Numerical Solutions of Nonlinear Radiative Heat Transfer Problems for Boundary Layer Flows

by

Ammar Mushtaq

Supervised by

Dr. Meraj Mustafa Hashmi

Research Centre for Modeling and Simulation,

National University of Sciences and Technology,

Sector H-12, Islamabad, Pakistan

2015

Numerical Solutions of Nonlinear Radiative Heat Transfer Problems for Boundary Layer Flows

by

Ammar Mushtaq

A dissertation submitted in partial fulfillment of the requirements for

Doctor of Philosophy

in

Computational Science and Engineering

Research Centre for Modeling and Simulation,

National University of Sciences and Technology,

Sector H-12, Islamabad, Pakistan

2015

Dedicated

To my Father

Acknowledgements

Alhamdulilah, what seemed to be a long endeavor four years ago is finally over. I would also like to thank the Government of Pakistan and National University of Sciences and Technology (NUST) for the financial support during my graduate studies. Looking back in time, there are many people who contributed directly or indirectly in this achievement and they all deserve my deepest gratitude.

Firstly, my profound regards to Dr. Meraj Mustafa Hashmi, my advisor and mentor for consistent guidance in my academic quest. It is indeed an honour for me to work with such a meticulous person. His regular motivation and unconditional help gave me courage to accomplish this work efficiently.

I would also like to thank my Master's research advisor Dr. Khalid Parvez, a very fatherly personality, who supported and counseled me in challenging situations. I also want to thank Dr. Muhammad Asif Farooq in School of Natural Sciences for teaching me MATLAB. Many thanks to my other advisory committee members, Drs. Imran Akhtar and Moniba Shams for their encouragement and assistance.

I wish to express my sicere thanks to Dr. Ahmed Ejaz Nadeem, Principal RCMS, for providing me with all the necessary facilities for the research. I would like to express gratitude to all of the Department faculty and staff for their help and support.

Special acknowledgments to my best friend Mr. Junaid Ahmed Khan for numerous occasions and memorable moments.

At the end, I pray from Almighty Allah, who bestowed all these blessings on me, to give me the strength and wisdom to use this knowledge the way He wants.

Ammar Mushtaq

Preface

Boundary layer flows subject to heat transfer have enormous industrial and engineering applications such as heat treatment of material travelling between a feed roll and wind-up roll, cooling of large metallic plates, cooling towers, solar water heating, distribution of moisture over groove fields, die forging, condensation processes, polymer extrusion and many others. In particular the radiative heat transfer is important in solar power technology, combustion applications such as fire, furnaces, IC engines, chemical engineering processes, various propulsion devices for aircrafts, missiles, satellites and space vehicles etc. A literature survey witnesses that boundary layer flow problems with linear Rosseland heat flux has been significantly addressed. This dissertation investigates some fundamental flow problems with the consideration of non-linear radiative heat transfer. Salient features affecting such flows have also been addressed. These include magnetic field, buoyancy forces, convective boundary, Brownian motion and thermophoretic diffusion due to nanoparticles, viscoelasticity, viscous dissipation and Joule heating. The developed differential system has been treated numerically through well known shooting method with fifth order Runge-Kutta integration. Numerical solutions through MATLAB builtin routine bvp4c are also presented in some cases.

Chapter 1 includes a detailed background of the boundary layer flows over moving or stationary surfaces and boundary layer flows of non-Newtonian fluids and nanofluids. Moreover, two-dimensional boundary layer equations for generalized Newtonian (power-law and Eyring-Powell fluids), viscoelastic fluids and nanofluids have been presented. Finally the numerical approach used in this dissertation is elaborated.

In Chapter 2, we emphasize the effects of nonlinear radiative heat transfer on the flow of Powell-Eyring fluid induced by a non-linearly stretching sheet. The arising non-linear problem is dealt numerically. Influences of parameters especially the radiation parameter on the flow fields are discussed. The main frame work of this chapter is submitted for

publication in **Open Physics**.

Chapter 3 describes the flow of upper-convected Maxwell (UCM) fluid affected by non-linear radiation heat transfer. UCM fluid is bounded by an isothermal stretching wall. Numerical solutions through both the shooting method and collocation method based MATLAB package bvp4c are evaluated. Comparison of the present computations with the previously reported results is also seen. The main findings of this chapter have been published in **Journal of Aerospace Engineering 27 (2014) 04014015. doi:10.1061/(ASCE)AS.1943-5525.0000361**.

Stagnation-point flow of power-law fluid with nonlinear radiative heat transfer is discussed in Chapter 4. The problem is first formulated and then investigated numerically for several values of embedded parameters. Power-law fluids of both shear-thinning and shear-thickening nature have been studied. The contents of this chapter have been published in **International Journal of Numerical Methods for Heat & Fluid Flow 25 (2015). doi:10.1108.2FHFF-05-2014-0147**.

Natural convective boundary layer flow of nanofluid with non-linear radiative heat flux is considered in chapter 5. The effects of magnetic field, Joule heating and viscous dissipation are also incorporated. Numerical solutions are discussed with the variation of interesting parameters. The main ideas of this study have been published in **PLoS ONE 9 (2014) e103946. doi:10.1371/journal.pone.0103946**

Two-dimensional flow of a nanofluid over a convectively heated radiative surface is described in chapter 6. Interesting aspects of Joule heating, viscous dissipation and magnetic field are also considered. Buongiorno's model for nanofluids is utilized in the formulation. At the end, the impact of physical parameters on the fields is sketched and analyzed. The main observations of this study are published in **Journal of the Taiwan Institute of Chemical Engineers 45 (2014) 1176-1183. doi:10.1016/j.jtice.2013.11.008**

In chapter 7, the non-linear radiative heat transfer analysis has been done for a moving electrically conducting fluid over a stationary or moving flat plate. Blasius and Sakiadis flow problems are obtained as special cases of this study. The numerical method is also able to simulate the model for both large and small values of the parameters. The graph-

ical results are obtained for several values of the parameters. The key results of this chapter have been accepted for publication in **International Journal of Numerical Methods for Heat & Fluid Flow**.

Non-linear thermal radiation is introduced for three-dimensional flow over a bidirectional stretching surface in chapter 8. The two-dimensional and axisymmetric flow cases are shown to be special cases for the model. Graphical illustrations showing the effect of parameters on the velocity, temperature, wall shear stress and wall heat transfer rate are presented and discussed. The obtained numerical solutions are found in excellent agreement with the available studies. The results of this chapter are published in **Zeitschrift Fur Naturforschung A 69 (2014) 705-713. doi:10.5560/zna.2014-0059**

Chapter 9 extends the idea of chapter 8 for an exponentially stretching surface. The exponential surface temperature distribution is considered for numerical simulations. Graphs for velocity and temperature functions are prepared and discussed. The computational results for wall shear stress and wall heat transfer rate are obtained. The contents of this chapter have been published in **Journal of the Taiwan Institute of Chemical Engineers 47 (2015) 43-49. doi:10.1016/j.jtice.2014. 10.011**.

Contents

Chapter 1

Introduction

This Chapter includes a detailed background of the boundary layer flows over moving or stationary surfaces, boundary layer flow of non-Newtonian fluids and some flow problems involving nanofluids. The governing equations for some flow problems considered in this dissertation are presented. Numerical approach adopted in this dissertation is also explained at the end.

1.1 Background

The study of flow over moving or stationary solid surfaces has been a prime interest of researchers mainly due to their variety of industrial and technological applications. For example, calculation of drag for the plate at zero incidence, metal and polymer extrusion processes, annealing and tinning of copper wires, paper production, manufacturing of plastic and rubber sheets, continuous cooling of fiber, metallic sheets or electronic chips, heat-treated materials travelling between a feed roll and a wind-up roll etc. In these processes the properties of the end product depends greatly on the rate of cooling, which is governed by the structure of the boundary layer near the moving strips. Prandtl in his revolutionary paper of 1904 suggested that the viscous effect in fluid are only present in a small region close to the surface known as boundary layer. The deduction of the boundary layer equations was one of the most successful advances in fluid mechanics. Using an order of magnitude analysis, the Navier-Stokes equations can be greatly simplified within the boundary layer. First of all Blasius [1] used Prandtl's boundary layer theory to investigate the flow over a stationary flat plate in the presence of uniform free stream. On the other hand, Sakiadis [2] investigated the boundary layer development over a moving plate in a calm fluid. Crane [3] investigated the Sakiadis' problem for a stretching sheet by assuming

linear variation in the velocity o the sheet with distance from the origin. After Crane's work, various studies dealing with two and three-dimensional boundary layer flows over stretching/ shrinking surfaces are addressed (see refs. [4-10]).

1.1.1 Non-Newtonian Fluids

Non-Newtonian fluid mechanics has been the subject of broad interest for research community during the last decade. Almost all industrial as well as biological fluids exhibit the non-linear relationship due to their different physical structures. These fluids are described through complicated nonlinear relationship between stress and deformation rate. Example include industrial fluids such as clay coatings and suspensions, drilling muds, liquid metal and alloys, oils and greases, ceramics, cosmetic products, plasma, mercury and paints. In the literature, a variety of fluid models have been proposed to understand the flow dynamics of these fluids. Among the most popular rheological models for non-Newtonian fluids is the power-law or Ostwald-de Waele model [11]. The power-law model is perhaps the widely discussed non-Newtonian fluid models that can be used to capture shear-thinning as well as shear-thickening effects. The former is a common characteristic of many fluids including blood, paints, ketchup etc. The constitutive equation for a power-law fluid can be expressed as:

$$S = K\left(\mathbf{tr}A^2\right)^{\frac{n-1}{2}} A, \tag{1.1}$$

where S is the extra stress tensor, $A = \nabla V + \nabla V^T$ is the first Rivilin-Ericksen tensor, K is consistency index and n is flow behavior index. Eq. (1.1) represents shear-thinning fluids for $n < 1$ and shear-thickening fluids for $n > 1$, while $n = 1$ indicates to Newtonian fluid. Th pioneering study on the boundary layer flow of power-law fluid was presented by Schowalter [12]. Anderson et al. [13] discussed the magnetohydrodynamics flow of a power-law fluid flow due to a stretching sheet. Prasad et al. [14] investigated the MHD flow of an electrically conducting power-law fluid over a stretching sheet maintained at variable surface temperature. Numerical solution for stagnation-point flow of power-law fluid was examined by Mahapatra et al. [15]. In this study, the characteristics of both pseudoplastic and Dilatant type power-law fluids were investigated. Salleh et al. [16] discussed the steady flow and heat transfer with Newtonian heating boundary condition. Kumari et al. [17] presented an interesting study on unsteady MHD stagnation point flow

of non-Newtonian fluid caused by an impulsive motion of stretching sheet from the rest. Patil et al. [18] examined the mixed convection flow due to a vertical stretching sheet with the power-law variation of the stretching velocity. The computations were performed by employing an implicit finite difference method combined with quasi-linearization technique. Postelnicu and Pop [19] discussed the numerical solution of Falkner-Skan boundary layer flow of a power-law fluid due to a stretching wedge. Recently, Griffiths et al. [20] reported the power-law fluid flow over a rotating disk. Similarity solutions were determine for the three-dimensional boundary layer and there stability was also discussed.

Differential type fluids have been extensively discussed by the researchers due to the fact that constitutive equations in differential type fluids are easily solvable for the stress components. However in rate type fluids the rheological equations are more complex than those of differential type fluids. Therefore it is difficult to eliminate the components of stress tensor from the momentum equation. Maxwell fluid model is perhaps the most commonly discussed viscoelastic fluid model that is capable of explaining the characteristics of fluid relaxation time. The constitutive equation for the upper-convected Maxwell model can be written as:

$$S + \lambda_1 \frac{DS}{Dt} = \mu A, \tag{1.2}$$

where S is the extra stress tensor, μ is the dynamic viscosity, A is the first Rivilin-Ericksen tensor, λ_1 is relaxation time and D/Dt is the upper-convected time derivative. Sakiadis flow of Maxwell fluid with different numerical and analytic approaches was discussed by Sadeghy et al. [21]. In another paper, Sadeghy et al. [22] discussed the stagnation-point flow of Maxwell fluid by using Chebyshev pseudo-spectral collocation-point method. Series solutions for flow of Maxwell fluid over a permeable stretching sheet were provided by Hayat et al. [23]. Stagnation-point flow of Maxwell fluid over a stretching sheet was addressed by Hayat and Sajid [24]. Mixed convection flow of Maxwell fluid subjected to uniform transverse magnetic field was considered by Kumari and Nath [25]. In this study the numerical solutions of the developed differential system were obtained by an explicit finite difference scheme. Alizadeh-Pahlavan et al. [26] employed two-parameter homotopy analytic technique to derive the solution of the corresponding problem by Hayat et al. [23]. Hayat et al. [27] investigated the stagnation-point flow of Maxwell fluid under the influence of magnetic force by using homotopy approach. Flow of Maxwell fluid past a permeable stretching surface was described by Raftari and Yildirim [28]. Recent studies

dealing the flow and heat transfer characteristics involving Maxwell fluid are [29-36].
The Powell-Eyring fluid model, although mathematically complex, is considered to be useful than the power-law fluid model because its constitutive relationships are developed from the kinetic theory of gases rather than empirical relationships. Further it can exactly describe the Newtonian flow behavior for both low and high shear rates. The constitutive equation for the Eyring-Powell model can be written as:

$$S = \mu \nabla V + \frac{1}{\beta} \sinh^{-1} \left(\frac{1}{C} \nabla V \right), \tag{1.3}$$

where S is the extra stress tensor, μ is the dynamic viscosity, ∇V is velocity gradient, $1/\beta$ is shear stress and C is the shear rate of the fluid. Now a days, the flow analysis of Powell-Eyring fluid has been given significant attention by the researchers. For instance, flow of Powell-Eyring fluid over a moving flat plate in a flowing fluid was discussed by Jalil et al. [37]. They used Keller-box approach to obtain the numerical solutions of the problem. Analytic and numerical solutions for flow of Powell-Eyring fluid caused by exponentially stretching sheet were derived by Mushtaq et al. [38]. Javed et al. [39] discussed theflow of an Erying-Powell fluid over a linearly stretching sheet Flow and heat transfer characteristics in Powell-Eyring fluid over a shrinking surface in the presence of free stream were investigated by Rosca and Pop [40]. Poonia and Bhargava [41] presented a finite element study of Powell-Eyring fluid flow and heat transfer by considering convective boundary condition. Series solutions for Powell-Eyring fluid flow past an inclined stretching sheet with non-uniform heat source were constructed by Hayat et al. [42]. Very recently, Panigrahi et al. [43] examined the mixed convection flow past a non-linearly stretching sheet by using Powell-Eyring fluid.

1.1.2 Nanofluids

Solar energy is probably the most suitable source of renewable energy that can meet the current energy requirements. The energy obtained from nature in the form of solar radiations can be directly transformed into heat and electricity. The idea of using small particles to collect solar energy was first investigated by Hunt [44] in the 1970s. Researchers concluded that with the addition of nanoparticles in the base fluids, heat transfer and the solar collection processes can be improved. Nanofluids are the new generation heat transfer fluids which possess much higher thermal conductivity at very low particle

concentrations than the conventional fluids. Researches have indicated that substitution of conventional coolants with the nanofluids may be beneficial in processes like engine cooling, improving heat transfer efficiency in chillers, domestic refrigerators/freezers, nuclear engineering and space and cooling of micro-electronics. The researchers not only discovered unexpected thermal properties of nanofluids but also proposed mechanisms behind the enhanced thermal properties of nanofluids and thus identified unusual opportunities to develop them as next generation coolants for computers and safe coolants for nuclear reactors. A combination of nanofluid with biotechnological components can provide potential applications in agriculture, pharmaceuticals and biological sensors. Various types of nanomaterials including nanoparticles, nanowires, nanofibers, nanostructures and nanomachines are used in biotechnological applications. The commercialization of nanobiotechnological products seems to have a potential future and within next a few years many new products of this nature are likely to be used. Nano and micro-fluidics is a new area with potential for engineering applications, especially for the development of new biomedical devices and procedures. The magnetic nanofluids possess both liquid and magnetic properties. These fluids have key importance in modulators, optical switches, optical gratings and tunable optical fiber filters. The magnetic nanoparticles are significant in medicine, construction of loud speakers, sink float separation, cancer therapy and tumor analysis. Magnetic nanoparticles are more important in biomedicinal applications as compared to other metallic particles because these can be used to control and manipulate the nanofluid through magnetic force. For instance, nanometer-sized iron particles can be used to deliver drugs and radiation in cancer patients without damaging the nearby healthy tissues [45-54].

Masuda et al. [55] discussed the alteration of thermal conductivity and viscosity by dispersing ultra-fine particles in the liquid. The terminology of nanofluid was first used by Choi [56] when he experimentally discovered a significant improvement in the heat transfer performance through the addition of small amount nanometer sized particles in the base fluids. This addition also causes scattering of the incident radiation which allows a deeper absorption within the fluid. Choi and Eastman [57] were the first to introduce the terminology of nanofluids when they experimentally discovered an effective way of controlling heat transfer rate using nanoparticles. Buongiorno [58] developed the non homogeneous equilibrium mathematical model for convective transport of nanofluids. He concluded that Brownian motion and thermophoretic diffusion of nanoparticles are the most important mechanisms for the abnormal convective heat transfer enhancement. Buongiorno and Hu

[59] discussed the heat transfer enhancement via nanoparticles for nuclear reactor application. Huminic and Huminic [60] showed that use of nanofluids in heat exchangers has advantage in the energy efficiency and it leads to better system performance. Later, Nield and Kuznetsov [61] and Kuznetsov and Nield [62] studied Cheng-Minkowycz problem of natural convective boundary layer flow in a porous medium saturated by a nanofluid and natural convective boundary-layer flow of a nanofluid past a vertical plate respectively. Khan and Pop [63] obtained the numerical solution of two-dimensional flow of nanofluid over a linearly stretching sheet using Keller-box method. Makinde and Aziz [64] extended the work of Khan and Pop [63] by implementing convective boundary condition for solving energy equation. Mustafa et al. [65] obtained series solution for stagnation-point flow of a nanofluid by using homotopy analysis method (HAM). Ahmad et al. [66] considered the classical Blasius and Sakiadis problems in nanofluids. Numerical solution for nanofluid flow past a stretching cylinder with non- uniform heat source/sink was considered by Rasekh et al. [67]. Ashorynejad et al. [68] investigated nanofluid flow over stretching cylinder in the presence of magnetic field. The effect of magnetic force on the boundary layer flow of nanofluid past a linearly stretching sheet has been reported by Ibrahim et al. [69]. Sheikholeslami et al. [70] also investigated the nanofluid flow with heat transfer in the presence of an applied magnetic field. It has been seen that the buoyancy forces stemming from the heating or cooling of the continuously moving surface alter the flow and thermal fields and thereby the heat transfer characteristics of the manufacturing process [71, 72]. The process of natural convection has been thoroughly explained in [73]. Aziz and Khan [74] solved the problem of natural convective flow of a nanofluid past a vertical plate with convective boundary conditions. Uddin et al. [75] obtained numerical solution for steady two dimensional MHD free convective boundary layer flow of an electrically conducting nanofluid past a vertical flat plate with Newtonian heating boundary condition. Kuznetsov and Nield [76] revised their classical natural convection flow problems in nanofluids [61,62] by taking into account zero nanoparticle wall mass flux condition. Recently, several interesting studies pertaining to boundary layer flows and heat transfer effect in nanofluids have been reported (see [77-85]).

1.1.3 Linear and Nonlinear Radiative Heat Transfer

The study of radiative heat transfer flow has significant importance in manufacturing industries for the design of reliable equipment, gas turbines, solar power technology, nuclear power plant, in combustion applications such as fire, furnaces, IC engines, chemical engineering processes, various propulsion devices for aircrafts, missiles, satellites and space vehicles etc. Particularly the thermal radiation effects are very important when the difference between the surface temperature and the ambient temperature is very large. In these cases the quality of final product largely depends on the rate of cooling which is governed by the structure of the thermal boundary layer near the moving plate/sheet. No doubt the thermal diffusivity of the liquids can also be enhanced by thermal radiation. Many researchers studied the radiation effects in the boundary layer flow using linearized Rosseland approximation for thermal radiation.

Raptis and Perdikis [86] studied the viscoelastic fluids motion under the influence of radiations. Seddeek [87] investigated the free convection flow past a semi-infinite plate with magnetic field, radiation and variable viscosity effects. Raptis et al. [88] examined the thermal radiation effect on the boundary layer flow of an electrically conducting viscous fluid. Bataller [89] discussed the classical Blasius problem for impermeable plate in the presence of thermal radiation. Mixed convection flow past a vertical plate with thermal radiation was investigated by Ishak [90]. He obtained the numerical solutions for some negative values of buoyancy parameter. Bhattacharyya [91] studied the effect of thermal radiation on the MHD boundary layer flow over a time-dependent shrinking sheet with internal heat generation fluids. Sakiadis flow subjected to thermal radiation was analyzed by Cortell [92]. Blasius flow of viscoelastic (second grade) fluid with thermal radiation was considered by Hayat et al. [93]. Mixed convection flow past a vertical plate with heat generation/absorption and thermal radiation was investigated by Gireesha et al. [94]. Hayat et al. [95] analytically discussed the melting heat transfer in the stagnation-point flow of Jeffrey fluid with thermal radiation. Recently, the influence of radiation in the unsteady flow of Powell-Eyring fluid past an inclined stretching surface has been examined by Hayat et al. [96]. Mahapatra et al. [97] obtained a numerical solution for MHD stagnation point flow of power-law fluid in the presence of thermal radiation and suction/ injection. Thermal radiation and viscous dissipation effects on the unsteady boundary layer flow of nanofluid over a stretching sheet were presented by Khan et al. [98]. Motsumi and Makinde [99] considered the similar effects on the nanofluid flow due to a continuously

moving permeable flat surface. Solar radiations on the nanofluid flow over a nonlinearly stretching sheet are considered by Hady et al. [100]. Behavior of nanoparticles on the Marangoni convection boundary layer flow with thermal radiation is addressed by Mat et al. [101]. The influence of solar energy radiations in the unsteady Hiemenz flow of nanofluid over a wedge was analyzed by Mohamad et al. [102]. Radiations due to solar energy in the natural convection flow of nanofluid past a vertical plate were considered by Kandasamy at al. [103]. They concluded that radiation effects due to solar energy become prominent through to the presence of nanoparticles in the base. Series solutions for flow of micropolar fluid under the impact of radiation have been computed by Shadloo et al. [104]. Numerical solution for free convective flow of nanofluid due to porous stretching sheet is discussed by Ferdows et al. [105]. Khan et al. [106] explored the magnetic field effects on the flow of nanofluid over a radiative surface. In another paper, Khan et al. [107] discussed the effects of heat generation, radiation and chemical reaction on the flow of nanofluid past a wedge.

Recently Magyari and Pantokratoras [108] showed that with the aid of simple rescaling of Prandtl number the results of the previous studies on the topic of thermal radiation for linearized Rosseland approximation can be recovered without even considering the thermal radiation term in the energy equation. Therefore it can be concluded that effect of thermal radiation on the flow using linearlized radiative heat transfer is trivial both physically and computationally. Keeping this in view, Rahman and El-tayeb [109] considered the radiation effects on the flow of an electrically conducting nanofluid by using non-linear Rosseland approximation. Pantokratoras and Fang [110] extended the work of Cortell [92] by considering non-linear radiations. In another paper, Pantokratoras and Fang [111] discussed Blasius flow under the influence of non-linear radiations. Mushtaq et al. [112] described the radiation effects on the flow of viscoelastic (Maxwell) fluid in the presence of non-linear radiations. Similar studies in this direction can be found in refs. [113-120].

1.2 Boundary Layer Equations

The governing equations of fluid flow motion are derived from the fundamental principles of conservation of mass, momentum and energy. The relation between shear stress and

strain rate through the rheological properties of the fluid can be of different forms. Here are the boundary layer equations for some of the most popular rheological models which will be used in the later chapter of this dissertation.

1.2.1 Power-Law Fluid

Consider a steady two-dimensional incompressible flow of Power-law fluid. Using the velocity field $V = [u(x, y), v(x, y), 0]$ and the stress tensor given in Eq. (1.1), the boundary layer equations of power-law model are:

$$\frac{\partial u}{\partial x} + \frac{\partial v}{\partial y} = 0, \tag{1.4}$$

$$u\frac{\partial u}{\partial x} + v\frac{\partial u}{\partial y} = -\frac{1}{\rho}\frac{dp}{dx} + \frac{K}{\rho}\frac{\partial}{\partial y}\left(\frac{\partial u}{\partial y}\right)^n. \tag{1.5}$$

In the above equations, u and v are the velocity components along the $x-$ and $y-$ directions, ρ is the fluid's density, p is the static pressure, K is the consistency index and n is the flow behavior index.

1.2.2 Upper-Convected Maxwell Fluid

Consider a steady two-dimensional incompressible flow of upper-convected Maxwell fluid. Using the velocity field $V = [u(x, y), v(x, y), 0]$ and the stress tensor given in Eq. (1.2), the boundary layer equations of UCM model are:

$$\frac{\partial u}{\partial x} + \frac{\partial v}{\partial y} = 0, \tag{1.6}$$

$$u\frac{\partial u}{\partial x} + v\frac{\partial u}{\partial y} + \lambda_1\left(u^2\frac{\partial^2 u}{\partial x^2} + v^2\frac{\partial^2 u}{\partial y^2} + 2uv\frac{\partial^2 u}{\partial x \partial y}\right) = -\frac{1}{\rho}\frac{dp}{dx} + \frac{\mu}{\rho}\frac{\partial^2 u}{\partial y^2}, \tag{1.7}$$

where μ is the dynamic viscosity, λ_1 is the relaxation time, ρ is the fluid's density, p is the static pressure, u and v are the velocity components in the $x-$ and $y-$ directions respectively.

1.2.3 Eyring-Powell Fluid

Consider a steady two-dimensional incompressible flow of Eyring-Powell fluid. Using the velocity field $V = [u(x, y), v(x, y), 0]$ and the stress tensor given in Eq. (1.3), the bound-

ary layer equations of Eyring-Powell model are:

$$\frac{\partial u}{\partial x} + \frac{\partial v}{\partial y} = 0, \tag{1.8}$$

$$u\frac{\partial u}{\partial x} + v\frac{\partial u}{\partial y} = -\frac{1}{\rho}\frac{dp}{dx} + \left(\nu + \frac{1}{\rho\beta C}\right)\frac{\partial^2 u}{\partial y^2} - \frac{1}{2\rho\beta C^3}\left(\frac{\partial u}{\partial y}\right)^2\frac{\partial^2 u}{\partial y^2}. \tag{1.9}$$

In the above equations, u and v are the velocity components along the $x-$ and $y-$ directions respectively, p is the static pressure, ν is the kinematic viscosity, ρ is the density of the fluid, β and C are the parameters of fluid material

1.3 Nanofluid

Nanofluids are engineered colloids made of a base fluid and nanoparticles 1– $100nm$. Therefore, we can develop a complete transport model for the nanofluid by treating the nanofluid as a two-component mixture (base fluid+nanoparticles). The boundary layer equations of steady incompressible nanofluid are:

$$\nabla \cdot V = 0, \tag{1.10}$$

$$(V \cdot \nabla)V = -\frac{1}{\rho_f}\nabla p + \nu_f \nabla^2 V, \tag{1.11}$$

$$(V \cdot \nabla)T = \alpha_f \nabla^2 T + \tau\Big[D_B(\nabla \cdot C)(\nabla \cdot T) + \frac{D_T}{T_\infty}(\nabla T)^2\Big], \tag{1.12}$$

$$(V \cdot \nabla)C = D_B \nabla^2 C + \frac{D_T}{T_\infty}\nabla^2 T, \tag{1.13}$$

where ν_f is the kinematic viscosity, ρ_f is the density of base fluid , $\tau = (\rho C_p)_p/(\rho C_p)_f$ is the ratio of effective heat capacity of the nanoparticle material to the effective heat capacity of the base fluid, α_f is thermal diffusivity of base fluid, T is the local temperature, C is local volume fraction of nanoparticles, D_B is Brownian diffusion coefficient and D_T is thermophoretic diffusion coefficient.

1.4 Shooting Method

The governing differential system for fluid flow and heat transfer phenomenons is generally a non-linear Boundary-Valued Problem (BVP). The boundary value problems can be solved using *finite difference method* or the iterative procedure known as *Shooting*

method. The later is preferred in the boundary layer flow problems because it uses fifth-order accurate Runge-Kutta scheme whereas finite difference method is only second order accurate. Other advantages of shooting method include its simple implementation as well as its faster convergence rate when compared to other numerical integration techniques. The basic idea of shooting method is as follows:
Consider the Blasius problem [1]

$$f''' + ff'' = 0, \quad f(0) = 0, \quad f'(0) = 0, \quad f'(\infty) = 1 \tag{1.14}$$

The equivalent first order equations are:

$$f' = \begin{pmatrix} f_1' \\ f_2' \\ f_3' \end{pmatrix} = \begin{pmatrix} f_2 \\ f_3 \\ -f_1 f_3 \end{pmatrix}, \tag{1.15}$$

with boundary conditions

$$f_1(0) = \alpha, \quad f_2(0) = 0, \quad f_2(\infty) = 1 \tag{1.16}$$

The solution of Eq. (1.15) is obtained using fifth order Runge-Kutta integration technique with following initial conditions

$$f_1(0) = 0, \quad f_2(0) = 0, \quad f_3(0) = u \tag{1.17}$$

This solution can agree with the original BVP for a suitable value of u. This means that $f_2(\infty)$ is a function of u; that is

$$f_2(\infty) = \theta(u) \tag{1.18}$$

$$r(u) = \theta(u) - 1 = 0 \tag{1.19}$$

where $r(u)$ is the boundary residual (difference between the computed and specified boundary value). Now Newton method can be used to determine the desired value of u such that the corresponding boundary condition is satisfied.

Chapter 2

Boundary layer flow of Powell-Eyring fluid subject to non-linear radiation heat transfer

2.1 Introduction

In this chapter, we address the flow and heat transfer characteristics in non-Newtonian Powell-Eyring fluid over a linearly stretching sheet. The novel idea of non-linear thermal radiation is taken into consideration. Appropriate similarity transformations are utilized to non-dimensionalize the governing boundary layer equations. The arising problem is strongly non-linear and involves important parameters including Powell-Eyring fluid parameters, temperature ratio parameter and Prandtl number. Shooting method with fifth-order Runge-Kutta integration technique is adopted to compute the numerical solution of the problem. We observe that an increase in wall to ambient ratio corresponds to a diminution in the heat transfer rate from the sheet. The influence of parameter on the velocity and temperature distributions is qualitatively opposite to that of parameter. The obtained results agree well the available studies in the literature in limiting cases.

2.2 Problem Formulation

We consider a steady two-dimensional incompressible flow of Powell Eyring fluid driven by a nonlinearly stretching sheet aligned with the $x-$ axis. Let $U_w(x) = ax$ be the velocity distribution across the sheet. The sheet is constant temperature T_w and T_∞ denotes

the ambient temperature. Under the usual boundary layer assumptions, the equations governing the conservation of mass, momentum and energy can be expressed as (see [38].):

$$\frac{\partial u}{\partial x}+\frac{\partial v}{\partial y}=0, \tag{2.1}$$

$$u\frac{\partial u}{\partial x}+v\frac{\partial u}{\partial y}=-\frac{1}{\rho}\frac{dp}{dx}+\left(\nu+\frac{1}{\rho\beta C}\right)\frac{\partial^2 u}{\partial y^2}-\frac{1}{2\rho\beta C^3}\left(\frac{\partial u}{\partial y}\right)^2\frac{\partial^2 u}{\partial y^2}, \tag{2.2}$$

$$u\frac{\partial T}{\partial x}+v\frac{\partial T}{\partial y}=\alpha\frac{\partial^2 T}{\partial y^2}-\frac{1}{\rho C_p}\left(\frac{\partial q_r}{\partial y}\right). \tag{2.3}$$

The boundary conditions in the present problem are as below:

$$\begin{aligned} &u=U_w(x)=ax,\ v=0,\ T=T_w \qquad \text{at } y=0,\\ &u\to 0,\ T\to T_\infty \qquad\qquad\qquad \text{as } y\to\infty. \end{aligned} \tag{2.4}$$

In the above equations $a>0$ is the stretching constant, u and v are the velocity components along the $x-$ and $y-$ directions respectively, ν is the kinematic viscosity, ρ is the density of the fluid, β and C are the parameters of fluid material, T is the fluid temperature and α is the thermal diffusivity. The radiative heat flux expression in Eq. (2.3) is given by the Rosseland formula [123] as

$$q_r=-\frac{4\sigma^*}{3k^*}\frac{\partial T^4}{\partial y}=-\frac{16\sigma^*}{3k^*}T^3\frac{\partial T}{\partial y}, \tag{2.5}$$

where σ^* and k^* are the Stefan-Boltzman constant and the mean absorption coefficient respectively. A huge simplification of Rosseland heat flux is possible if T^4 in Eq. (2.5) is expanded about the ambient temperature T_∞ and then higher order terms are neglected (through the assumption of small temperature differences within the flow), as done by many authors previously [86-107]. This means to simply replace T^3 in Eq. (2.5) with T_∞^3. Now Eq. (2.3) can be written as

$$u\frac{\partial T}{\partial x}+v\frac{\partial T}{\partial y}=\left(\alpha+\frac{16\sigma^*T_\infty^3}{3\rho C_p k^*}\right)\frac{\partial^2 T}{\partial y^2}. \tag{2.6}$$

However if we utilize the complete expression of Rosseland heat flux, Eq. (2.3) results in a highly non-linear partial differential equation given below:

$$u\frac{\partial T}{\partial x}+v\frac{\partial T}{\partial y}=\frac{\partial}{\partial y}\left[\left(\alpha+\frac{16\sigma^*T^3}{3\rho C_p k^*}\right)\frac{\partial T}{\partial y}\right]. \tag{2.7}$$

Introducing the following dimensionless variables

$$\eta=y\sqrt{\frac{a}{\nu}},\ u=ax\frac{df}{d\eta},\ v=-\sqrt{a\nu}f,\ \theta=\frac{T-T_\infty}{T_w-T_\infty}. \tag{2.8}$$

Eq.(2.1) is identically satisfied and Eqs.(2.2) and (2.6-2.7) become

$$\Big(1+K\Big)\frac{d^3f}{d\eta^3} - K\Lambda\left(\frac{d^2f}{d\eta^2}\right)^2\frac{d^3f}{d\eta^3} + f\frac{d^2f}{d\eta^2} - \left(\frac{df}{d\eta}\right)^2 = 0, \tag{2.9}$$

$$\left(\frac{1+Rd}{Pr}\right)\frac{d^2\theta}{d\eta^2} + f\frac{d\theta}{d\eta} = 0, \tag{2.10}$$

$$\frac{1}{Pr}\frac{d}{d\eta}\left[\left(1+Rd\Big(1+(\theta_w-1)\theta\Big)^3\right)\frac{d\theta}{d\eta}\right] + f\frac{d\theta}{d\eta} = 0, \tag{2.11}$$

with corresponding boundary conditions

$$\begin{aligned} &f(0)=0,\ f'(0)=1,\ \theta(0)=1,\\ &f'(\infty)\to 1,\ \theta(\infty)\to 0, \end{aligned} \tag{2.12}$$

where $K = 1/\mu\beta C$ and $\Lambda = U_w^3/2\nu x C^2$ are the dimensionless fluid parameters, $\theta_w = T_w/T_\infty$ is the temperature ratio parameter, $Pr = \nu/\alpha$ is the Prandtl number, and $Rd = 16\sigma^* T_\infty^3/3kk^*$ is the radiation parameter.

Physical quantities of practical interest in this study are the skin friction coefficient C_f and the local Nusselt number Nu_x defined as

$$\begin{aligned} C_f &= \frac{\tau_w}{\rho U_w^2};\ \tau = \left(\mu+\frac{1}{\beta C}\right)\left(\frac{\partial u}{\partial y}\right)_{y=0} - \frac{1}{6\beta C^3}\left(\frac{\partial u}{\partial y}\right)^3_{y=0},\\ Nu_x &= \frac{xq_w}{k(T_w-T_\infty)};\ q_w = -k\left(\frac{\partial T}{\partial y}\right)_{y=0} + (q_r)_{y=0}, \end{aligned} \tag{2.13}$$

where τ_w is the wall shear stress and q_w is the wall heat flux. Now using dimensionless quantities from Eq. (2.8) in Eq. (2.13), we get

$$\begin{aligned} Re_x^{1/2}C_f &= (1+K)f''(0) - \frac{K\Lambda}{3}\Big(f''(0)\Big)^3,\\ Re_x^{-1/2}Nu_x &= -\Big[1+Rd\theta_w^3\Big]\theta'(0) = Nur, \end{aligned} \tag{2.14}$$

where $Re_x = U_w x/\nu$ is the local Reynolds number.

2.3 Numerical Method

The solutions of dimensionless ordinary differential equations (2.9-2.11) with the boundary conditions (2.12) have been obtained numerically using fourth-fifth order Runge-Kutta method based shooting technique. For this purpose the boundary value problem (BVP) (2.9)-(2.12) is transformed to initial value problem (IVP). Before employing the Runge-Kutta integration scheme, first we reduce the governing differential equations into a set

of first order ODEs. Let $x_1 = \eta, x_2 = f, x_3 = f', x_4 = f'', x_5 = \theta, x_6 = \theta'$. We obtain the following system:

$$\begin{pmatrix} x_1' \\ x_2' \\ x_3' \\ x_4' \\ x_5' \\ x_6' \end{pmatrix} = \begin{pmatrix} 1 \\ x_3 \\ x_4 \\ \frac{x_3^2 - x_2 x_4}{1+K-K\Lambda x_4^2} \\ x_6 \\ \frac{-Prx_2x_6 - 3Rdx_6^2(\theta_w-1)\left(1+(\theta_w-1)x_5\right)^2}{1+Rd\left(1+(\theta_w-1)x_5\right)^3} \end{pmatrix}, \tag{2.15}$$

and the corresponding initial conditions are:

$$\begin{pmatrix} x_1 \\ x_2 \\ x_3 \\ x_4 \\ x_5 \\ x_6 \end{pmatrix} = \begin{pmatrix} 0 \\ 0 \\ 1 \\ u_1 \\ 1 \\ u_2 \end{pmatrix}. \tag{2.16}$$

The above nonlinear coupled ODEs along with initial conditions are solved using fourth-fifth order Runge-Kutta integration technique. Suitable values of the unknown initial conditions u_1 and u_2 are approximated through Newton's method until the boundary conditions at infinity $f'(\infty)$, and $\theta(\infty)$ are satisfied. The computations have been performed by using MATLAB. The maximum value of η_∞, to each group of parameters is determined when the values of unknown boundary conditions at $\eta = 0$ do not change to a successful loop with error less than 10^{-7}.

2.4 Numerical Results and Discussion

This section is devoted to study the effects of various physical parameters on velocity, temperature, skin friction coefficient and local Nusselt number. In this regard, numerically computed data is presented in both, tabular and graphical forms. Table 2.1 provides the variation in skin friction coefficient as dimensionless fluid parameters K, Λ change. In this table we compared the numerical results of present study, in which shooting method with fourth-fifth order Runge-Kutta method and Javed et al. [39]. The results are in

excellent agreement with the previously published data. The magnitude of the skin friction coefficient significantly increases with an increase in K. However there is a decrease in the coefficient of skin friction when Λ is increased. From the industrial point of view this is a useful result since the power generation involved in displacing the fluid over the sheet can be reduced by assuming larger values of Λ. Table 2.2 presents the variation in local Nusslet number for various embedded parameters of the considered problem. The thermal boundary layer thickness decreases when K is increased. This results in a larger rate of heat transfer at the stretching sheet. Further the magnitude of the local Nusselt number slightly decreases with an increase in Λ.

Figs 2.1 displays the velocity distribution profile for dimensionless fluid parameters K and Λ. An increase in K may be either regarded as a decrease in the viscosity or a decrease in rheological effects of the Powell–Eyring fluid. Here we notice that velocity and boundary layer thickness are increasing functions of K . This observation leads to the conclusion that the increase in the elastic effects of the Powell–Eyring fluid leads to a thinner momentum boundary layer. Whereas, an increase in Λ shift the profiles towards the boundary, indicating a diminution in the boundary layer thickness. This notion is quite understandable since an increase in Λ accompanies with a decrease in kinematic viscosity. In case of Λ as defined in previous section Λ is inversely proportional to the kinematic viscosity ν thus increasing this dimensionless fluid parameter would provide a diminution in the momentum boundary layer however the magnitude is very minor as shown in Fig 2.1. The influence of K and Λ on the skin friction coefficient is plotted in Fig. 2.2. It can be seen that increasing Λ increases the skin friction coefficient while increasing K decreases the skin friction coefficient.

Figure 2.3 indicates that the temperature profiles move towards the boundary when Pr is increased causing a reduction in the thermal boundary layer thickness. Physically this is attributed to the fact that a larger Prandtl number has a relatively lower thermal diffusivity. Thus an increase in Pr reduces the conduction and thereby increases the variation in the thermal characteristics. In other words, profiles become increasingly steeper when Pr is increased. There is a slight decrease in the temperature θ when K is increased for large values of Pr. Effects of temperature parameter θ_w and Λ are depicted in Fig. 2.4. Increasing values of θ_w indicates larger wall temperature compared to ambient. As a result temperature θ is an increasing function of θ_w. Moreover the profiles become S-shaped indicating the occurrence of adiabatic case for sufficiently larger value of $\theta_w > 5$. It is well known in boundary layer theory that the thermal boundary layer thickness, depends

on the value of the thermal diffusivity. When the thermal diffusivity is large the thermal boundary layer thickness is large and vice-versa. In case of nonlinear thermal radiation, the thermal diffusivity includes the whole quantity $(\alpha + 16\sigma^* T^3/3\rho C_p k^*)$ (Eq. (2.7)), that is, the sum of the classical thermal diffusivity α and the second term, and is variable across the boundary layer due to the corresponding temperature change. This means that near the plate, where the fluid temperature is large the above thermal diffusivity is large whereas far away from the plate, where the temperature is low, the thermal diffusivity is low. The large thermal diffusivity near the plate causes a small temperature gradient while a smaller thermal diffusivity far from the wall causes an increasing temperature gradient, creating thus of the inflexion point. On the other hand, the effects of Λ has a little effect on thermal boundary layer. Figs. 2.5 and 2.6 compare the results of linear and non-linear radiation for different values of Rd when $\theta_w = 1.1$ and $\theta_w = 1.5$ respectively. It is seen that linear and non-linear results match each other better at $\theta_w = 1.1$ when compared with $\theta_w = 1.5$. The profiles show a significant deviation as the radiation parameter is gradually increased, a fact that can be understood through a comparison of Eqs. (2.10) and (2.11). Thus it can be concluded that linear and non-linear radiation results match up smoothly when θ_w is close to one (say $\theta_w = 1.1$) and Rd is sufficiently small (say $Rd < 1$).

Figs. 2.7 and 2.8 illustrate the effects of dimensionless fluid parameters K and Λ , Prandtl number Pr, temperature parameter θ_w and radiation parameter Rd on reduced Nusselt number $-\theta'(0)$. Increasing the Pr decrease thermal boundary layer as already discussed in Fig. 2.3. Therefore the local Nusselt number, being proportional to the initial slope, increases with an increase in Pr. Fig. 2.8 plots the wall temperature gradient versus θ_w for different values of radiation parameter Rd. It is worth pointing here that when $\theta_w \approx 1$, corresponding to the case of linear radiative heat flux. Also, when $\theta_w \approx 1, \theta'(0)$ when tends to a constant value for sufficiently smaller values of $Rd \approx 0.005$, which is in accordance with the previous studies on nonlinear radiation [109-120].

2.5 Conclusions

The non-Newtonian flow and heat transfer induced by a nonlinearly stretched surface have been investigated. The numerical study assumes that the temperature across the sheet is controlled convectively. Following are the major results of this study:

a. It is found that hydrodynamic/ momentum boundary layer decreases and thermal

boundary layer decreases with an increase in dimensionless fluid parameter Λ. Further, these effects are minor for both velocity and temperature profiles.

b. On increasing dimensionless fluid parameter K there is a significant increase in momentum boundary layer.

c. While increasing dimensionless fluid parameter K temperature profile reduces and converge towards a certain profile.

d. In the non-linear Rosseland approximation the temperature profiles are S-shaped with an inflection point with an increase in temperature ratio parameter.

e. An increase in wall to ambient temperature ratio rises the fluid's temperature and thermal boundary layer thickness. Heat transfer rate $\theta'(0)$ tends to zero as temperature ratio parameter is increased.

Table 2.1: Comparison of Skin friction coefficient $Re_x^{1/2}C_f$ with (Javed et al. [39]) for different values of parameters.

Λ/K	0.2	0.6	1.0
0.0	-1.09545	-1.26491	-1.41422
	(-1.0954)	(-1.2649)	(-1.4142)
0.5	-1.08782	-1.24977	-1.3961
	(-1.0878)	(-1.2498)	(-1.3961)
1.0	-1.07975	-1.23294	-1.37578
	(-1.0798)	(-1.2329)	(-1.3758)

Table 2.2: Values of local Nusselt number $-\theta'(0)$ for different values of parameters.

K	Λ	Pr	$Rd = 0$	$Rd = 1$		
				Linear	Non-linear Radiation	
				Radiation	$\theta_w = 1.1$	$\theta_w = 3$
1	1	2	0.96899	0.63925	0.57091	0.08494
		4	1.43597	0.96899	0.86795	0.14554
		7	1.95095	1.33297	1.19587	0.21405
		10	2.36293	1.62422	1.45827	0.26908
	0	7	1.95919	1.34025	1.20259	0.21611
	0.5		1.95547	1.33693	1.19952	0.21514
	1		1.95095	1.33297	1.19587	0.21405
	2		1.93612	1.32071	1.18463	0.21105
0	1	7	1.89542	1.27616	1.14277	0.18870
0.5			1.92753	1.30947	1.17394	0.20391
1			1.95095	1.33297	1.19587	0.21405
2			1.98112	1.36295	1.22383	0.22675

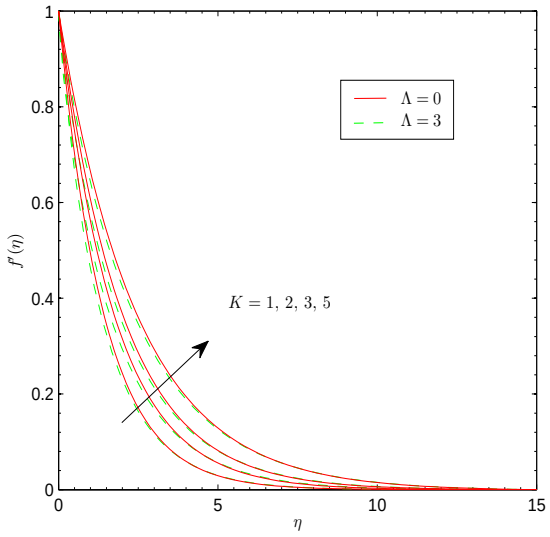

Figure 2.1: Effect of K and Λ on f'.

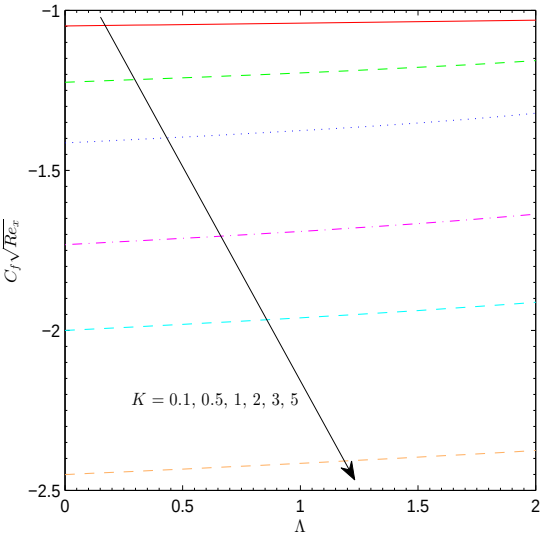

Figure 2.2: Effect of K and Λ on $Re_x^{1/2}C_f$.

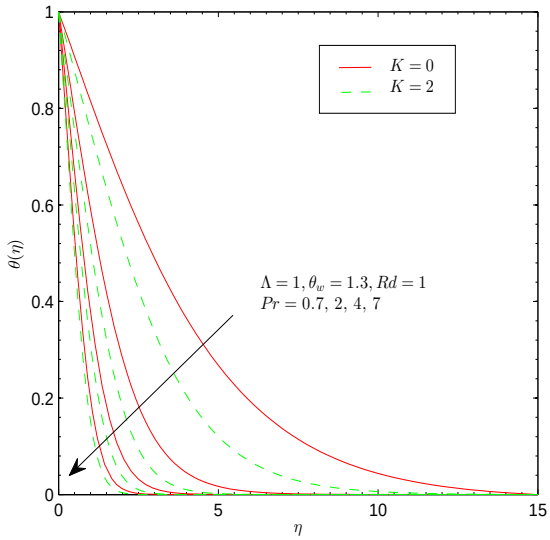

Figure 2.3: Effect of K and Pr on θ.

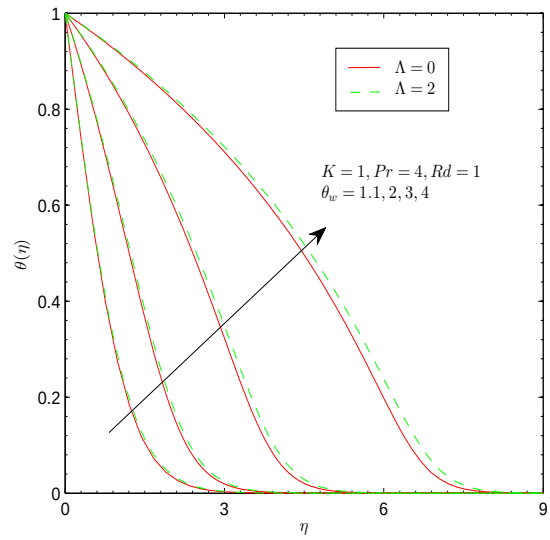

Figure 2.4: Effect of θ_w and Λ on θ.

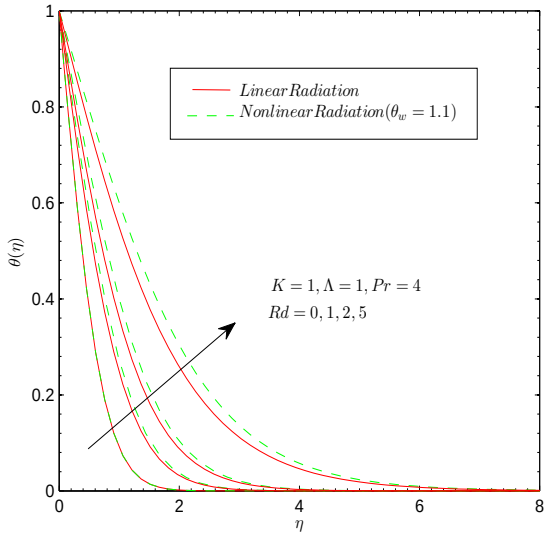

Figure 2.5: Effect of Rd on θ.

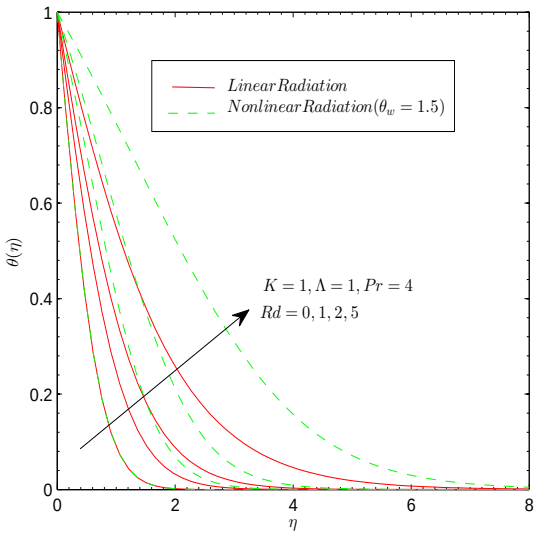

Figure 2.6: Effect of Rd on θ.

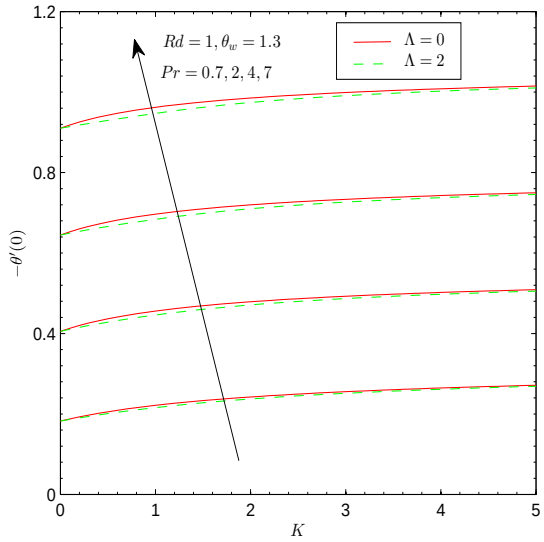

Figure 2.7: Effect of K, Λ and Pr on $-\theta'(0)$.

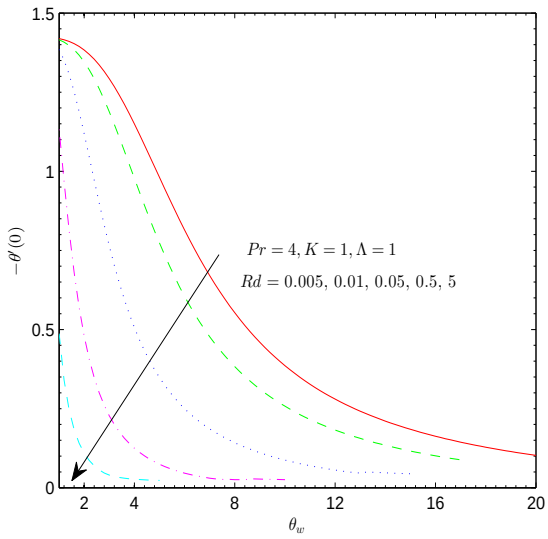

Figure 2.8: Effect of θ_w and Rd on $-\theta'(0)$.

Chapter 3

Stagnation-point flow of upper-convected Maxwell fluid using non-linear Rosseland thermal radiation

3.1 Introduction

Laminar steady two-dimensional incompressible flow of upper-convected Maxwell (UCM) fluid over a linearly stretching surface is reported in this chapter. Influence of non-linear thermal radiation. The developed nonlinear problems have been solved by shooting method using fourth-order Runge-Kutta method. An entirely different aspect of nonlinear Rosseland approximation for thermal radiation for UCM are captured. The solutions are validated with the built in solver *bvp4c* of the software $MATLAB$. Numerical results are tabulated and graphs for velocity distribution and temperature field are sketched to examine the behaviors of interesting parameters entering into the problem.

3.2 Problem Formulation

We consider the steady flow of an incompressible Maxwell fluid over a stretching sheet situated at $y = 0$. Heat transfer analysis in the presence of viscous dissipation and thermal radiation is considered. Let $U_w(x) = ax$, be the velocity of the stretching sheet while the velocity of external flow is $U_\infty(x) = bx$, where a, b are positive constants (see Fig. 3.1).

The boundary layer equations governing the steady two-dimensional stagnation-point flow

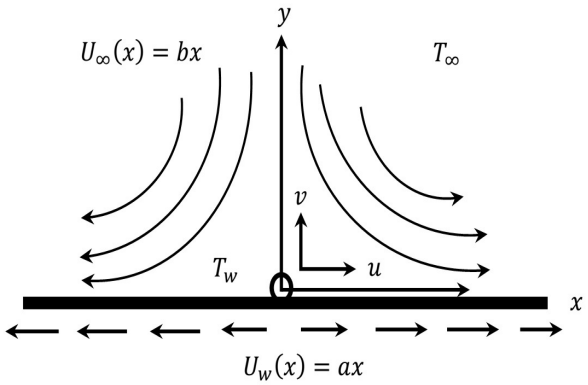

Figure 3.1: Schematic of the physical model.

of Maxwell fluid are:

$$\frac{\partial u}{\partial x} + \frac{\partial v}{\partial y} = 0, \tag{3.1}$$

$$u\frac{\partial u}{\partial x} + v\frac{\partial u}{\partial y} + \lambda_1\left(u^2\frac{\partial^2 u}{\partial x^2} + v^2\frac{\partial^2 u}{\partial y^2} + 2uv\frac{\partial^2 u}{\partial x \partial y}\right) = -\frac{1}{\rho}\frac{dp}{dx} + \nu\frac{\partial^2 u}{\partial y^2}, \tag{3.2}$$

where ν is the kinematic viscosity, λ_1 is the relaxation time, u and v are the velocity components in the $x-$ and $y-$directions respectively. The boundary conditions in the present problem are:

$$\begin{aligned} &u = U_w(x) = ax,\ v = 0, && \text{at } y = 0, \\ &u \to U_\infty(x) = bx, && \text{as } y \to \infty. \end{aligned} \tag{3.3}$$

Invoking the following similarity transformations:

$$\eta = y\sqrt{\frac{a}{\nu}},\ u = ax\frac{df}{d\eta},\ v = -\sqrt{a\nu}f. \tag{3.4}$$

Eq. (3.1) is identically satisfied and Eq. (3.2) becomes

$$\frac{d^3 f}{d\eta^3} + f\frac{d^2 f}{d\eta^2} - \left(\frac{df}{d\eta}\right)^2 + K\left(2f\frac{df}{d\eta}\frac{d^2 f}{d\eta^2} - f^2\frac{d^3 f}{d\eta^3}\right) + \lambda^2 = 0, \tag{3.5}$$

with corresponding boundary condition

$$f(0) = 0,\ f'(0) = 1,\ f'(\infty) \to \lambda, \tag{3.6}$$

where $\lambda = b/a$ is ratio of the free stream velocity to the velocity of the stretching sheet and $K = \lambda_1 a$ is the dimensionless viscoelastic parameter (Deborah number). For $K = 0$ and $\lambda = 1$, Eq. (3.5) subject to the boundary conditions (3.6) reduces to the classical problem first considered by Hiemenz.

3.3 Heat Transfer Analysis

Under usual boundary layer assumptions, the energy equation in the presence of thermal radiation and viscous dissipation effects is given by:

$$u\frac{\partial T}{\partial x}+v\frac{\partial T}{\partial y}=\alpha\frac{\partial^2 T}{\partial y^2}+\frac{\nu}{C_p}\left(\frac{\partial u}{\partial y}\right)^2-\frac{1}{\rho C_p}\left(\frac{\partial q_r}{\partial y}\right), \tag{3.7}$$

The relevant boundary conditions in this situation are:

$$T=T_w \text{ at } y=0;\ T\to T_\infty \text{ as } y\to\infty, \tag{3.8}$$

where T is the temperature, α is the thermal diffusivity, C_p is the specific heat at constant pressure and q_r is the radiative heat flux, T_w, T_∞ are the sheet temperature and the ambient fluid temperature respectively with $T_w > T_\infty$. Using the Rosseland approximation for thermal radiation [123] and applying to optically thick media, the radiative heat flux is simplified as:

$$q_r=-\frac{4\sigma^*}{3k^*}\frac{\partial T^4}{\partial y}=-\frac{16\sigma^*}{3k^*}T^3\frac{\partial T}{\partial y}, \tag{3.9}$$

where σ^* and k^* are the Stefan-Boltzman constant and the mean absorption coefficient respectively. Now (3.7) can be expressed as:

$$u\frac{\partial T}{\partial x}+v\frac{\partial T}{\partial y}=\frac{\partial}{\partial y}\left[\left(\alpha+\frac{16\sigma^*T^3}{3\rho C_p k^*}\right)\frac{\partial T}{\partial y}\right]+\frac{\nu}{C_p}\left(\frac{\partial u}{\partial y}\right)^2. \tag{3.10}$$

It is worth mentioning here that in the previous studies on thermal radiation T^4 in Eq. (3.9) was expanded about the ambient temperature T_∞. However in the present case this has been avoided to obtain more meaningful and practically useful results. Two kinds of thermal boundary conditions at the wall are considered and are treated separately in the following sections. Defining the non-dimensional temperature $\theta=(T-T_\infty)/T_w-T_\infty)$. Eq. (3.10) takes the following form

$$\frac{1}{Pr}\frac{d}{d\eta}\left[\left(1+Rd\Big(1+(\theta_w-1)\theta\Big)^3\right)\frac{d\theta}{d\eta}\right]+f\frac{d\theta}{d\eta}+Ec\left(\frac{d^2f}{d\eta^2}\right)^2=0, \tag{3.11}$$

with the following boundary conditions

$$\theta(0)=1,\ \theta(\infty)\to 0, \tag{3.12}$$

where $Pr=\nu/\alpha$ is the Prandtl number, $Ec=U_w^2/C_p(T_w-T_\infty)$ is the Eckert number and $Rd=16\sigma^*T_\infty^3/3kk^*$ is the radiation parameter. We notice that $x-$ coordinate could not be eliminated from the energy equation. Thus we look for the availability of local

similarity solutions.

The heat transfer rate at the sheet in this case can be calculated using the local Nusselt number Nu_x defined as

$$Nu_x = \frac{xq_w}{k(T_w - T_\infty)};\ q_w = -k\left(\frac{\partial T}{\partial y}\right)_{y=0} + (q_r)_{y=0}, \tag{3.13}$$

where q_w is the wall heat flux. Now using dimensionless quantities we get

$$Re_x^{-1/2} Nu_x = -\Big[1 + Rd\theta_w^3\Big]\theta'(0) = Nur. \tag{3.14}$$

where $Re_x = U_w x/\nu$ is the local Reynolds number.

3.4 Numerical Method

The solutions of dimensionless ordinary differential equations (3.5 and 3.11) with the boundary conditions (3.12 and 3.6) have been obtained numerically using fourth-fifth order Runge-Kutta method based shooting technique. For this purpose the boundary value problem (BVP) (3.5) and (3.11) is transformed to initial value problem (IVP). Before employing the Runge-Kutta integration scheme, first we reduce the governing differential equations into a set of first order ODEs. Let $x_1 = \eta, x_2 = f, x_3 = f', x_4 = f'', x_5 = \theta, x_6 = \theta'$. We obtain the following system:

$$\begin{pmatrix} x_1' \\ x_2' \\ x_3' \\ x_4' \\ x_5' \\ x_6' \end{pmatrix} = \begin{pmatrix} 1 \\ x_3 \\ x_4 \\ \frac{x_3^2 - (1+2Kx_3)x_2x_4 - \lambda^2}{1+Kx_2^2} \\ x_6 \\ \frac{-Pr\left(x_2x_6 + Ec^* x_4^2\right) - 3Rdx_6^2(\theta_w - 1)\left(1+(\theta_w-1)x_5\right)^2}{1+Rd\left(1+(\theta_w-1)x_5\right)^3} \end{pmatrix}. \tag{3.15}$$

and the corresponding initial conditions:

$$\begin{pmatrix} x_1 \\ x_2 \\ x_3 \\ x_4 \\ x_5 \\ x_6 \end{pmatrix} = \begin{pmatrix} 0 \\ 0 \\ 1 \\ u_1 \\ 1 \\ u_2 \end{pmatrix}. \tag{3.16}$$

The above nonlinear coupled ODEs along with initial conditions are solved using fourth-fifth order Runge-Kutta integration technique.

3.5 Numerical Results and Discussion

The physical interpretation to the graphical and numerical results has been presented in this section. The effects of viscoelastic parameter (Deborah number) K and velocity ratio λ on velocity profiles can be easily examined from Fig. 3.2. The Deborah number can be defined as the ratio of the relaxation time characterizing the time it takes for the fluid to adjust to applied stresses or deformations and the fluid's characteristic time. It incorporates both the elasticity and viscosity of the fluid. Here the present work can be reduced to the case of Newtonian fluid by choosing $K = 0$. An increase in the values of K corresponds to a reduction in the velocity and the boundary layer thickness. Here the viscoelasticity produces tensile stress which opposes the fluid motion and as a consequence the horizontal velocity decreases. The decrease in the momentum boundary layer thickness with an increase in K induces an increase in the absolute value of the velocity gradient at the surface. It is also noticed that increase in K leads to an enhancement of the thermal boundary layer. The value of the temperature gradient at the surface increases with an increase in K as shown in Tables 3.2 and 3.3. In other words the heat transfer rate at the bounding surface increases when the viscoelastic effects strengthen. It is noticed that velocity ratio λ has a dual behavior on the momentum boundary layer. It is clear that velocity profiles move closer to the bounding surface, that is $\eta = 0$, with an increase in λ when $\lambda > 1$. Here the sheet velocity $U_w(x)$ is less than the velocity of external stream $U_\infty(x)$. The straining motion near the stagnation region increases which give rise to the acceleration of the external stream. This causes a significant reduction in the boundary layer thickness and consequently the horizontal velocity increases. On the other hand, when $\lambda < 1$, the flow has an inverted boundary layer structure. Here the sheet velocity $U_w(x)$ is greater than the velocity of external stream $U_\infty(x)$. Moreover the boundary layer is not formed for $\lambda = 1$.

Figure 3.3 shows the behavior of radiation parameter Rd on the temperature θ. Here unlike previously reported works on the topic, the temperature function in the term representing thermal radiation effect is not further expanded in Taylor's series about the ambient temperature. In contrast with the linearized Rosseland approximation consid-

ered by Magyari and Pantokratoras [108] the radiation parameter in the present case has a strong influence on the thermal boundary layer as can be seen from Fig. 3.3. As expected the temperature and the thermal boundary layer thickness are increasing functions of Rd. Further the heat transfer rate at the sheet drastically increases with an increase in Rd in the present case when compared with Magyari and Pantokratoras [108].

The Prandtl number is defined as the ratio of momentum diffusivity to the thermal diffusivity. Thus it can be used to increase the rate of cooling in conducting flows. Temperature profiles for different values of Pr have been shown in the Fig. 3.4. It is pertinent to mention that the liquids are characterized by small values of $Pr(\ll 1)$, which have high thermal conductivity but low viscosity, while large values of $Pr(\gg 1)$ represent the high-viscosity oils. Specifically, Prandtl number $Pr = 0.72, 1.0$ and 7.0 correspond to air, electrolyte solution such as salt water and water, respectively. Fig. 3.4 indicates that profiles move closer to the boundary as Pr increases indicating a diminution in the thickness of thermal boundary layer. Physically this is attributed to the fact that increasing values of Pr decrease the thermal diffusivity of the fluid which in turn corresponds to a thinner thermal boundary layer. In this work the variation in the temperature θ with an increase in Pr is larger than that studied by Magyari and Pantokratoras [108] for the linearized Rosseland approximation.

Figure 3.5 captures the influence of Eckert number or equivalently viscous dissipation on the temperature. It is quite obvious that in a viscous fluid flow the viscosity of the fluid will take kinetic energy from the motion of the fluid and transform it into internal energy of the fluid that heats up the fluid. This process is partially irreversible and is referred to as viscous dissipation. It is worth stating here that viscous dissipation effect (the generation of heat due to friction caused by shear in the flow) is prominent when the fluid is largely viscous or flowing at a high speed. The results are shown for $Rd = 0$ and $Rd = 1$. We observed that temperature and the thermal boundary layer thickness are increasing functions of Eckert number and this observation is true with and without thermal radiation effects.

Table 3.1 shows the comparison of present solutions for $f''(0)$ and $\theta'(0)$ with those reported by Mahapatra and Gupta [7]. The results are in very good agreement for all the considered values of λ. The numerical values of local Nusselt number are given for various parametric values in Table 3.2. Irrespective of velocity ratio λ we observe a significant increase in the local Nusselt number as the thermal radiation effect strengthens. We noticed earlier in the graphical results that temperature profiles become increasingly steeper

as Pr increases. As a result the Nusselt number, being proportional to the initial slope, increases with an increase in Pr.

3.6 Concluding Remarks

Thermal radiation effect on the boundary layer flow of an upper-convected Maxwell (UCM) fluid over a stretching sheet is studied. In this chapter the temperature function in the radiation term of energy equation is not further expanded about the ambient temperature. This gives us confidence that present results are more practically useful and meaningful in comparison to the previously reported studies on the topic. The major points of this chapter can be summarized as follows:

a. The velocity ratio λ has a dual behavior on the momentum boundary layer i.e increase in K assists the velocity for $\lambda > 1$ while the velocity field decreases when K is increased in the case $\lambda < 1$. Moreover the boundary layer does not exist and $f''(0) = 0$ when $\lambda = 1$.

b. The magnitude of temperature gradient is an increasing function of both λ and Pr. Further the deviation in the temperature profiles is more pronounced for smaller values of Ec when compared with its larger values.

c. Irrespective of the velocity ratio λ, $|\theta'(0)|$ decreases with an increase in K. This result is similar in the presence and absence of thermal radiation effects.

d. In the present analysis, the temperature profiles show huge deviation when the radiation effects strengthen which is different from the previously reported studies.

e. The current analysis for the case of viscous fluid can be recovered by choosing $K = 0$.

Table 3.1: Comparison of values of $f''(0)$ and $\theta'(0)$ with those of Mahapatra and Gupta [7] at different values of η_∞.

λ	Mahapatra & Gupta [7]		Present Solution					
			$\eta_\infty = 10$		$\eta_\infty = 50$		$\eta_\infty = 100$	
	$f''(0)$	$-\theta'(0)$	$f''(0)$	$-\theta'(0)$	$f''(0)$	$-\theta'(0)$	$f''(0)$	$-\theta'(0)$
0.1	-0.9694	0.081	-0.9694	0.1264	-0.9694	0.0812	-0.9694	0.0812
0.2	-0.9181	0.099	-0.9181	0.1320	-0.9181	0.0990	-0.9181	0.0990
0.5	-0.6673	0.136	-0.6673	0.1507	-0.6673	0.1356	-0.6673	0.1356
2.0	2.0176	0.241	2.0175	0.2415	2.0175	0.2410	2.0175	0.2410
3.0	4.7296	0.289	4.7293	0.2901	4.7293	0.2901	4.7293	0.2900

Table 3.2: The heat transfer rate at the wall $\theta'(0)$ for various parametric values.

λ	θ_w	Pr	K	Ec	Rd	$-\theta'(0)$	
						bvp4c	Shooting
0.1	1	7	0.2	0.2	1	1.02719	1.02718
					0	1.45281	1.45278
				0.5	1	0.65858	0.65857
					0	0.79582	0.79579
			0.5	0.2	1	0.97234	0.97234
					0	1.37093	1.37092
				0.5	1	0.55359	0.55358
					0	0.62211	0.62209
	2	0.72	0.1	0.2	1	0.08621	0.08621
					0	0.42219	0.42219
				0.5	1	0.07548	0.07548
					0	0.33499	0.33499
0.3	2	7	0.1	0.2	1	0.42027	0.42027
					0	1.63361	1.63361
0.8	2	7		0.5	1	0.52539	0.52539
					0	2.02325	2.02324

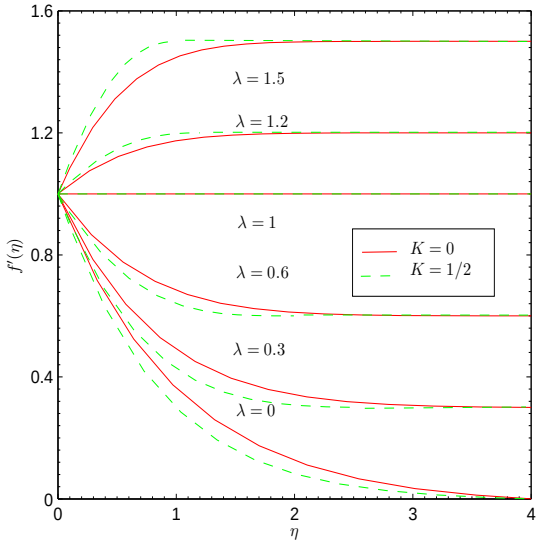

Figure 3.2: Effect of K and λ on $f'(\eta)$.

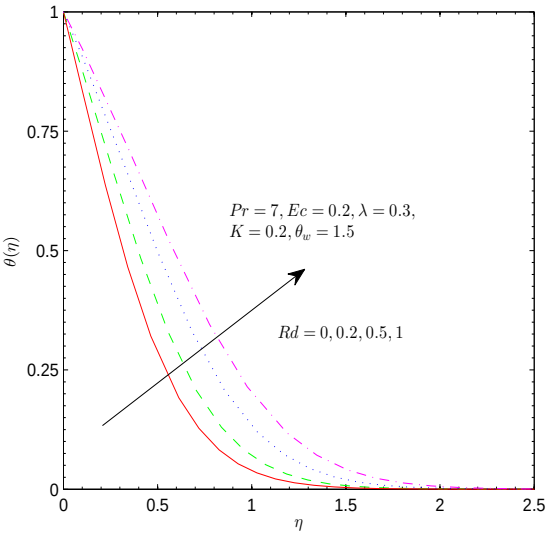

Figure 3.3: Effect of Rd on θ.

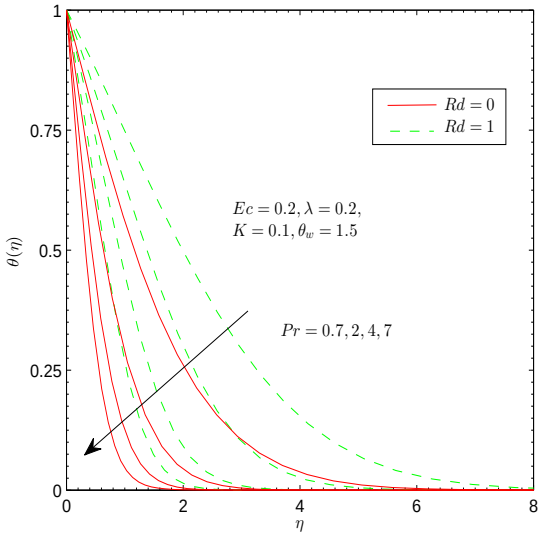

Figure 3.4: Effect of Pr on θ.

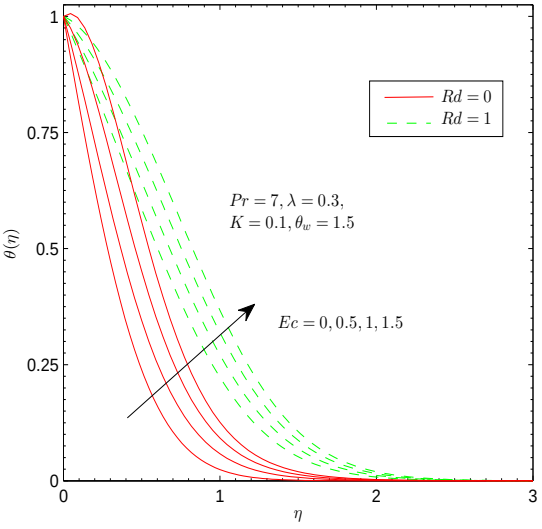

Figure 3.5: Effect of Ec on θ.

Chapter 4

Non-linear radiative heat flux in the flow of power-law fluid

4.1 Introduction

Non-linear radiation heat transfer problem is investigated for the stagnation-point flow of non-Newtonian fluid obeying the power-law model. Power-law fluids of both shear-thinning (pseudoplastic) and shear-thickening (dilatant) nature have been considered. Boundary layer equations are non-dimensionalized and then solved for the numerical solutions by fifth order Runge-Kutta method integration based shooting technique. It is seen that wall temperature gradient approaches the zero value with an increase in wall to ambient temperature ratio. The numerical values of skin friction coefficient and wall heat flux are computed and discussed. Different from the linear radiation heat transfer problem (which can be simply reduced to rescaling of Prandtl number by a factor containing the radiation parameter), here the energy equation is strongly non-linear and it involves an additional temperature ratio parameter $\theta_w = T_w/T_\infty$. This parameter allows studying the thermal characteristics for small/large temperature differences in the flow. The results also reveal an existence of point of inflection for the temperature distribution for sufficiently large wall to ambient temperature ratio. Moreover temperature increases and heat transfer from the plate decreases with an increase in the radiation parameter. Heat transfer rate at the sheet is bigger in dilatant (shear-thickening) fluids when compared with the pseudoplastic (shear-thinning-fluid).

4.2 Problem Formulation

Consider a two-dimensional incompressible flow of an electrically conducting power-law fluid near a stagnation-point towards an isothermal elastic stretching sheet along the horizontal direction. The sheet is maintained at constant temperature T_w while T_∞ is the ambient fluid's temperature. The sheet is linearly stretched in its own plane with the velocity $U_w(x) = ax$, and velocity of the external flow is $U_\infty(x) = bx$, where $a, b > 0$ are constants. The flow is under the influence of uniform transverse magnetic field of strength B_0 and induced magnetic field is neglected on the basis of small magnetic Reynold's number. In the present problem when $b/a > 1$, the free stream velocity is greater than the stretching sheet velocity and hence $\partial u/\partial y > 0$. On the other hand, when $b/a < 1$, the flow has inverted boundary layer structure. In this case the velocity of the sheet exceeds the velocity of external stream. Thus $\partial u/\partial y < 0$ and $b/a < 1$, as indicated by Mahapatra et al. [15]. The boundary layer equations governing the flow of power-law fluid and heat transfer in presence of thermal radiation are expressed as (see Mahapatra et al. [15]):

$$\frac{\partial u}{\partial x} + \frac{\partial v}{\partial y} = 0, \tag{4.1}$$

$$u\frac{\partial u}{\partial x} + v\frac{\partial u}{\partial y} = -\frac{1}{\rho}\frac{dp}{dx} + \frac{K}{\rho}\frac{\partial}{\partial y}\left(\frac{\partial u}{\partial y}\right)^n - \frac{\sigma B_0^2}{\rho}u, \tag{4.2}$$

$$u\frac{\partial T}{\partial x} + v\frac{\partial T}{\partial y} = \alpha\frac{\partial^2 T}{\partial y^2} - \frac{1}{\rho C_p}\left(\frac{\partial q_r}{\partial y}\right). \tag{4.3}$$

The boundary conditions in the present problem are as below:

$$\begin{aligned} &u = U_w(x) = ax,\ v = 0,\ T = T_w && \text{at } y = 0, \\ &u \to U_\infty(x) = bx,\ v \to -by,\ T \to T_\infty && \text{as } y \to \infty. \end{aligned} \tag{4.4}$$

In the above equations, u and v are the velocity components along the $x-$ and $y-$ directions, ρ is the fluid's density, p is the static pressure, K is the consistency index and n is the flow behavior index, σ is the conductance of the fluid, T is the temperature, α is the thermal diffusivity, C_p is the specific heat at constant pressure and q_r is the radiative heat flux. Using Rosseland formula for the raidative heat flux

$$q_r = -\frac{4\sigma^*}{3k^*}\frac{\partial T^4}{\partial y} = -\frac{16\sigma^*}{3k^*}T^3\frac{\partial T}{\partial y}, \tag{4.5}$$

where σ^* and k^* are the Stefan-Boltzman constant and the mean absorption coefficient respectively. A huge simplification of Rosseland heat flux is possible if T^4 in Eq. (4.5) is expanded about the ambient temperature T_∞ and then higher order terms are neglected

(through the assumption of small temperature differences within the flow), as done by many authors previously [86-107]. This means to simply replace T^3 in Eq. (4.5) with T_∞^3. Now Eq. (4.3) can be written as

$$u\frac{\partial T}{\partial x}+v\frac{\partial T}{\partial y}=\left(\alpha+\frac{16\sigma^* T_\infty^3}{3\rho C_p k^*}\right)\frac{\partial^2 T}{\partial y^2}. \tag{4.6}$$

However if we utilize the complete expression of Rosseland heat flux, Eq. (4.3) results in a highly non-linear partial differential equation given below:

$$u\frac{\partial T}{\partial x}+v\frac{\partial T}{\partial y}=\frac{\partial}{\partial y}\left[\left(\alpha+\frac{16\sigma^* T^3}{3\rho C_p k^*}\right)\frac{\partial T}{\partial y}\right]. \tag{4.7}$$

Introducing the following dimensionless variables

$$\begin{aligned}&\psi=\left(\frac{K/\rho}{a^{1-2n}}\right)^{\frac{1}{n+1}}x^{\frac{2n}{n+1}}f,\ \eta=y\left(\frac{a^{2-n}}{K/\rho}\right)^{\frac{1}{n+1}}x^{\frac{1-n}{n+1}},\\&u=\frac{\partial\psi}{\partial y},\ v=-\frac{\partial\psi}{\partial x},\ \theta=\frac{T-T_\infty}{T_w-T_\infty}.\end{aligned} \tag{4.8}$$

Eq. (4.1) is identically satisfied and Eqs. (4.2), (4.6) and (4.7) with the boundary conditions (4.4) reduce to:

$$n\left[sgn(\lambda-1)\frac{d^2f}{d\eta^2}\right]^{n-1}\frac{d^3f}{d\eta^3}+\left(\frac{2n}{n+1}\right)f\frac{d^2f}{d\eta^2}-\left(\frac{df}{d\eta}\right)^2+M\left(\lambda-\frac{df}{d\eta}\right)+\lambda^2=0, \tag{4.9}$$

$$\left(\frac{1+Rd}{Pr}\right)\frac{d^2\theta}{d\eta^2}+\left(\frac{2n}{n+1}\right)f\frac{d\theta}{d\eta}=0, \tag{4.10}$$

$$\frac{1}{Pr}\frac{d}{d\eta}\left[\left(1+Rd\Big(1+(\theta_w-1)\theta\Big)^3\right)\frac{d\theta}{d\eta}\right]+\left(\frac{2n}{n+1}\right)f\frac{d\theta}{d\eta}=0, \tag{4.11}$$

with the corresponding boundary conditions

$$\begin{aligned}&f(0)=0, f'(0)=1, \theta(0)=1,\\&f'(\infty)\to\lambda, \theta(\infty)\to 0,\end{aligned} \tag{4.12}$$

where $sgn(.)$ stand for signum function, $Pr=(K/\rho)^{\left(\frac{2}{n+1}\right)}x^{-2\left(\frac{1-n}{n+1}\right)}/\alpha a^{3\left(\frac{1-n}{n+1}\right)}$ is the Prandtl number, $\lambda=b/a$ is ratio of the free stream velocity to the velocity of the stretching sheet, $M=\sigma B_0^2/\rho a$ is the and magnetic field parameter, $\theta_w=T_w/T_\infty$ is the temperature ratio parameter, and $Rd=16\sigma^* T_\infty^3/3kk^*$ is the radiation parameter.

It is important to note that since $x-$coordinate could not be eliminated from the momentum equation therefore the local similarity solutions of above equations are possible which give the behaviors of parameters at a fixed location above the boundary. Physical

quantities of interest are the skin friction coefficient and local Nusselt number are defined in [15]. These can be expressed in the dimensionless form as:

$$\begin{aligned} &\frac{1}{2}Re_x^{1/1+n}C_f = \Big[sgn(\lambda-1)f''(0)\Big]^n, \\ &Re_x^{-1/n+1}Nu_x = -\Big[1+Rd\theta_w^3\Big]\theta'(0) = Nur, \end{aligned} \tag{4.13}$$

where $Re_x = (U_w)^{2-n}x^n/(K/\rho)$ is the local Reynolds number.

4.3 Numerical Method

The solutions of dimensionless ordinary differential equations (4.9-4.11) with the boundary conditions (4.12) have been obtained numerically using fourth-fifth order Runge-Kutta method based shooting technique. For this purpose the boundary value problem (BVP) (4.9)-(4.12) is transformed to initial value problem (IVP). Let $x_1 = \eta, x_2 = f, x_3 = f', x_4 = f'', x_5 = \theta, x_6 = \theta'$. We obtain the following system:

$$\begin{pmatrix} x_1' \\ x_2' \\ x_3' \\ x_4' \\ x_5' \\ x_6' \end{pmatrix} = \begin{pmatrix} 1 \\ x_3 \\ x_4 \\ \frac{x_3^2-\left(\frac{2n}{n+1}\right)x_2x_4+Mx_3-M\lambda-\lambda^2}{n[sgn(\lambda-1)x_4]^{n-1}} \\ x_6 \\ \frac{-\left(\frac{2n}{n+1}\right)Prx_2x_6-3Rdx_6^2(\theta_w-1)\Big(1+(\theta_w-1)x_5\Big)^2}{1+Rd\Big(1+(\theta_w-1)x_5\Big)^3} \end{pmatrix}, \tag{4.14}$$

and the corresponding initial conditions are:

$$\begin{pmatrix} x_1 \\ x_2 \\ x_3 \\ x_4 \\ x_5 \\ x_6 \end{pmatrix} = \begin{pmatrix} 0 \\ 0 \\ 1 \\ u_1 \\ 1 \\ u_2 \end{pmatrix}. \tag{4.15}$$

The above nonlinear coupled ODEs along with initial conditions are solved using fourth-fifth order Runge-Kutta integration technique.

4.4 Numerical Results and Discussion

In order to test the accuracy of the numerical method, the results of $-f''(0)$ and $-\theta'(0)$ are compared with those obtained by Mahapatra et al. [15] in Table 2.1 for the case of linear thermal radiation (Eq. (4.10)). The results are found in excellent agreement with for various values of n and λ. As expected, the velocity gradient $f''(0)$ is negative for $\lambda < 1$ and positive when $\lambda > 1$. It is also found that variation in $f''(0)$ with n is non-monotonic when the velocity ratio λ largely differs from 1, a fact that is already demonstrated in Mahapatra et al. [15].

To gain physical insight on the behavior of parameters entering in the solution, we have shown the plots of velocity, temperature, skin friction coefficient and Nusselt number (see Figs. 4.1-4.10). Fig. 4.1 shows the effects of magnetic field on the horizontal component of velocity with the variation in velocity ratio λ. The flow has an inverted boundary layer structure when velocity of the stretching sheet is greater than the free stream velocity i.e. $\lambda < 1$. Further boundary layer is not formed when $\lambda = 1$. With a gradual increase in M, the Lorentz force associated with the magnetic field increases and it produces more resistance to the transport phenomena. Due to this reason the boundary layer thickness is a decreasing function of M. Fig. 4.1 is complimenting this behavior since profiles smoothly approach the free stream condition at shorter distance from the sheet when M is increased. Fig. 4.2 illustrates the effect of power law index n on the velocity field $f'(\eta)$ for both the cases $\lambda > 1$ and $\lambda < 1$. It is clear from this figure that when $\lambda < 1$, the velocity at a point in the neighborhood of the stretching sheet increases with increase in n and when $\lambda > 1$ and an opposite trend is depicted for $\lambda < 1$. In both the cases, the boundary layer thickness decreases with an increase in n. Fig. 4.3 captures the behavior of power-law index n on the horizontal component of velocity f'. f' is an increasing function of n. However, the variation in f' with n is found to be non-monotonic just close to the stretching wall. It can be further noted that profiles approach the free stream condition λ faster when n is increased. This shows a reduction in the momentum boundary layer thickness. Skin friction coefficient $f''(0)$ versus the magnetic field parameter M is plotted for different values of λ in Fig. 4.4. It is clear that results complement the observations made from Table 4.1 and from Figs. 4.1, 4.2 and 4.3.

Fig. 4.5 indicates that thermal boundary layer thins and profiles become steeper, when n is increased. This leads to the conclusion that wall heat transfer rate is greater in dilatant fluids than in pseudo plastic fluid. The variation in temperature function θ with the

Prandtl number Pr is seen in Fig. 4.6. Increasing values of Pr corresponds to a decrease in thermal diffusion and shorter penetration depth for thermal boundary layer. Fig. 4.6 demonstrates that fluid's temperature decreases and profiles tend to merge at small distances from the sheet as Pr increases indicating a diminution in thermal boundary layer thickness. This variation is of similar magnitude for any considered value of n. It is also observed that profiles become increasingly steeper with an augmentation in Pr revealing an increase in wall slope of temperature function $\theta'(0)$. Fig. 4.7 shows that increasing values of θ_w corresponds to an increase in wall temperature (T_w) which eventually rises the fluid's temperature. As depicted by Pantokratoras and Fang [110] the profiles become broader and change from normal shape to the S-shaped thicker profiles when θ_w is gradually increased revealing that wall temperature gradient tends to zero value with an increment in wall to ambient temperature ratio. It is worth mentioning here that when $\theta_w \approx 1$, the corresponding profiles represent the case of linearized radiative heat flux, a fact that is evident from Eq. (4.11). Interestingly the variations are significant in the case $\lambda = 0.2$ when compared with $\lambda = 1.5$. In Fig. 4.8 we have presented the influence of radiation parameter Rd on the temperature θ for both linear and non-linear radiative heat flux cases. It is found that rise in temperature function with the variation in Rd becomes significant in case of large wall to ambient temperature ratio. When $\theta_w = 2$, thermal boundary layer thins and profiles change to S-shape when Rd tends to zero value. Fig. 4.9 shows the variation of wall temperature gradient versus M with the variations in λ and Pr. The wall temperature gradient increases with increasing the Prandtl number (as described earlier in Fig. 4.6) for any considered value of λ. On the other hand $|\theta'(0)|$ is an increasing function of M when $\lambda > 1$ and a decreasing function of M when $\lambda < 1$. Fig. 4.10 displays the interesting plots of $\theta'(0)$ against θ_w with the variation in radiation parameter Rd. As noted earlier in Fig. 4.7, the profiles of $\theta'(0)$ reach the zero value as θ_w is gradually increased. Further when θ_w is close to one, the wall heat flux approaches to a constant finite value as Rd tends to zero. Notably, this outcome is not true in case of non-linear radiation heat transfer case ($\theta_w \gg 1$).

4.5 Conclusions

The problem of non-linear radiation heat transfer for MHD stagnation-point flow of an electrically conducting power-law fluid is investigated. The inclusion of non-linear radiation term in the energy equation led to strongly non-linear but interesting differential

equations. Unlike the linear radiation heat transfer problem, which simply reduces to the re-scaling of Prandtl number by a factor involving the radiation parameter, the present problem is governed by an additional temperature ratio parameter. The velocity and temperature distributions are computed through shooting method. Following are the important observations of current analysis.

a. Velocity in the horizontal direction increases/decreases with an increase in magnetic field strength when the ratio of free stream velocity to the stretching sheet velocity (λ) is greater/less than one.

b. The variation in velocity distribution with power-law index (n) is non-monotonic when λ largely differs from one.

c. Wall heat transfer rate decreases with an increase in wall to ambient temperature ratio (θ_w). Moreover, it approaches to zero value for sufficiently large θ_w. A significant variation in temperature function is accounted in the case $\lambda < 1$ when compared with $\lambda > 1$.

d. Temperature is an increasing function of radiation parameter while it decreases when Prandtl number is increased.

e. Unlike previously reported results on thermal radiations effect, current results are valid for both small as well as large temperature differences between plate and environment.

Table 4.1: Comparison of results for $-f''(0)$ and $-\theta'(0)$ with Mahapatra et al. [15] when $Pr = 2.0$,$Nr = 1.0 = 3/4Rd$ and $M = 0.5$ for linearized radiation case.

λ	n	$-f''(0)$			$-\theta'(0)$		
		Ref	Present		Ref	Present	
		[15]	Shooting	bvp4c	[15]	Shooting	bvp4c
0.2	0.4	1.5176	1.5179	1.5179	0.3919	0.3920	0.3920
	0.6	1.2506	1.2506	1.2506	0.4659	0.4660	0.4660
	0.8	1.1356	1.1356	1.1356	0.5156	0.5151	0.5151
	1.0	1.0768	1.0768	1.0768	0.5504	0.5498	0.5498
2.0	0.4	-4.1322	-4.1322	-4.1322	0.7347	0.7247	0.7247
	0.6	-2.9827	-2.9827	-2.9827	0.8128	0.8128	0.8128
	0.8	-2.4445	-2.4445	-2.4445	0.8722	0.8721	0.8721
	1.0	-2.1363	-2.1363	-2.1363	0.9155	0.9155	0.9155

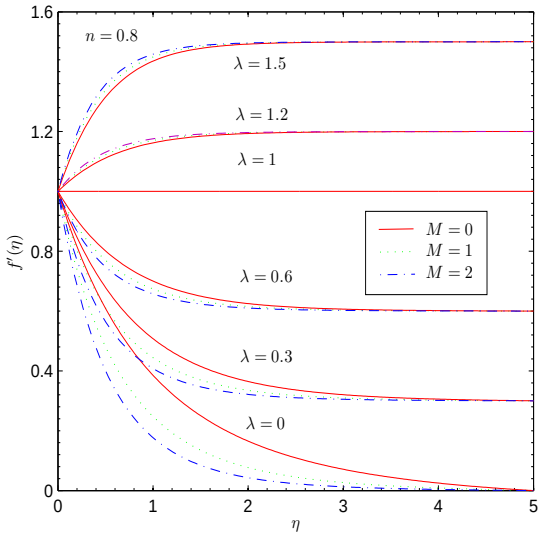

Figure 4.1: Effect of M and λ on f'.

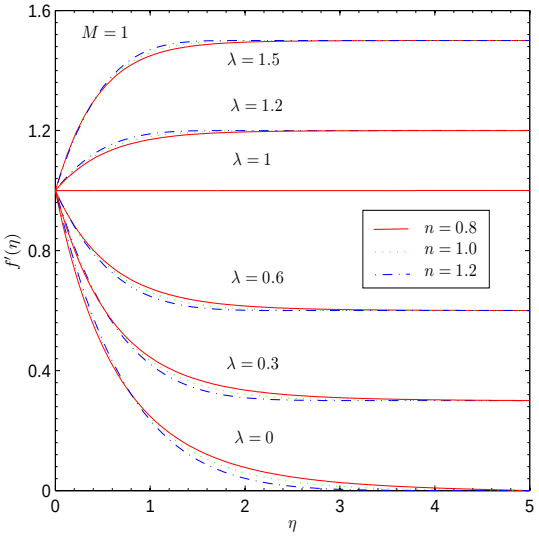

Figure 4.2: Effect of n and λ on f'.

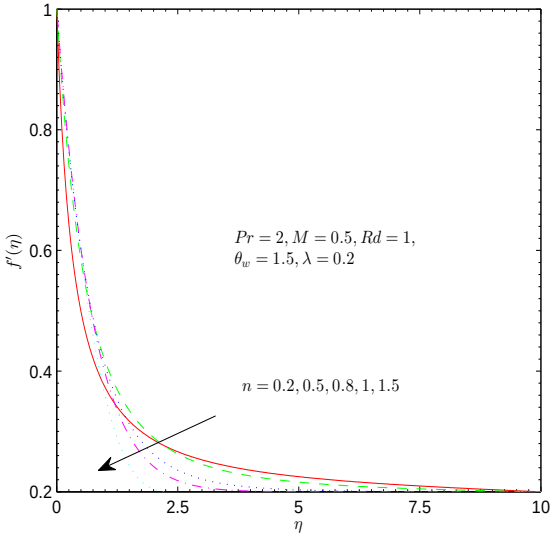

Figure 4.3: Effect of n on f'.

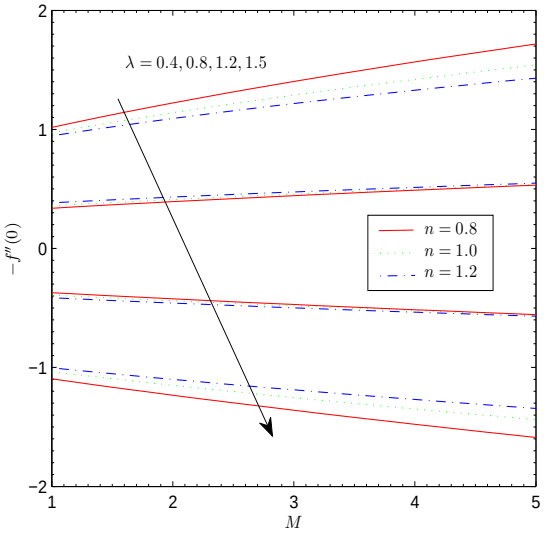

Figure 4.4: Effect of M, n and λ on $-f''(0)$.

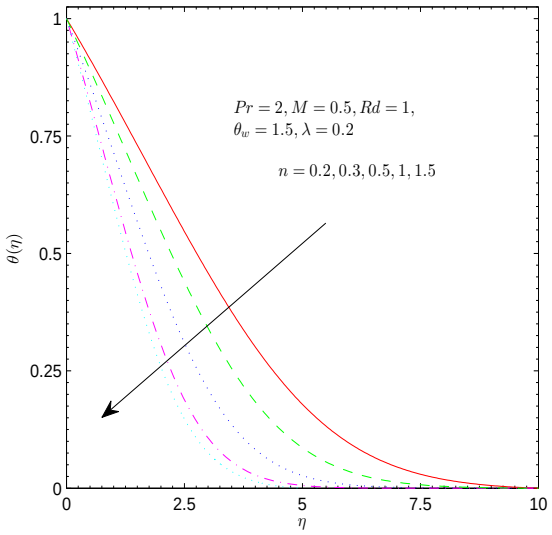

Figure 4.5: Effect of n on θ.

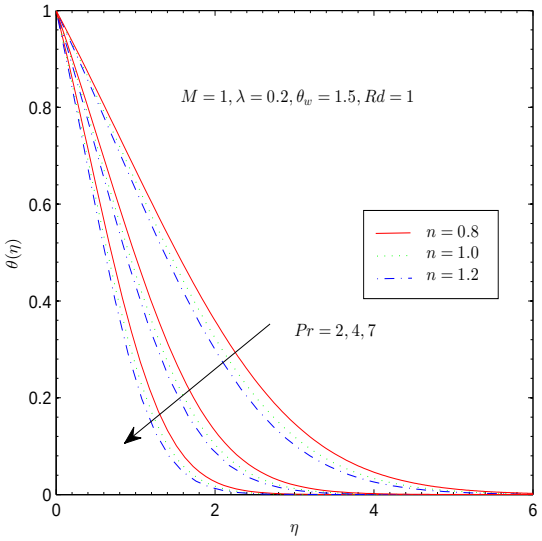

Figure 4.6: Effect of n and Pr on θ.

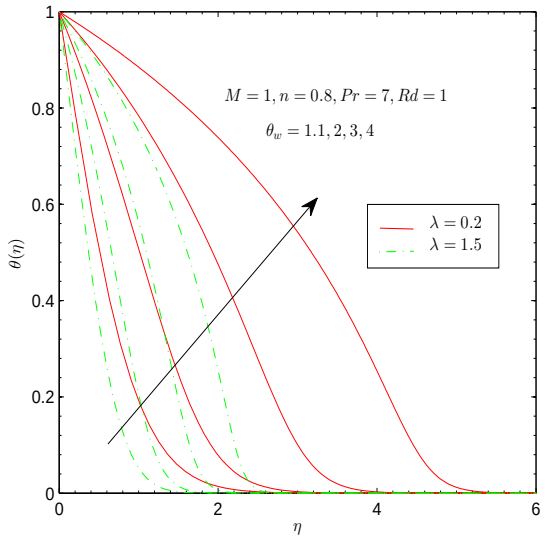

Figure 4.7: Effect of θ_w and λ on θ.

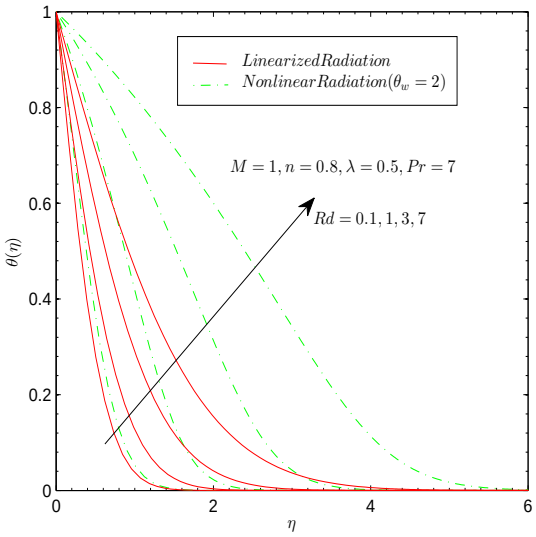

Figure 4.8: Effect Rd on θ.

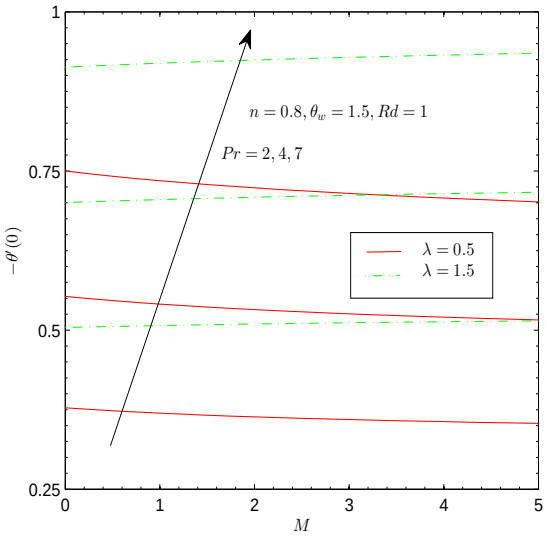

Figure 4.9: Effect of Pr, λ, M on $-\theta'(0)$.

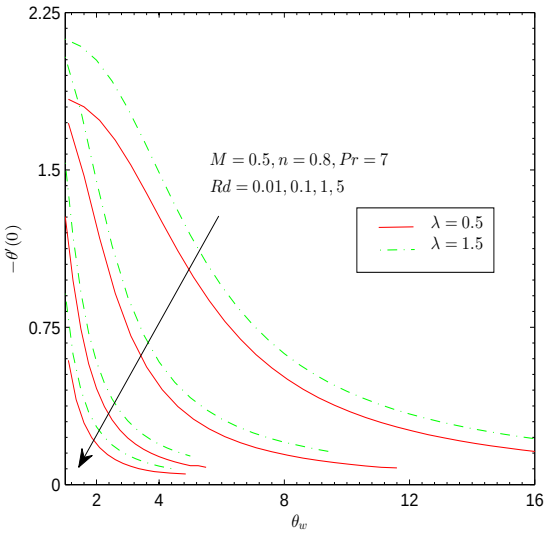

Figure 4.10: Effect of θ_w, λ, Rd on $-\theta'(0)$.

Chapter 5

Non-linear thermal radiation in natural convection flow of nanofluid adjacent to vertical plate

5.1 Introduction

The problem of natural convective boundary layer flow of nanofluid past a vertical plate is discussed in the presence of nonlinear radiative heat flux. The effects of magnetic field, Joule heating and viscous dissipation are also taken into consideration. The governing partial differential equations are transformed into a system of coupled nonlinear ordinary differential equations via similarity transformations and then solved numerically using the Runge–Kutta fifth order method with shooting technique. The results reveal an existence of point of inflection for the temperature distribution for sufficiently large wall to ambient temperature ratio. Temperature and thermal boundary layer thickness increase as Brownian motion and thermophoretic effects intensify. Moreover temperature increases and heat transfer from the plate decreases with an increase in the radiation parameter.

5.2 Problem Formulation

We consider laminar two-dimensional boundary layer flow of nanofluid past a vertical plate located at $y = 0$. The magnetic field of strength $B(x) = B_0 x^{-1/4}$ is applied in the $y-$ direction whereas the induced magnetic field is neglected subject to the assumption of small magnetic Reynolds number. Heat transfer analysis is carried out in the presence

of nonlinear thermal radiation, Joule heating and viscous dissipation effects. The plate is maintained at constant temperature T_w whereas T_∞ denotes the ambient fluid's temperature (see Fig. 5.1).

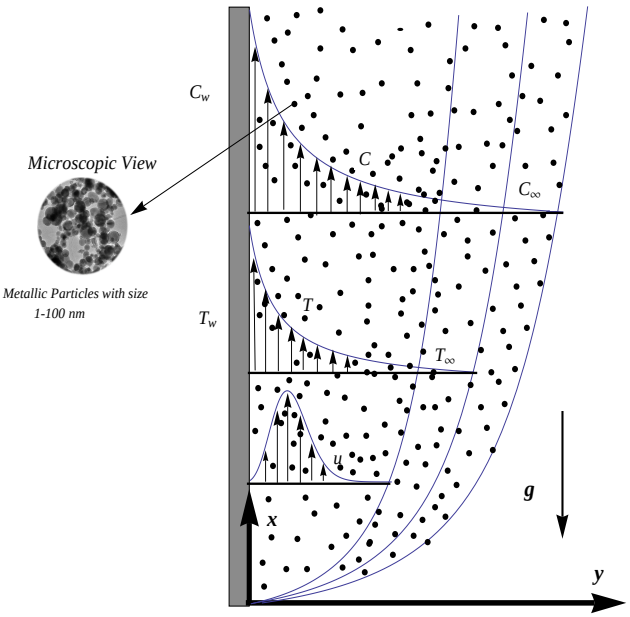

Figure 5.1: Sketch of the problem and coordinate system.

Using the standard boundary layer assumptions and the Oberbeck-Boussinesq approximation we obtain the following boundary layer equations governing the steady incompressible flow of nanofluid (see Nield and Kuznetsov [54] and Kuznetsov and Nield [55])

$$\frac{\partial u}{\partial x}+\frac{\partial v}{\partial y}=0, \tag{5.1}$$

$$u\frac{\partial u}{\partial x}+v\frac{\partial u}{\partial y}=\nu_f\frac{\partial^2 u}{\partial y^2}-\frac{\sigma B^2}{\rho_f}u+\frac{g}{\rho_f}\left[(1-C_\infty)\,\rho_f\beta\,(T-T_\infty)-(\rho_p-\rho_f)\,(C-C_\infty)\right], \tag{5.2}$$

$$\begin{aligned} u\frac{\partial T}{\partial x}+v\frac{\partial T}{\partial y}=&\alpha_f\frac{\partial^2 T}{\partial y^2}-\frac{1}{(\rho C_p)_f}\left(\frac{\partial q_r}{\partial y}\right)+\frac{\nu_f}{(C_p)_f}\left(\frac{\partial u}{\partial y}\right)^2+\frac{\sigma B^2}{(\rho C_p)_f}u^2\\ &+\tau\left[D_B\left(\frac{\partial C}{\partial y}\frac{\partial T}{\partial y}\right)+\frac{D_T}{T_\infty}\left(\frac{\partial T}{\partial y}\right)^2\right], \end{aligned} \tag{5.3}$$

$$u\frac{\partial C}{\partial x}+v\frac{\partial C}{\partial y}=D_B\frac{\partial^2 C}{\partial y^2}+\frac{D_T}{T_\infty}\frac{\partial^2 T}{\partial y^2}. \tag{5.4}$$

The boundary conditions in the present problem are as below:

$$\begin{aligned} &u=0,\ v=0,\ T=T_w,\ C=C_w && \text{at } y=0,\\ &u\to 0,\ T\to T_\infty,\ C\to C_\infty && \text{as } y\to\infty. \end{aligned} \tag{5.5}$$

In the above equations, u and v are the velocity components along the $x-$ and $y-$ directions, ρ_f and ρ_p are the densities of base fluid and nanoparticles material respectively, σ is the conductance of the fluid, T is the local temperature, β is volumetric thermal expansion coefficient of base fluid, $\tau = (\rho C_p)_p/(\rho C_p)_f$ is the ratio of effective heat capacity of the nanoparticle material to the effective heat capacity of the base fluid, α_f is thermal diffusivity of base fluid, C is local volume fraction of nanoparticles, q_r is nonlinear radiative heat flux, D_B is Brownian diffusion coefficient and D_T is thermophoretic diffusion coefficient. The radiative heat flux expression in Eq. (5.3) is given by the Rosseland formula [123] as

$$q_r = -\frac{4\sigma^*}{3k^*}\frac{\partial T^4}{\partial y} = -\frac{16\sigma^*}{3k^*}T^3\frac{\partial T}{\partial y}, \tag{5.6}$$

where σ^* and k^* are the Stefan-Boltzman constant and the mean absorption coefficient respectively. Now Eq. (5.3) can be written as

$$\begin{aligned} u\frac{\partial T}{\partial x} + v\frac{\partial T}{\partial y} =& \frac{\partial}{\partial y}\left[\left(\alpha_f + \frac{16\sigma^* T^3}{3\left(\rho C_p\right)_f k^*}\right)\frac{\partial T}{\partial y}\right] + \frac{\nu_f}{\left(C_p\right)_f}\left(\frac{\partial u}{\partial y}\right)^2 + \frac{\sigma B^2}{\left(\rho C_p\right)_f}u^2 \\ &+ \tau\left[D_B\left(\frac{\partial C}{\partial y}\frac{\partial T}{\partial y}\right) + \frac{D_T}{T_\infty}\left(\frac{\partial T}{\partial y}\right)^2\right]. \end{aligned} \tag{5.7}$$

Introducing the following dimensionless variables

$$\begin{aligned} &\psi = \alpha_f Ra_x^{1/4} f,\ u = \frac{\partial \psi}{\partial y},\ v = -\frac{\partial \psi}{\partial x}, \\ &\eta = \frac{y}{x}Ra_x^{1/4},\ \theta = \frac{T - T_\infty}{T_w - T_\infty},\ \phi = \frac{C - C_\infty}{C_w - C_\infty}. \end{aligned} \tag{5.8}$$

Eq. (5.1) is identically satisfied and Eqs. (5.2), (5.4) and (5.7) with the boundary conditions (5.5) reduce to:

$$\frac{d^3 f}{d\eta^3} + \frac{1}{4Pr}\left[3f\frac{d^2 f}{d\eta^2} - 2\left(\frac{df}{d\eta}\right)^2\right] - M\frac{df}{d\eta} + \theta - Nr\phi = 0, \tag{5.9}$$

$$\begin{aligned} \frac{d}{d\eta}\left[\left(1 + Rd\Big(1 + (\theta_w - 1)\theta\Big)^3\right)\frac{d\theta}{d\eta}\right] + \frac{3}{4}f\frac{d\theta}{d\eta} + Nb\frac{d\theta}{d\eta}\frac{d\phi}{d\eta} + Nt\left(\frac{d\theta}{d\eta}\right)^2 \\ + PrEc\left[\left(\frac{d^2 f}{d\eta^2}\right)^2 + M\left(\frac{df}{d\eta}\right)^2\right] = 0, \end{aligned} \tag{5.10}$$

$$\frac{d^2\phi}{d\eta^2} + \frac{3}{4}Lef\frac{d\phi}{d\eta} + \frac{Nt}{Nb}\frac{d^2\theta}{d\eta^2} = 0, \tag{5.11}$$

with corresponding boundary conditions

$$\begin{aligned} &f(0) = 0,\ f'(0) = 0,\ \theta(0) = 1,\ \phi(0) = 1, \\ &f'(\infty) \to 0,\ \theta(\infty) \to 0,\ \phi(\infty) \to 0, \end{aligned} \tag{5.12}$$

where Ra_x is the local Rayleigh number, M is the magnetic parameter, Nr is the buoyancy ratio parameter, Nb is Brownian motion parameter, Nt is the thermophoresis parameter, Rd is the radiation parameter, Pr is the Prandtl number, θ_w is sheet to ambient temperature ratio, Ec is the Eckert number and Le is the Lewis number. These parameters are defined as under:

$$\begin{cases} Ra_x = \dfrac{(1-C_\infty)\, g\beta\,(T_w - T_\infty)\, x^3}{\nu_f \alpha_f},\ Nr = \dfrac{(\rho_p - \rho_f)\,(C_w - C_\infty)}{(1-C_\infty)\,\rho_f \beta\,(T_w - T_\infty)}, \theta_w = \dfrac{T_w}{T_\infty}, \\ Rd = \dfrac{16\sigma^* T_\infty^3}{3kk^*},\ Pr = \dfrac{\nu_f}{\alpha_f},\ M = \dfrac{\sigma B^2}{\rho_f \nu_f}\sqrt{\dfrac{x}{C_1}},\ C_1 = \dfrac{(1-C_\infty)\, g\beta\,(T_w - T_\infty)}{\nu_f \alpha_f}, \\ Nt = \dfrac{\tau D_T\,(T_w - T_\infty)}{T_\infty \alpha_f},\ Nb = \dfrac{\tau D_B\,(C_w - C_\infty)}{\alpha_f},\ Ec = \dfrac{\alpha_f^2 C_1 x}{C_p\,(T_w - T_\infty)},\ Le = \dfrac{\alpha_f}{D_B}. \end{cases} \tag{5.13}$$

The quantities of practical interest in this study are the local skin friction coefficient C_f , the local Nusselt number Nu_x and the local Sherwood number Sh_x which are defined as:

$$\begin{aligned} C_f &= \frac{\tau_w x^2}{(\mu\alpha)_f Ra_x^{3/4}};\ \tau_w = \mu_f \left(\frac{\partial u}{\partial y}\right)_{y=0}, \\ Nu_x &= \frac{x q_w}{k(T_w - T_\infty)};\ q_w = -k\left(\frac{\partial T}{\partial y}\right)_{y=0} + (q_r)_{y=0}, \\ Sh_x &= \frac{x j_w}{D_B(C_w - C_\infty)};\ j_w = -D_B\left(\frac{\partial C}{\partial y}\right)_{y=0}, \end{aligned} \tag{5.14}$$

where τ_w is the wall shear stress, q_w is the wall heat flux and j_w is the wall mass flux. Now using dimensionless quantities from Eq. (5.8) in Eq. (5.14), we get

$$\begin{aligned} &C_f = f''(0), \\ &Ra_x^{1/4} Nu_x = -\Big[1 + Rd\theta_w^3\Big]\theta'(0) = Nur, \\ &Ra_x^{1/4} Sh_x = -\phi'(0) = Shr. \end{aligned} \tag{5.15}$$

5.3 Numerical Method

The dimensionless mathematical problems given in Eqs. (5.9)-(5.11) with the boundary conditions (5.12) have been solved for the numerical solutions via shooting method. Before employing the Runge-Kutta integration scheme, first we reduce the governing differential equations into a set of first order ODEs. Let $x_1 = \eta, x_2 = f, x_3 = f', x_4 = f'', x_5 = \theta, x_6 = \theta', x_7 = \phi, x_8 = \phi'$. We obtain the following system:

$$\begin{pmatrix} x_1' \\ x_2' \\ x_3' \\ x_4' \\ x_5' \\ x_6' \\ x_7' \\ x_8' \end{pmatrix} = \begin{pmatrix} 1 \\ x_3 \\ x_4 \\ Mx_3 + Nrx_7 - x_5 - \frac{1}{4Pr}(3x_2x_4^2 - 2x_3^2) \\ x_6 \\ \frac{-Nbx_6x_8 - Ntx_6^2 - PrEc\left(x_4^2 + Mx_3^2\right) - \frac{3}{4}x_2x_6 - 3Rdx_6^2(\theta_w - 1)\left(1 + (\theta_w - 1)x_5\right)^2}{1 + Rd\left(1 + (\theta_w - 1)x_5\right)^3} \\ x_8 \\ -\frac{3}{4}Lex_2x_8 - \frac{Nt}{Nb}x_6' \end{pmatrix}, \tag{5.16}$$

and the corresponding initial conditions are:

$$\begin{pmatrix} x_1 \\ x_2 \\ x_3 \\ x_4 \\ x_5 \\ x_6 \\ x_7 \\ x_8 \end{pmatrix} = \begin{pmatrix} 0 \\ 0 \\ 1 \\ u_1 \\ 1 \\ u_2 \\ 1 \\ u_3 \end{pmatrix}. \tag{5.17}$$

The above nonlinear coupled ODEs along with initial conditions are solved using fourth-fifth order Runge-Kutta integration technique.

5.4 Numerical Results and Discussion

To assess the accuracy of code, the results are compared with Kuznetsov and Nield [62] in a limiting case and found in very good agreement (see Table 5.1). Table 5.2 provides the numerical values of wall temperature gradient and wall concentration gradient for different values of M, Ec, Pr and Nr with the other parameters fixed. It may be noted here that values of parameters Nb, Nt, Rd, Ec, M and Nr characterize the strengths of Brownian motion, thermophoresis, thermal radiation, viscous dissipation and Joule heating respectively. Thus we can take any value of these parameters in the range $0 \leq Nb, Nt, Rd, Ec, M, Nr < \infty$. The larger the values of these parameters the greater will be the corresponding effect. In absence of magnetic field ($M = 0$) , there is a de-

crease in $|\theta'(0)|$ and increase in $|\phi'(0)|$ with an increase in the viscous dissipation effect. These variations increase with the higher values of Prandtl number (i.e. $Pr = 3, 5$), as can be observed from Table 5.2. This is primarily due to the fact that the Prandtl number controls the relative thickness of the momentum and thermal boundary layers. Therefore increasing values of Pr reduces conduction but enhances pure convection as well as variations in thermal characteristics due to viscous dissipation or joule heating. It is seen that in the presence of viscous dissipation and Joule heating effects, heat flux at the wall decreases with an increase in Pr. This outcome is in accordance with Makinde et al. [132]. In Table 5.3 the computed values of $|\theta'(0)|$ and $|\phi'(0)|$ are given for various values of Nb, Nt, Le and Rd with the other parameters fixed. It is found that in absence of thermal radiation there is significant reduction in wall temperature gradient when Nb and Nt are increased and this variation is smaller in the presence of thermal radiation. Fig. 5.2 describes the influences of radiation and magnetic field on the dimensionless velocity profiles. The vertical ($x-$component) of velocity increases to a maximum value and asymptotically reaches to zero value near the edge of boundary layer. Fig. 5.2 also indicates that hydrodynamic boundary layer is thicker at $Rd = 2$ than at $Rd = 0$. On the other hand the boundary layer becomes thinner when magnetic field strength is increased. The decrease in momentum transport is due to the presence of Lorentz force induced by the applied magnetic field perpendicular to the flow. Fig. 5.3 shows the variations in velocity profiles with an augmentation in Nr for three different values of Pr. In accordance with Kuznetsov and Nield [62] and Aziz and Khan [74], as Prandtl number is increased from $Pr = 1$ to $Pr = 5$ the hydrodynamic boundary layer becomes thicker. Further a decrease in the vertical component of velocity with an increment in Nr is accounted and this decrease is of similar magnitude for $Pr = 1, 3, 5$. It is worth mentioning here that Pr=1 corresponds to the electrolyte solution such as salt water. The Prandtl number between 5.4 and 5.5 represents $R - 12$ refrigerant. For water-based nanofluid the Prandtl number is between 6 and 7. Physically when Nr is increased, the fluid is under the influence of stronger buoyancy force which reduces the vertical component of velocity. Fig. 5.4 plots the wall velocity gradient versus Pr with the variation in Nr. The results are presented for three different values of M. It is clear that wall shear stress can be decreased by either increasing the strength of magnetic field or by increasing the buoyancy-ratio parameter Nr. The behavior of Joule heating on the thermal boundary layer can be visualized from Fig. 5.5. $Ec = 0$ corresponds to the case when there is no viscous dissipation effect. For a weaker viscous dissipation effect i.e. when $Ec = 0.1$,

there is a minor growth in the thermal boundary layer thickness with an increase in M and this variation increases as viscous dissipation effect is strengthened. It is seen that for stronger viscous dissipation effect, the resistance in the fluid motion caused by the Lorentz force and by friction enhances the temperature. As viscous dissipation effect gets strengthened (i.e. Ec changes from ($Ec = 0$ to $Ec = 0.2$) the fluid's temperature near the vicinity of the plate becomes greater than the plate's temperature which results in reverse heat flow close to the plate as can be seen from Fig. 5.5. We therefore expect the reduced Nusselt number $\breve{}\theta'(0)$ to be negative in this situation. The influence of Brownian motion and thermophoresis parameters on the temperature profiles is presented in Fig. 5.6. Increase in the Brownian motion leads to significant movement of nanoparticles within the base fluid which eventually increases the fluid's kinetic energy and thus temperature rises. The thermal boundary layer also becomes thicker as thermophoretic effect is increased. Interestingly the variations in temperature function with Nb and Nt becomes less when radiation parameter Rd is increased from $Rd = 0$ to $Rd = 2$. In Fig. 5.7 the green line is obtained for linear radiation problem and red lines are computed through Eq. (5.10) with the variation in θ_w. Increasing values of θ_w indicates larger wall temperature compared to ambient. As a result temperature θ is an increasing function of θ_w. Moreover the profiles become S-shaped (earlier pointed out by Pantokratoras and Fang [110]) indicating the occurrence of adiabatic case for sufficiently larger value of $\theta_w > 10$. It is worth pointing here that when $\theta_w \approx 1$, temperature profiles are close to corresponding profiles for the case of linear radiative heat flux. Figs. 5.8 and 5.9 compare the results of linear and non-linear radiation for different values of Rd when $\theta_w = 1.1$ and $\theta_w = 3$ respectively. It is seen that linear and non-linear results match each other better at $\theta_w = 1.1$ when compared with $\theta_w = 3$. The profiles show a significant deviation as the radiation parameter is gradually increased. Thus it can be concluded that linear and non-linear radiation results match up smoothly when θ_w is close to one (say $\theta_w = 1.1$) and Rd is sufficiently small (say $Rd < 0.5$).

Fig. 5.10 depicts the thermophoretic effect on the nanoparticle volume fraction ϕ. For hot surfaces, thermophoresis tends to blow the nanoparticle volume fraction boundary layer away from the surface since a hot surface repels the sub-micron sized particles from it, thereby forming a relatively particle-free layer near the surface. As a consequence, the nanoparticle distribution does not exist closer to the plate. It can also be seen that there is a significant increase in ϕ with an increase in Nt for a weaker Brownian motion ($Nb = 0.1$). The change in nanoparticle volume fraction profiles with an increase in Nt

becomes smaller as the Brownian motion strengthens i.e. when Nb changes from 0.1 to 0.5. The behavior of Lewis number Le on ϕ can be interpreted from Fig. 5.11. Increasing values of Le corresponds to a decrease in mass diffusivity or less Brownian diffusion and eventually less penetration depth for concentration boundary layer. It is noticeable that values of Le around $0.3 - 1.62$ represent various gases which include hydrogen, methane, ethylene and propane. Moreover the concentration ϕ is a decreasing function of Rd.
Fig. 5.12 shows the variation in reduced Nusselt number with Nb for different values of Nt. This Fig. is complimenting the data shown in Table 5.2. It is seen that $|\theta'(0)|$ is a decreasing function of Nt and this decrease is of similar magnitude for any value of M and Nb. Physically a stronger thermophoretic force drives the nanoparticles from the plate to the fluid invoking a particle-free layer near the plate. Fig. 5.13 plots the wall temperature gradient versus θ_w for different values of radiation parameter Rd. When $\theta_w \approx 1, \theta'(0)$ tends to a constant value for sufficiently smaller values of $Rd \approx 0.001$ which is in accordance with Cortell [113]. Fig. 5.14 indicates that variation in $\phi'(0)$ with Brownian motion and thermophoresis effects is similar for $Le = 1$ and $Le = 5$. It should be noted here that behaviors of parameters on the velocity, temperature, local nanoparticle volume fraction and heat transfer rate discussed above are in accordance with the previous studies [61, 62, 74] and even with Kuznetsov and Nield [76] about the revised boundary condition for nanoparticle volume fraction.

5.5 Concluding Remarks

The present work investigates the influence of nonlinear thermal radiation on the natural convective boundary layer flow of an electrically conducting nanofluid past a vertical plate. Different from the linear radiation problem, the present problem is governed by an additional temperature ratio parameter. Mathematical model incorporates the effects of Joule heating and viscous dissipation in the energy equation. The solutions are computed numerically by shooting method with fourth-fifth-order Runge-Kutta integration technique. The major conclusions are listed below:

a. Temperature increases and profiles become S-shaped with an increase in temperature ratio parameter and decrease in thermal radiation parameter revealing the existence of the point of inflection for temperature distribution.

b. Unlike previously reported results on thermal radiations effect, current results are

valid for both small ($\theta_w \approx 1$) as well as large temperature differences ($\theta_w > 1$) between plate and environment.

c. Temperature θ increases and thermal boundary layer thickens when Nb and Nt are increased. The variation in temperature function is of smaller magnitude for a stronger thermal radiation effect.

d. Increase in the strengths of Brownian motion and thermophoresis effects results in the decrease of heat transfer from the plate.

e. Temperature θ increases and heat transfer from the plate decreases by increasing Joule heating and viscous dissipation effects.

f. The points c, d and e still hold in case of linear radiation and differences in the behaviors of parameters (except the radiation parameter) are only quantitative.

With the inclusion of non-linear radiation term, which allows both small and large temperature differences in the flow, the current work may lead to better understanding of the absorption of incident solar radiation and its transition into the nanoparticle working fluid. Further natural convection in nanofluids has vital importance in next generation solar film collectors, nuclear reactor application, heat exchangers etc.

Table 5.1: Comparison of current results of $-\theta'(0)$ with Kuznetsov and Nield [62] with $Le = 10, Nr = Nb = Nt = 10^{-5}$ in the absence of M, Ec and Rd.

Pr	1	10	100	1000
Present	0.401007	0.463285	0.481067	0.483602
Kunetsov & Nield [62]	0.401	0.463	0.481	0.484

Table 5.2: Variation of Nusselt number $(-\theta'(0))$ and Sherwood number $(-\phi'(0))$ when $Nt = Nb = 0.1, Le = 5, \theta_w = 1.5$ and $Rd = 1$.

Pr	Nr	$M = 0$				$M = 1$			
		$Ec = 0$		$Ec = 0.1$		$Ec = 0$		$Ec = 0.1$	
		$-\theta'(0)$	$-\phi'(0)$	$-\theta'(0)$	$-\phi'(0)$	$-\theta'(0)$	$-\phi'(0)$	$-\theta'(0)$	$-\phi'(0)$
1	0	0.1925	0.8844	0.1812	0.8941	0.1542	0.7479	0.1422	0.7572
	0.5	0.1861	0.8370	0.1773	0.8449	0.1464	0.6875	0.1372	0.6958
	1	0.1784	0.7776	0.1719	0.7841	0.1361	0.6037	0.1296	0.6122
3	0	0.2201	0.9460	0.1720	0.9883	0.1618	0.7634	0.1176	0.7982
	0.5	0.2128	0.8992	0.1740	0.9355	0.1531	0.7013	0.1186	0.7332
	1	0.2042	0.8419	0.1742	0.8734	0.1418	0.6158	0.1167	0.6485
5	0	0.2305	0.9690	0.1363	1.0524	0.1635	0.7670	0.0786	0.8329
	0.5	0.2229	0.9226	0.1457	0.9954	0.1547	0.7044	0.0867	0.7660
	1	0.2140	0.8662	0.1530	0.9306	0.1431	0.6185	0.0920	0.6821

Table 5.3: Values of Nusselt number $(-\theta'(0))$ and Sherwood number $(-\phi'(0))$ when $M = 0.5, Nr = 0.2, Pr = 0.7, \theta_w = 1.5$ and $Ec = 0.1$.

Nt	Nb	$Le = 2$				$Le = 10$			
		$Rd = 0$		$Rd = 1$		$Rd = 0$		$Rd = 1$	
		$-\theta'(0)$	$-\phi'(0)$	$-\theta'(0)$	$-\phi'(0)$	$-\theta'(0)$	$-\phi'(0)$	$-\theta'(0)$	$-\phi'(0)$
0.1	0.2	0.2738	0.4332	0.1516	0.5299	0.2686	0.9416	0.1528	1.0277
	0.5	0.2286	0.4770	0.1433	0.5379	0.2107	0.9653	0.1434	1.0292
	0.8	0.1879	0.4929	0.1352	0.5411	0.1634	0.9765	0.1344	1.0308
0.2	0.2	0.2624	0.3967	0.1494	0.5228	0.2570	0.9427	0.1508	1.0315
	0.5	0.2199	0.4712	0.1415	0.5366	0.2016	0.9751	0.1416	1.0324
	0.8	0.1807	0.4938	0.1336	0.5412	0.1562	0.9872	0.1328	1.0337
0.3	0.2	0.2517	0.3665	0.1473	0.5163	0.2461	0.9489	0.1489	1.0353
	0.5	0.2117	0.4674	0.1398	0.5356	0.1930	0.9861	0.1398	1.0357
	0.8	0.1738	0.4958	0.1320	0.5414	0.1494	0.9983	0.1312	1.0367

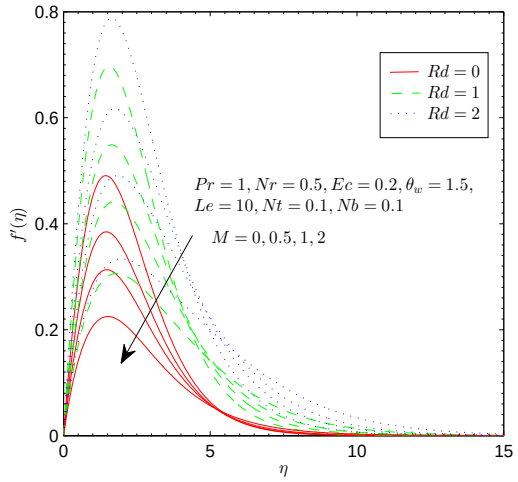

Figure 5.2: Effect of Rd and M on f'.

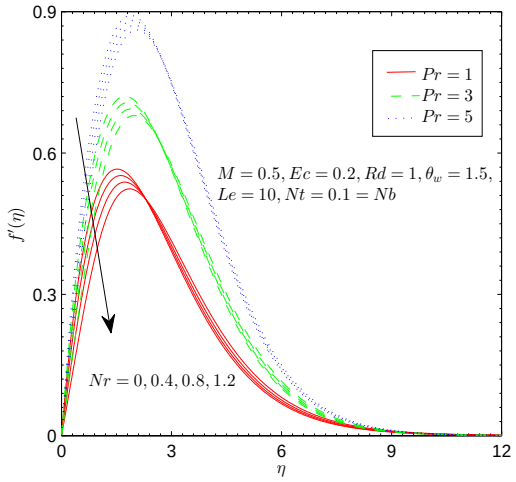

Figure 5.3: Effect of Pr and Nr on f'.

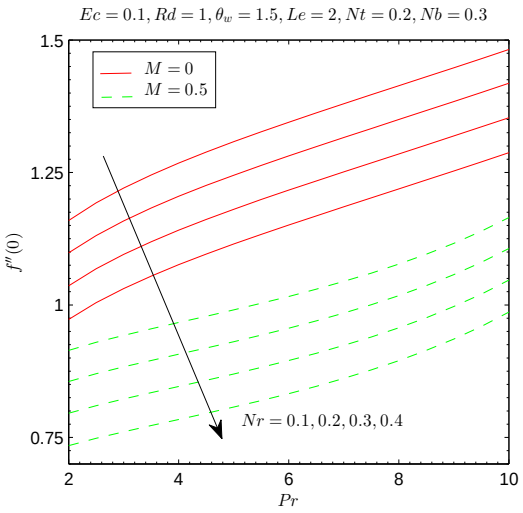

Figure 5.4: Variation of $-f''(0)$.

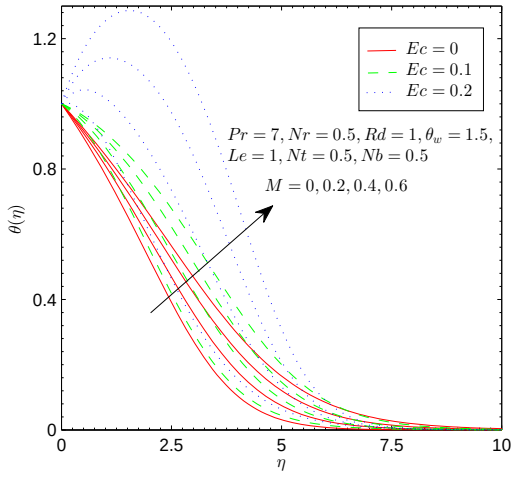

Figure 5.5: Effect of M and Ec on θ.

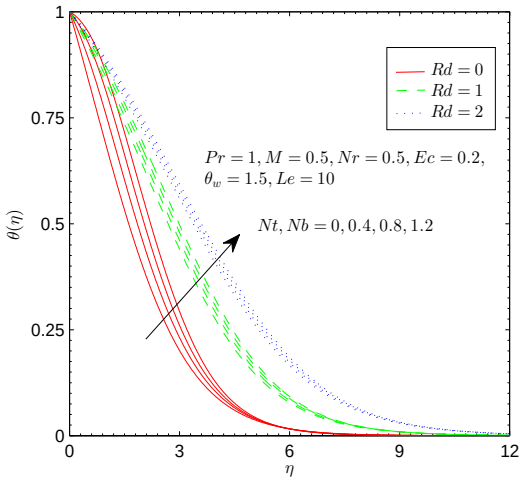

Figure 5.6: Effect of Nt, Nb and Rd on θ.

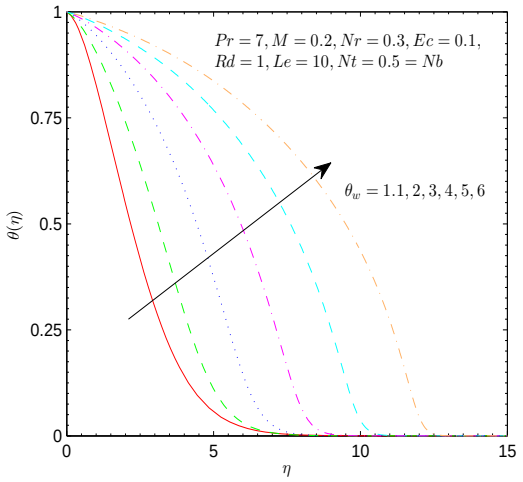

Figure 5.7: Effect of θ_w on θ.

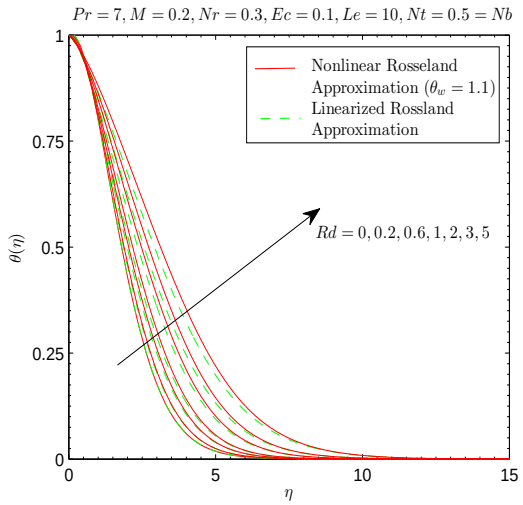

Figure 5.8: Effect of Rd on θ.

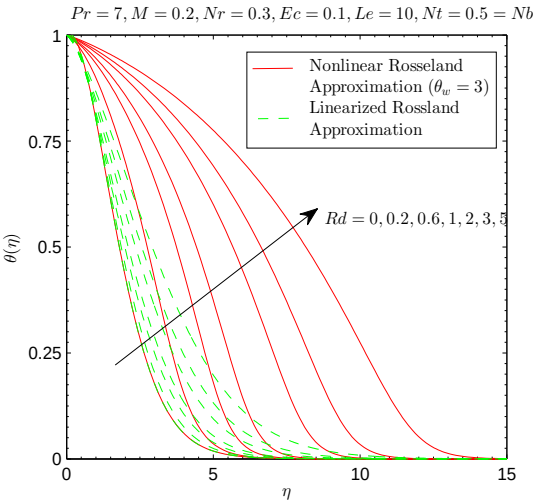

Figure 5.9: Effect of Rd on θ.

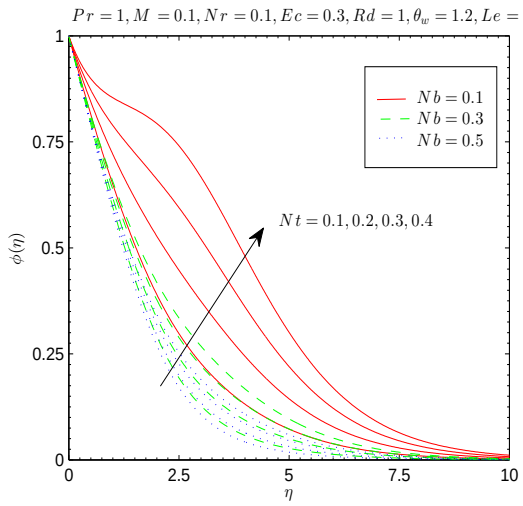

Figure 5.10: Effect of Nt and Nb on ϕ.

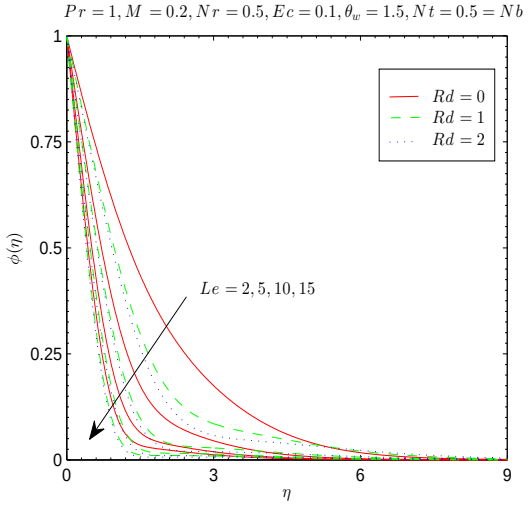

Figure 5.11: Effect of Rd and Le on ϕ.

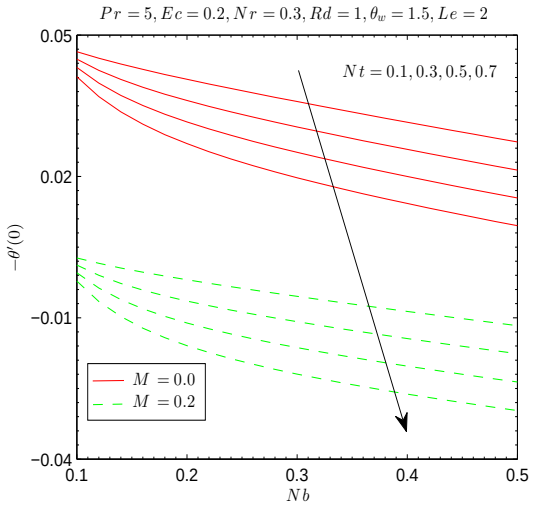

Figure 5.12: Variation of $-\theta'(0)$.

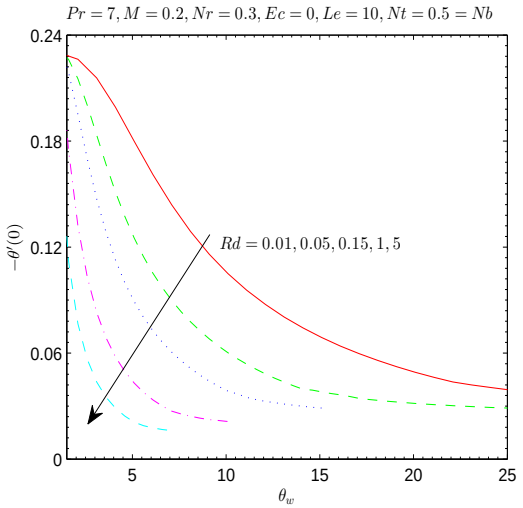

Figure 5.13: Effect of θ_w and Rd on $-\theta'(0)$.

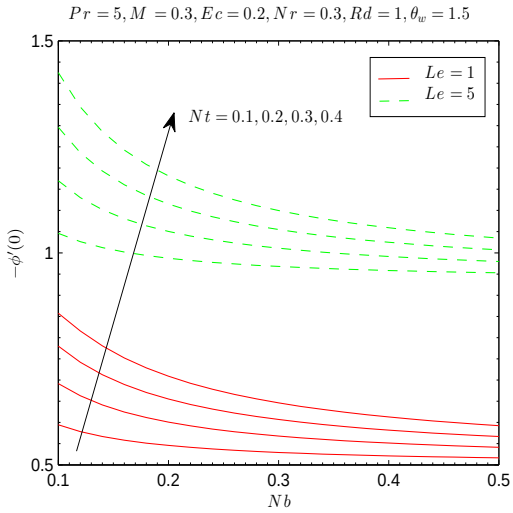

Figure 5.14: Effect of Nb, Nt and Le on $-\phi'(0)$.

Chapter 6

Stagnation-point flow of nanofluid under the effect of non-linear radiative heat transfer

6.1 Introduction

Radiation effects in the two-dimensional stagnation-point flow of viscous nanofluid due to solar energy are investigated. Heat transfer subject to non-linear thermal radiation, Joule heating, viscous dissipation and convective boundary conditions is considered. The governing equations are simplified through the boundary layer assumptions and then transformed into non-dimensional forms by appropriate transformations. The resulting differential systems are solved numerically through fifth order Runge-Kutta method using a shooting technique. The influences of different parameters are explained through graphs for velocity, temperature and concentration and numerical values of local Nusselt and Sherwood numbers. A comparative analysis of the solutions is performed through previous studies in some limiting cases. Both the temperature and wall temperature gradient are increasing functions of the radiation parameter. The excessive movement of nanoparticles in the base fluids results in the deeper absorption of solar radiations in the liquids.

6.2 Problem Formulation

Let us consider the two-dimensional incompressible boundary layer flow of nanofluid over a convectively heated stretching sheet located at $y = 0$. The sheet is stretched through

two equal and opposite forces along $x-$axis by keeping the origin fixed with the velocity $U_w = ax$. Let $U_\infty(x) = bx$ be the fluid's velocity outside the boundary layer. A uniform magnetic field of strength B_0 is applied in the transverse direction to the flow. The fluid is assumed to be slightly conducting, so that the magnetic Reynolds number is much less than unity and hence the induced magnetic field is negligible in comparison with the applied magnetic field. Further, it is also assumed that the external electrical field is zero and the electric field due to the polarization of charges is negligible. Heat transfer analysis is carried out in the presence of thermal radiation, Joule heating and viscous dissipation effects. The combined effects of Brownian motion and thermophoresis due to the presence of nanoparticles are considered. T_f denotes the convective surface temperature while T_∞ is the ambient fluid's temperature. The steady boundary layer equations governing the two-dimensional incompressible stagnation-point flow of nanofluid can be written as

$$\frac{\partial u}{\partial x} + \frac{\partial v}{\partial y} = 0, \tag{6.1}$$

$$u\frac{\partial u}{\partial x} + v\frac{\partial u}{\partial y} = U_\infty \frac{dU_\infty}{d\eta} + \nu_f \frac{\partial^2 u}{\partial y^2} + \frac{\sigma B^2}{\rho_f}\left(U_\infty - u\right), \tag{6.2}$$

$$\begin{aligned} u\frac{\partial T}{\partial x} + v\frac{\partial T}{\partial y} =& \alpha_f \frac{\partial^2 T}{\partial y^2} - \frac{1}{(\rho C_p)_f}\left(\frac{\partial q_r}{\partial y}\right) + \frac{\nu_f}{(C_p)_f}\left(\frac{\partial u}{\partial y}\right)^2 + \frac{\sigma B^2}{(\rho C_p)_f}\left(U_\infty - u\right)^2 \\ &+ \tau\left[D_B\left(\frac{\partial C}{\partial y}\frac{\partial T}{\partial y}\right) + \frac{D_T}{T_\infty}\left(\frac{\partial T}{\partial y}\right)^2\right], \end{aligned} \tag{6.3}$$

$$u\frac{\partial C}{\partial x} + v\frac{\partial C}{\partial y} = D_B\frac{\partial^2 C}{\partial y^2} + \frac{D_T}{T_\infty}\frac{\partial^2 T}{\partial y^2}. \tag{6.4}$$

The relevant boundary conditions for convective heat transfer can be written as :

$$\begin{aligned} &u = U_w(x) = ax,\ v = 0,\ -k\frac{\partial T}{\partial y} = h\left(T - T_f\right),\ C = C_w \qquad \text{at } y = 0, \\ &u \to U_\infty(x) = bx,\ T \to T_\infty,\ C \to C_\infty \qquad\qquad\qquad \text{as } y \to \infty. \end{aligned} \tag{6.5}$$

In the above equations, u and v are the velocity components along the $x-$ and $y-$ directions, ρ_f and ρ_p are the densities of base fluid and nanoparticles material respectively, σ is the conductance of the fluid, T is the local temperature, $\tau = (\rho C_p)_p/(\rho C_p)_f$ is the ratio of effective heat capacity of the nanoparticle material to the effective heat capacity of the base fluid, α_f is thermal diffusivity of base fluid, C is local volume fraction of nanoparticles, q_r is nonlinear radiative heat flux, D_B is Brownian diffusion coefficient and D_T is thermophoretic diffusion coefficient. The radiative heat flux expression in Eq. (6.3) is given by the Rosseland formula [118] as

$$q_r = -\frac{4\sigma^*}{3k^*}\frac{\partial T^4}{\partial y} = -\frac{16\sigma^*}{3k^*}T^3\frac{\partial T}{\partial y}, \tag{6.6}$$

where σ^* and k^* are the Stefan-Boltzman constant and the mean absorption coefficient respectively. Now Eq. (6.3) can be written as

$$\begin{aligned} u\frac{\partial T}{\partial x}+v\frac{\partial T}{\partial y} =&\frac{\partial}{\partial y}\left[\left(\alpha_f+\frac{16\sigma^* T^3}{3\left(\rho C_p\right)_f k^*}\right)\frac{\partial T}{\partial y}\right]+\frac{\nu_f}{\left(C_p\right)_f}\left(\frac{\partial u}{\partial y}\right)^2+\frac{\sigma B^2}{\left(\rho C_p\right)_f}\left(U_\infty-u\right)^2 \\ &+\tau\left[D_B\left(\frac{\partial C}{\partial y}\frac{\partial T}{\partial y}\right)+\frac{D_T}{T_\infty}\left(\frac{\partial T}{\partial y}\right)^2\right]. \end{aligned} \tag{6.7}$$

Introducing the following dimensionless variables

$$\begin{aligned} &\eta=y\sqrt{\frac{a}{\nu_f}},\ u=ax\frac{df}{d\eta},\ v=-\sqrt{\nu_f a}f, \\ &\theta=\frac{T-T_\infty}{T_f-T_\infty},\ \phi=\frac{C-C_\infty}{C_w-C_\infty}. \end{aligned} \tag{6.8}$$

Eq. (6.1) is identically satisfied and Eqs. (6.2), (6.4) and (6.7) with the boundary conditions (6.5) reduce to:

$$\frac{d^3 f}{d\eta^3}+f\frac{d^2 f}{d\eta^2}-\left(\frac{df}{d\eta}\right)^2+M\left(\lambda-\frac{df}{d\eta}\right)+\lambda^2=0, \tag{6.9}$$

$$\begin{aligned} \frac{1}{Pr}\frac{d}{d\eta}\left[\left(1+Rd\Big(1+(\theta_w-1)\theta\Big)^3\right)\frac{d\theta}{d\eta}\right]+f\frac{d\theta}{d\eta}+Nb\frac{d\theta}{d\eta}\frac{d\phi}{d\eta}+Nt\left(\frac{d\theta}{d\eta}\right)^2 \\ +Ec\left[\left(\frac{d^2 f}{d\eta^2}\right)^2+M\left(\lambda-\frac{df}{d\eta}\right)^2\right]=0, \end{aligned} \tag{6.10}$$

$$\frac{d^2\phi}{d\eta^2}+Scf\frac{d\phi}{d\eta}+\frac{Nt}{Nb}\frac{d^2\theta}{d\eta^2}=0, \tag{6.11}$$

with corresponding boundary conditions

$$\begin{aligned} &f(0)=0,\ f'(0)=0,\ \theta'(0)=-Bi\left[1-\theta(0)\right],\ \phi(0)=1, \\ &f'(\infty)\to\lambda,\ \theta(\infty)\to 0,\ \phi(\infty)\to 0, \end{aligned} \tag{6.12}$$

where M is the magnetic parameter, Nb is Brownian motion parameter, Nt is the thermophoresis parameter, Bi is the Biot number, Rd is the radiation parameter, Pr is the Prandtl number, θ_w is hot fluid to ambient temperature ratio, Ec is the Eckert number and Sc is the Schmidt number. These parameters are defined as under:

$$\begin{cases} \lambda=\dfrac{b}{a},\ Bi=\dfrac{h}{k}\sqrt{\dfrac{\nu_f}{a}},\ Rd=\dfrac{16\sigma^* T_\infty^3}{3kk^*},\ Pr=\dfrac{\nu_f}{\alpha_f},\ M=\dfrac{\sigma B^2}{\rho_f a},\ ,\theta_w=\dfrac{T_f}{T_\infty}, \\ Nt=\dfrac{\tau D_T\left(T_w-T_\infty\right)}{T_\infty\alpha_f},\ Nb=\dfrac{\tau D_B\left(C_w-C_\infty\right)}{\alpha_f},\ Ec=\dfrac{U_w^2}{C_p\left(T_w-T_\infty\right)},\ Sc=\dfrac{\nu_f}{D_B}. \end{cases} \tag{6.13}$$

The quantities of practical interest in this study are the local Nusselt number Nu_x and the local Sherwood number Sh_x which are defined as:

$$\begin{aligned} Nu_x &= \frac{xq_w}{k(T_f - T_\infty)};\ q_w = -k\left(\frac{\partial T}{\partial y}\right)_{y=0} + (q_r)_{y=0}, \\ Sh_x &= \frac{xj_w}{D_B(C_w - C_\infty)};\ j_w = -D_b\left(\frac{\partial C}{\partial y}\right)_{y=0}, \end{aligned} \tag{6.14}$$

where q_w is the wall heat flux and j_w is the wall mass flux. Now using dimensionless quantities from Eq. (6.8) in Eq. (6.14), we get

$$\begin{aligned} \frac{Nu_x}{\sqrt{Re_x}} &= -\Big[1 + Rd\theta_w^3\Big]\theta'(0) = Nur, \\ \frac{Sh_x}{\sqrt{Re_x}} &= -\phi'(0) = Shr, \end{aligned} \tag{6.15}$$

where $Re_x = U_w x/\nu$ is the local Reynolds number.

6.3 Numerical Method

The dimensionless mathematical problems given in Eqs. (6.9)-(6.11) with the boundary conditions (6.12) have been solved for the numerical solutions via shooting method. Before employing the Runge-Kutta integration scheme, first we reduce the governing differential equations into a set of first order ODEs. Let $x_1 = \eta, x_2 = f, x_3 = f', x_4 = f'', x_5 = \theta, x_6 = \theta', x_7 = \phi, x_8 = \phi'$. We obtain the following system:

$$\begin{pmatrix} x_1' \\ x_2' \\ x_3' \\ x_4' \\ x_5' \\ x_6' \\ x_7' \\ x_8' \end{pmatrix} = \begin{pmatrix} 1 \\ x_3 \\ x_4 \\ x_3^2 - x_2x_4 - M(\lambda - x_3) - \lambda^2 \\ x_6 \\ \frac{-Pr\left(Nbx_6x_8 + Ntx_6^2 + Ec\left(x_4^2 + M(\lambda - x_3)^2\right) + x_2x_6\right) - 3Rdx_6^2(\theta_w - 1)\left(1 + (\theta_w - 1)x_5\right)^2}{1 + Rd\left(1 + (\theta_w - 1)x_5\right)^3} \\ x_8 \\ -Scx_2x_8 - \frac{Nt}{Nb}x_6' \end{pmatrix}, \tag{6.16}$$

and the corresponding initial conditions are:

$$\begin{pmatrix} x_1 \\ x_2 \\ x_3 \\ x_4 \\ x_5 \\ x_6 \\ x_7 \\ x_8 \end{pmatrix} = \begin{pmatrix} 0 \\ 0 \\ 1 \\ u_1 \\ u_2 \\ -Bi(1-u_2) \\ 1 \\ u_3 \end{pmatrix}. \tag{6.17}$$

The above nonlinear coupled ODEs along with initial conditions are solved using fourth-fifth order Runge-Kutta integration technique.

6.4 Numerical Results and Discussion

To ascertain the accuracy of our results, the values of $-\theta'(0)$ and $\phi'(0)$ are compared with those of Makinde and Aziz [64] in the absence of viscous dissipation, Joule heating and thermal radiation effects. A decent agreement is observed for all the considered values of parameters as can be seen from 6.1. This gives us confidence that our results are accurate and more general than the existing attempts in the literature. The influence of Brownian motion and thermophoresis effects on the dimensionless heat and mass transfer rates can be observed from Tables 6.2 and 6.3 which give numerical values of $-\theta'(0)$ and $-\phi'(0)$ for various values of Nb and Nt. Table 6.2 shows that for a weaker Brownian motion ($Nb = 0.1$), there is a decrease in Nur with an increase in Nt. However as the strength of Brownian motion increases (i.e Nb changes from 0.1 to 0.5) the decrease in Nur becomes significant with an increase in Nt. This notion is understandable since the strengthened Brownian motion corresponds to the intense motion of nanoparticles which are driven from the stretching wall to the quiescent fluid. The numerical values are given with and without thermal radiation effects. It is clear that heat transfer rate at the wall $|\theta'(0)|$ is an increasing function of radiation parameter. It is also noticed that for a given Nb, the decrease in Nur with Nt is larger in the case of $Rd = 0$ when compared with $Rd = 1$. Table 6.3 provides the data given in Table 6.2for the reduced Sherwood number Shr. Here it is clear that Shr drastically decreases when Nt is increased. This is due to the

fact that stronger thermophoretic effect tends to blow the nanoparticles volume fraction away from the surface since the hot surface repels the sub-micron sized particles from it, thereby forming a relatively particle-free layer near the surface. This decrease is uniform for both weaker and stronger Brownian motions.

Fig. 6.1 displays the temperature profiles for different values of Nb with and without thermal radiation effects. In nanofluids the Brownian motion takes place due to the size of nanoparticles which is of nanometer scale, at this level the particles motion and its effect on the fluid has a pivotal role in the heat transfer. An increase in Nb corresponds to the effective motion of nanoparticles within the flow. The intensity of this chaotic motion increases the kinetic energy of the nanoparticles and as a consequence the nanofluid's temperature rises. This experimental fact was discovered by Brown in 1827. Here the results are given for $Rd = 0, Rd = 1$ and $Rd = 2$. We observe that in absence of radiation effects $Rd = 0$ the increasing values of Nb accompany with the flatter profiles near the stretching wall. Thus slope of tangent to these at the wall $|\theta'(0)|$ decreases. On the other hand this decrease in $|\theta'(0)|$ with an increase in Nb is negligible when $Rd = 1$. Fig. 6.2 presents the variations of nanoparticle volume fraction with Nb. A minor decrease in ϕ is accounted only away from the sheet for a stronger Brownian motion.

Figs. 6.3 and 6.4 depict the influence of thermophoretic diffusion of nanoparticles on the thermal and concentration boundary layers. From the definition of thermophoretic parameter Nt it is obvious that larger values of Nt correspond to the larger temperature difference and shear gradient. Thus increase in Nt leads to the larger temperature inside the boundary layer as depicted in the Fig. 6.3. This Fig. also shows a decrease in the temperature gradient at the sheet as the thermophoretic effect intensifies. The nanoparticles volume fraction, being strong function of Nt, significantly increases with an increment in Nt (see Fig. 6.4). We also conclude from Fig. 6.3 that decreasing rate in the wall temperature gradient can be reduced by incorporating thermal radiation effects.

Fig. 6.5 shows the behavior of Prandtl number Pr on the thermal boundary layer. For the smaller Prandtl number the temperature gradient near the surface is smaller than the velocity gradient, and for the fluids with Prandtl number greater than one, the temperature gradient is steeper than the velocity gradient. Prandtl number, being the ratio of momentum diffusivity to the thermal diffusivity, is large for the fluids which are highly conducive but have low viscosity such as air and some other gases. On the other hand large Prandtl number fluids including water, ethylene glycol and engine oil have high viscosity but low thermal diffusivity. Fig. 6.5 indicates that increase in Pr corresponds to

a decrease in thermal diffusivity which thereby increases variations in the thermal characteristics and decreases the fluid's temperature and thermal boundary layer thickness. It is also clear from the Fig. that profiles for θ becomes increasingly steeper near the wall as Pr increases. As a result the wall temperature gradient $\theta'(0)$ increases with an increase in Pr. Fig. 6.6 is prepared to perceive the effects of viscous dissipation on the thermal boundary layer. In a viscous fluid flow the viscosity of the fluid takes kinetic energy from the motion of the fluid and transforms it into internal energy that heats up the fluid. This process is partially irreversible and is referred to as viscous dissipation. Regardless of the radiation parameter Rd, the fluid's temperature significantly rises as Ec is increased. Fig. 6.7 depicts the influence of convective heating on temperature θ. The larger values of Bi accompany with the stronger convective heating at the sheet which rises the temperature gradient at the sheet. This allows the thermal effect to penetrate deeper into the quiescent fluid. Due to this reason the temperature and thermal boundary layer thickness are increasing functions of Bi. Here the results for constant wall temperature case $\theta(0) = 1$ can be recovered by assuming sufficiently larger Biot number. Further $Bi = 0$ corresponds to the case of insulated sheet. The concentration field is driven by the temperature gradient and since temperature is an increasing function of Bi, thus one would expect an increase in ϕ with an increase in Bi. This outcome is depicted in Fig. 6.8. Fig. 6.9 shows the influence of Schmidt number Sc on ϕ. In accordance with Makinde and Aziz [64], the temperature θ increases with an increase in Sc only close to the stretching sheet. The effects of Lewis number on the concentration boundary layer are depicted in the Fig. 6.10. As Schmidt number Sc gradually increases, this corresponds to weaker molecular diffusivity and thinner concentration boundary layer (see Fig. 6.10). Fig. 6.11 shows that thermal boundary layer significantly grows when the magnetic field strength is increased. On the other hand a minor increase in the nanoparticles volume fraction is observed for large values of M. In the Figs. 6.11 and 6.12, the plots are given for three different values of the radiation parameter. Figs. 6.13 and 6.14 show the graphical representations for the combined influence of Nb and Nt on the dimensionless wall temperature and concentration gradients.

6.5 Conclusions

Radiation effects in the laminar two-dimensional flow of nanofluid over a convectively heated stretching sheet are analyzed. Heat transfer analysis is performed in the presence

of thermal radiation, Joule heating and viscous dissipation. In contrast to the previous studies, the nonlinear radiative heat flux in the Rosseland approximation is considered. This gives us confidence that the present results are more meaningful and practically useful than the previous studies. The boundary layer equations are non-dimensionalized through appropriate similarity transformations and the resulting differential system has been solved for the numerical solutions. The graphical and numerical results are presented with and without thermal radiation effects and the behaviors of essential parameters are thoroughly addressed. The main findings of this study can be summarized as follows:

a. The velocity ratio λ has a dual behavior on the momentum boundary layer. The presence of magnetic field yields a Lorentz force which opposes the fluid velocity. As a result the momentum boundary layer thins as the magnetic field effect strengthens.

b. The temperature and thermal boundary layer thickness are decreasing functions of Prandtl number Pr. The reduced Nusselt number increases when Pr is increased.

c. Regardless of the selected value of radiation parameter Rd, the temperature increases as the Brownian motion and thermophoretic effects are simultaneously increased. The nanoparticles volume fraction is found to decrease upon increasing the Brownian motion parameter. These outcomes are in accordance with the previous studies in the limiting cases (see Khan and Pop [63] and Makinde and Aziz [64]).

d. In future studies on thermal radiation, present work can play a fundamental part on absorption of the incident solar radiation and transiting it to the working fluid by convection.

e. The numerical results of dimensionless wall temperature gradient are compared with those of Makinde and Aziz [64] in the absence of thermal radiation effects and found in an excellent agreement.

f. The results for the case of ordinary fluid and with constant wall temperature can be recovered as special cases of the present work.

Table 6.1: Comparison of values of Nur, Shr and $\theta(0)$ with Makinde and Aziz [64] when $Nt = Nb = 0.5$ and $Rd = 0$.

Pr	Bi	Sc	Makinde and Aziz [64]			Present Solution		
			Nur	Shr	$\theta(0)$	Nur	Shr	$\theta(0)$
1	0.1	5	0.0789	1.5477	0.2107	0.07893	1.54769	0.21069
2			0.0806	1.5554	0.1938	0.08062	1.55543	0.19382
5			0.0735	1.5983	0.2655	0.07344	1.59833	0.26551
10			0.0387	1.7293	0.6132	0.03867	1.72932	0.61329
5	1.0	5	0.1476	1.6914	0.8524	0.14756	1.69139	0.85244
	10		0.1550	1.7122	0.9845	0.15498	1.71222	0.98450
	100		0.1557	1.7144	0.9984	0.15556	1.71437	0.99844
	10^3		0.1557	1.7146	1.0000	0.15572	1.71461	1.00000
	0.1	10	0.0647	2.3920	0.3531	0.06468	2.39201	0.35316
		15	0.0600	2.9899	0.4001	0.05998	2.99003	0.40018
		20	0.0570	3.4881	0.4296	0.05704	3.48817	0.42961

Table 6.2: Values of reduced Nusselt number $-\theta'(0)$ when $Pr = 7, M = 0.5, \lambda = 0.5, Ec = 0.2, \theta_w = 1.5, Sc = 10$ and $Bi = 0.1$.

Nb	Rd	Nt				
		0.1	0.2	0.2	0.4	0.5
0.1	0	0.078493	0.077537	0.076442	0.075166	0.073656
	1	0.081387	0.081022	0.080637	0.080230	0.079801
0.2	0	0.070373	0.068407	0.066014	0.063031	0.059173
	1	0.078183	0.077692	0.077171	0.076620	0.076035
0.3	0	0.058202	0.054148	0.048904	0.041866	0.032143
	1	0.074496	0.073853	0.073172	0.072449	0.071680
0.4	0	0.040852	0.033208	0.023188	0.010383	-0.004342
	1	0.070375	0.069565	0.068707	0.067795	0.066831
0.5	0	0.018834	0.007372	-0.005876	-0.019231	-0.030718
	1	0.065911	0.064929	0.063892	0.062798	0.061644

Table 6.3: Values of reduced Sherwood number $-\phi'(0)$ when $Pr = 7, M = 0.5, \lambda = 0.5, Ec = 0.2, \theta_w = 1.5, Sc = 10$ and $Bi = 0.1$.

Nb	Rd	Nt				
		0.1	0.2	0.2	0.4	0.5
0.1	0	2.44780	2.52829	2.62012	2.72554	2.84752
	1	2.40369	2.43301	2.46505	2.49998	2.53793
0.2	0	2.43727	2.50668	2.58749	2.68274	2.79717
	1	2.39810	2.42085	2.44530	2.47153	2.49962
0.3	0	2.44012	2.51441	2.60310	2.71068	2.84202
	1	2.39670	2.41772	2.44007	2.46381	2.48899
0.4	0	2.44673	2.52969	2.62826	2.74174	2.86094
	1	2.39623	2.41660	2.43807	2.46071	2.48446
0.5	0	2.45314	2.54097	2.63684	2.73130	2.81466
	1	2.39605	2.41605	2.43696	2.45878	2.48150

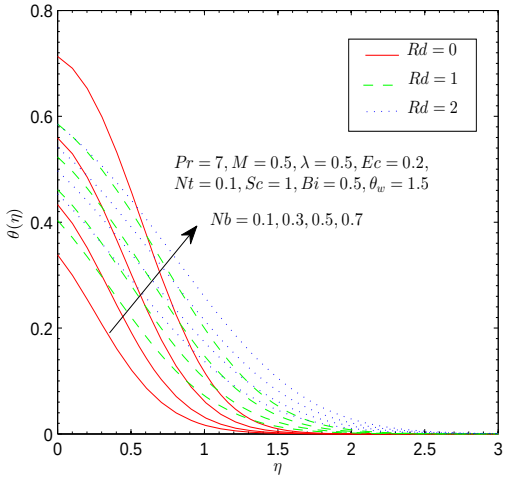

Figure 6.1: Effect of Nb and Rd on θ.

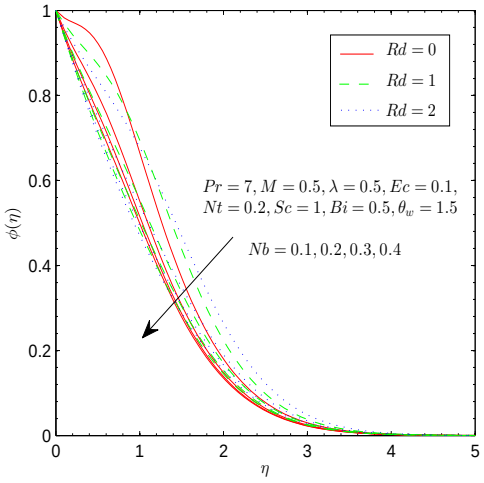

Figure 6.2: Effect of Nb and Rd on ϕ.

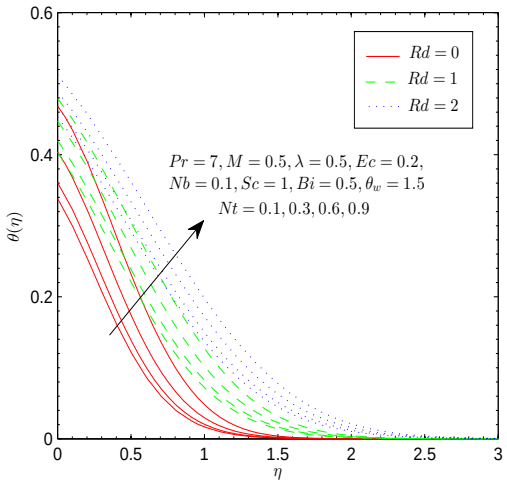

Figure 6.3: Effect of Nt and Rd on θ.

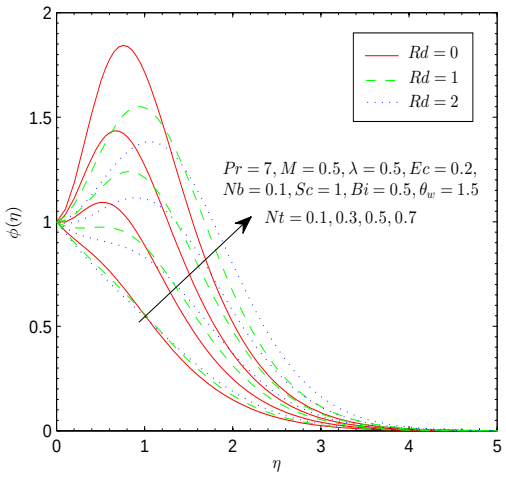

Figure 6.4: Effect of Nt and Rd on ϕ.

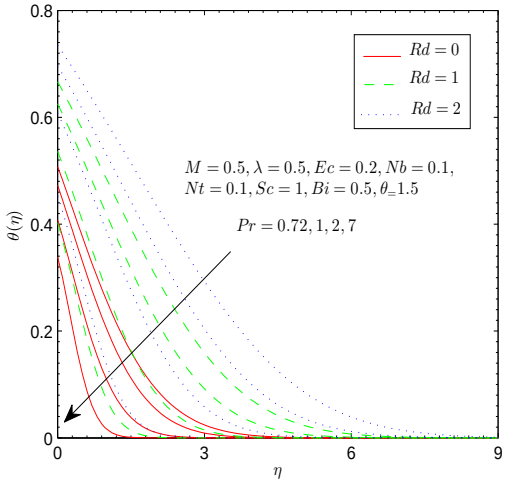

Figure 6.5: Effect of Rd and Pr on θ.

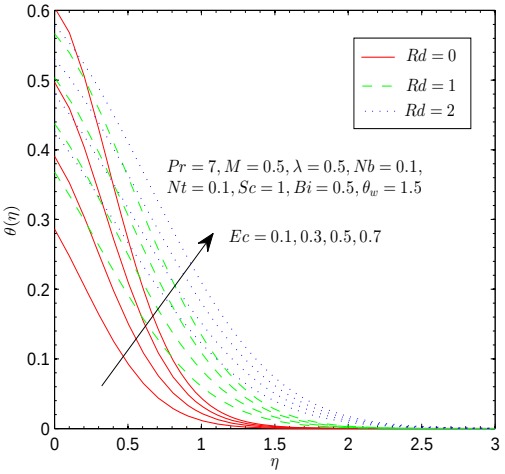

Figure 6.6: Effect of Ec and Rd on θ.

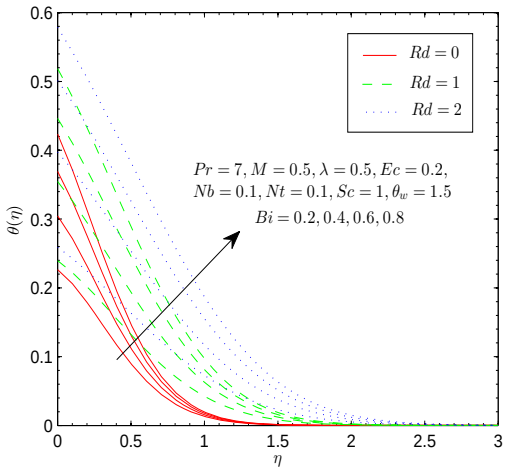

Figure 6.7: Effect of Bi and Rd on θ.

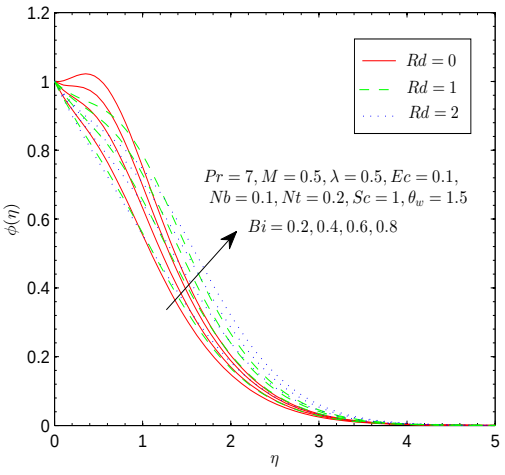

Figure 6.8: Effect of Bi and Rd on ϕ.

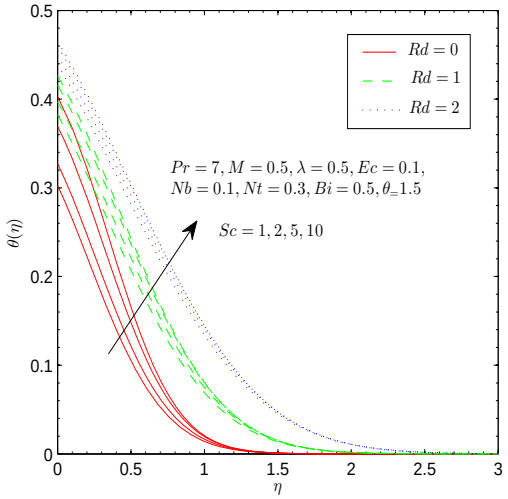

Figure 6.9: Effect of Sc and Rd on θ.

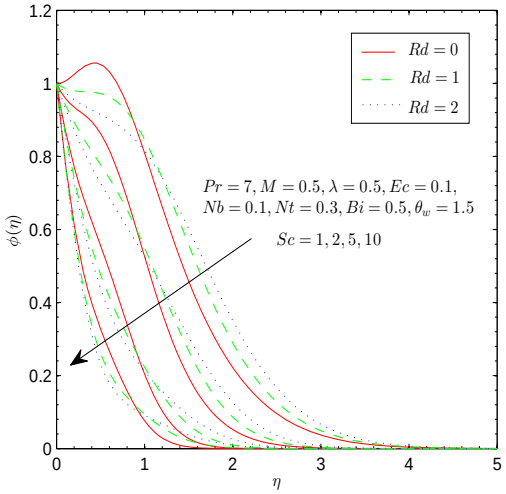

Figure 6.10: Effect of Sc and Rd on ϕ.

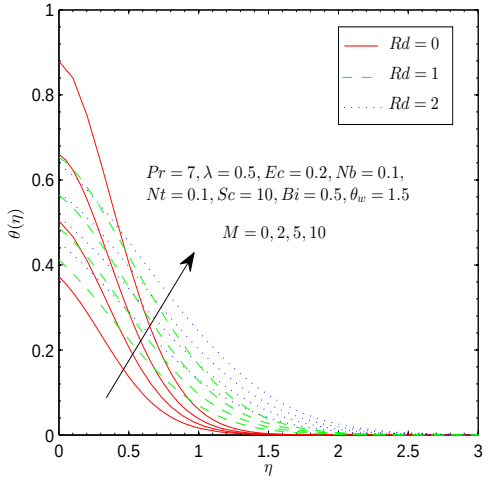

Figure 6.11: Effect of M and Rd on θ.

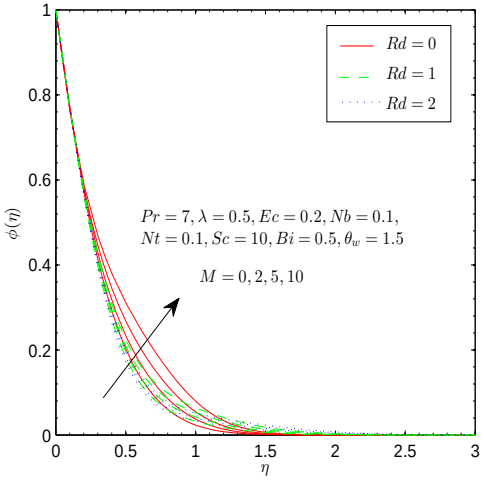

Figure 6.12: Effect of M and Rd on ϕ.

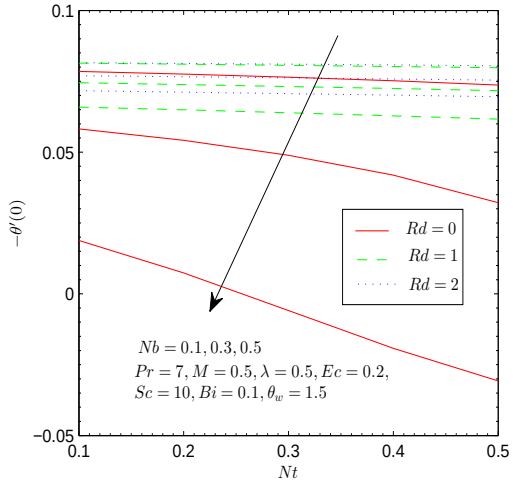

Figure 6.13: Effect of Nt, Nb, Rd on Nur.

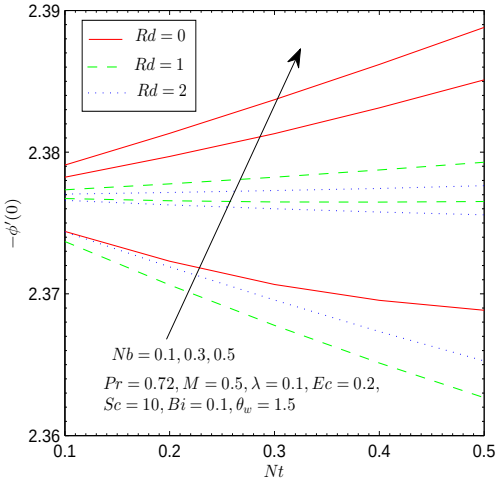

Figure 6.14: Effect of Nt, Nb, Rd on Shr.

Chapter 7

About non-linear radiative heat flux in the boundary layer flow over a moving rigid plate

7.1 Introduction

A laminar two-dimensional incompressible flow of an electrically conducting fluid over a moving flat plate with a parallel free stream is considered. Nonlinear radiative heat transfer with Joule heating and viscous dissipation effects is analyzed. The governing equations are first reduced into self-similar forms and then solved for the numerical solutions by shooting method. The results are compared with the available studies is some special cases and found in excellent agreement. It is noticed that an increase in the magnetic field strength leads to a decrease in the momentum boundary layer thickness and enhancement in the rate of heat transfer from the plate. It is also observed that temperature and heat transfer from the plate increase when radiation effect is strengthened.

7.2 Problem Formulation

Consider the two-dimensional incompressible flow and heat transfer over a moving flat plate in the presence of parallel free stream. The plate (situated at $y = 0$) is moving with the constant velocity U_w and U_∞ be the fluid velocity outside the boundary layer. The magnetic field of strength $B(x) = B_0 x^{-1/2}$ is applied in the vertical direction whereas the induced magnetic field is neglected by assuming small magnetic Reynolds number.

Heat transfer analysis subject to nonlinear thermal radiation is performed. In addition, the combined effects of Joule heating and viscous dissipation are taken into account. The plate is maintained at constant temperature T_w while T_∞ denotes the ambient fluid temperature.

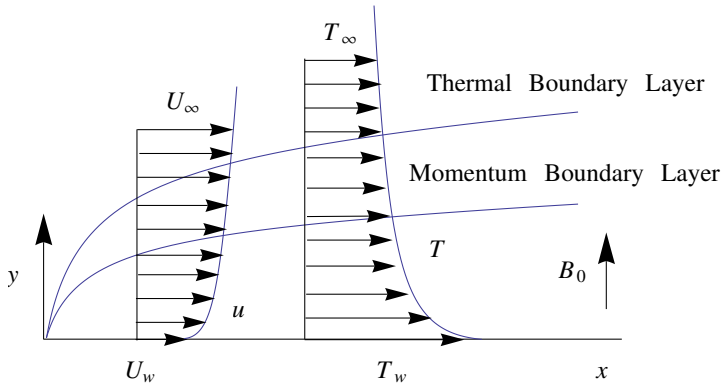

Figure 7.1: Physical sketch of the problem.

The boundary layer equations governing the flow and heat transfer are (see Cortell [8])

$$\frac{\partial u}{\partial x}+\frac{\partial v}{\partial y}=0, \tag{7.1}$$

$$u\frac{\partial u}{\partial x}+v\frac{\partial u}{\partial y}=\nu\frac{\partial^2 u}{\partial y^2}+\frac{\sigma B^2}{\rho}\left(U_\infty-u\right), \tag{7.2}$$

$$u\frac{\partial T}{\partial x}+v\frac{\partial T}{\partial y}=\alpha\frac{\partial^2 T}{\partial y^2}-\frac{1}{\rho C_p}\left(\frac{\partial q_r}{\partial y}\right)+\frac{\nu}{C_p}\left(\frac{\partial u}{\partial y}\right)^2+\frac{\sigma B^2}{\rho C_p}\left(U_\infty-u\right)^2. \tag{7.3}$$

The boundary conditions in the present problem are as below:

$$\begin{aligned} &u=U_w,\ v=0,\ T=T_w \qquad \text{at } y=0,\\ &u\to U_\infty,\ T\to T_\infty \qquad\quad \text{as } y\to\infty. \end{aligned} \tag{7.4}$$

In the above equations u and v are the velocity components along the $x-$ and $y-$ directions respectively, ν is the kinematic viscosity, ρ is the density of the fluid, σ is the conductance of the fluid, T is the temperature, α is the thermal diffusivity, C_p is the specific heat at constant pressure and q_r is the radiative heat flux. The radiative heat flux expression in Eq. (7.3) is given by the Rosseland formula [123] as

$$q_r=-\frac{4\sigma^*}{3k^*}\frac{\partial T^4}{\partial y}=-\frac{16\sigma^*}{3k^*}T^3\frac{\partial T}{\partial y}, \tag{7.5}$$

where σ^* and k^* are the Stefan-Boltzman constant and the mean absorption coefficient respectively. Now Eq. (7.3) can be written as

$$u\frac{\partial T}{\partial x}+v\frac{\partial T}{\partial y}=\frac{\partial}{\partial y}\left[\left(\alpha+\frac{16\sigma^*T^3}{3\rho C_pk^*}\right)\frac{\partial T}{\partial y}\right]+\frac{\nu}{C_p}\left(\frac{\partial u}{\partial y}\right)^2+\frac{\sigma B^2}{\rho C_p}\left(U_\infty-u\right)^2. \tag{7.6}$$

Introducing the following dimensionless variables

$$\eta=y\sqrt{\frac{U}{2\nu x}},\ u=U\frac{df}{d\eta},\ v=-\sqrt{\frac{U\nu}{2x}}\left(f-\eta\frac{df}{d\eta}\right),\ \theta=\frac{T-T_\infty}{T_w-T_\infty}, \tag{7.7}$$

where $U=U_w+U_\infty$ now Eq.(7.1) is identically satisfied and Eqs.(7.2) and (7.6) become

$$\frac{d^3f}{d\eta^3}+f\frac{d^2f}{d\eta^2}+M\left(\gamma-\frac{df}{d\eta}\right)=0, \tag{7.8}$$

$$\frac{1}{Pr}\frac{d}{d\eta}\left[\left(1+Rd\Big(1+(\theta_w-1)\theta\Big)^3\right)\frac{d\theta}{d\eta}\right]+f\frac{d\theta}{d\eta}+Ec\left(\frac{d^2f}{d\eta^2}\right)^2+2MEc\left(\gamma-\frac{df}{d\eta}\right)^2=0, \tag{7.9}$$

with corresponding boundary conditions

$$\begin{aligned}&f(0)=0,\ f'(0)=1-\gamma,\ \theta(0)=1,\\&f'(\infty)\to\gamma,\ \theta(\infty)\to 0,\end{aligned} \tag{7.10}$$

where $M=\sigma B_0^2/\rho U$ is the Hartman number, $\gamma=U_\infty/U$ is the velocity ratio, $Ec=U^2/C_p(T_w-T_\infty)$ is the Eckert number, $\theta_w=T_w/T_\infty$ is the temperature ratio parameter, $Pr=\nu/\alpha$ is the Prandtl number, and $Rd=16\sigma^*T_\infty^3/3kk^*$ is the radiation parameter. Physical quantities of practical interest in this study are the skin friction coefficient C_f and the local Nusselt number Nu_x defined as

$$\begin{aligned}C_f&=\frac{\tau_w}{\rho U^2};\ \tau_w=\mu\left(\frac{\partial u}{\partial y}\right)_{y=0},\\Nu_x&=\frac{xq_w}{k(T_w-T_\infty)};\ q_w=-k\left(\frac{\partial T}{\partial y}\right)_{y=0}+(q_r)_{y=0},\end{aligned} \tag{7.11}$$

where τ_w is the wall shear stress and q_w is the wall heat flux. Now using dimensionless quantities from Eq. (7.7) in Eq. (7.11), we get

$$\begin{aligned}\frac{\sqrt{2Re_x}}{2}C_f&=f''(0),\\\frac{Nu_x}{\sqrt{2Re_x}}&=-\Big[1+Rd\theta_w^3\Big]\theta'(0)=Nur,\end{aligned} \tag{7.12}$$

where $Re_x=Ux/\nu$ is the local Reynolds number. It is worth mentioning here that when $\gamma=1$, Eq. (7.8) subject to the boundary conditions (7.10) reduces to classical Blasius problem [1] while $\gamma=0$ corresponds to the Sakiadis flow problem [2].

7.3 Numerical Method

The dimensionless mathematical problems given in Eqs. (7.8)-(7.9) with the boundary conditions (7.10) have been solved numerically by shooting method with fourth-fifth-order Runge-Kutta integration technique. Before employing the Runge-Kutta integration scheme, first we reduce the governing differential equations into a set of first order ODEs. Let $x_1 = \eta, x_2 = f, x_3 = f', x_4 = f'', x_5 = \theta, x_6 = \theta'$. We obtain the following system:

$$\begin{pmatrix} x_1' \\ x_2' \\ x_3' \\ x_4' \\ x_5' \\ x_6' \end{pmatrix} = \begin{pmatrix} 1 \\ x_3 \\ x_4 \\ M\left(x_3 - \gamma\right) - x_2 x_4 \\ x_6 \\ \frac{-Pr\left(x_2 x_6 + Ec x_4^2 + 2MEc(x_3-\gamma)^2\right) - 3Rd x_6^2(\theta_w - 1)\left(1+(\theta_w-1)x_5\right)^2}{1+Rd\left(1+(\theta_w-1)x_5\right)^3} \end{pmatrix}, \tag{7.13}$$

and the corresponding initial conditions are:

$$\begin{pmatrix} x_1 \\ x_2 \\ x_3 \\ x_4 \\ x_5 \\ x_6 \end{pmatrix} = \begin{pmatrix} 0 \\ 0 \\ 1-\gamma \\ u_1 \\ 1 \\ u_2 \end{pmatrix}. \tag{7.14}$$

The above nonlinear coupled ODEs along with initial conditions are solved using fourth-fifth order Runge-Kutta integration technique. The computed results for $f''(0)$ are compared with those of Cortell [8] and found in very good agreement as can be seen from Table 7.1.

7.4 Numerical Results and Discussion

Fig. 7.2 depicts the variation in the horizontal velocity with an increase in the velocity ratio parameter γ. It is seen that velocity increases and the boundary layer thickness decreases with an increase in γ when $0 \leq \gamma < 0.5$. The flow has an inverted boundary layer structure and the velocity of the plate is greater than the free stream velocity in

this range of γ. The velocity field f' is an increasing function of γ when $\gamma > 0.5$. When γ is increased in this case, the velocity profiles approach the free stream velocity at large distance from the plate indicating an increase in the momentum boundary layer thickness. The behavior of Hartman number M on the velocity distribution is examined for two different values of γ (see Fig. 7.3). The results reveal that velocity decreases with an increase in M when $\gamma < 0.5$. However velocity is directly proportional to the magnetic field strength when $\gamma > 0.5$. In both these cases, the profiles approach the free stream at smaller values of η when M is increased. This leads to the conclusion that momentum boundary layer thins when magnetic field strength is increased for any considered value of γ. This opposition in the momentum transport is due to the occurrence of Lorentz force induced by the applied magnetic field perpendicular to the flow.

Dimensionless skin friction coefficient versus the velocity ratio γ has been plotted for different values of M in the Fig. 7.4. The magnitude of skin friction coefficient increases with an increase in M. When $0 \leq \gamma < 0.5$, the wall velocity gradient is negative (i.e $\partial u/\partial y|_{y=0} < 0$) (as pointed out by Cortell [8]) and continues to decrease with an increment in γ. On the other hand when $\gamma > 0.5$, shear stress at the plate is positive and increases when γ is increased.

Fig. 7.5 shows the influence of Prandtl number Pr on the temperature distribution. For a smaller Prandtl number fluid (such as air and other gases) the thermal diffusivity is dominant (i.e heat conduction is very effective compared to pure convection). On the other hand, convection becomes dominant in transferring energy from the plate compared to pure conduction in case of large Prandtl number fluid (such as water, engine oil etc.). Thus increase in Pr corresponds to decrease the thermal boundary layer thickness and increase in the rate of heat transfer at the plate. Moreover the variation in thermal boundary layer thickness is pronounced for a stronger thermal radiation effect.

The impact of Joule heating on the temperature θ can be described from Fig. 7.6. The resistance offered by Lorentz force to the fluid motion enhances the temperature and consequently the thermal boundary layer thickens. The increase in temperature θ with an increase in M is significant when the thermal radiation effect is enhanced. Fig. 7.7 depicts the effect of Eckert number Ec on the temperature distribution. The process in which kinetic energy from the fluid motion is irreversibly converted into internal energy (that heats up the fluid) is known as viscous dissipation. Increasing values of Ec indicates larger heat generation due to friction which rises the temperature. Interestingly, the viscous dissipation effect has a minor impact on the temperature distribution for sufficiently

large values of the radiation parameter. The bigger temperature ratio parameter $\theta_w = T_w/T_\infty$ indicates larger temperature at the plate compared to ambient. Increase in θ_w corresponds to hotter surface which consequently rises the fluid temperature (see Fig. 7.8). Fig. 7.9 shows that, irrespective of the chosen range of values of velocity ratio γ, the temperature θ increases with an increase in γ. Fig. 6.7.10 plots the wall temperature gradient versus θ_w for different values of radiation parameter Rd. When $\theta_w \cong 1$, $-\theta'(0)$ tends to a constant value for sufficiently smaller values of Rd which is in accordance with Cortell [113]. Table 7.2 provides the numerical values of wall temperature gradient for various values of parameters. $\theta'(0)$ is negative since the plate is hotter than the fluid and heat, therefore, flows from the plate to the fluid. It can be observed from Fig. 7.5 that temperature profiles become increasingly steeper near the wall by increasing Pr (i.e by assuming larger convection compared to conduction). In other words, the local Nusselt number (being directly proportional to the wall slope of temperature function) increases with an increase in Pr. It is observed that heat transfer from the plate can be enhanced by increasing the magnetic field strength. The behaviors of M and Ec on the local Nusselt number are similar in a qualitative sense. An augmentation in θ_w corresponds to decrease the rate of heat transfer from the plate. As already indicated by Cortell [113], $|\theta'(0)|$ approaches the zero value for sufficiently bigger values of θ_w. It is quite obvious that increase in radiation parameter Rd enhances the heat flux from the plate which escalates the magnitude of local Nusselt number.

7.5 Concluding Remarks

Nonlinear radiation heat transfer effects on the steady flow over a moving plate in a uniform free stream are studied. The inclusion of nonlinear radiative effects in the energy equation led to highly nonlinear but interesting differential equation. It is worth mentioning here that similarity solution is possible only when magnetic field strength is proportional to $x^{-1/2}$. The numerical solutions are computed by shooting method. The major conclusions drawn in this work may be summarized as:

a. In contrast to the linear radiative heat transfer problem, the present problem involves an additional temperature ratio parameter ($\theta_w = T_w/T_\infty$) which is an indicator of the difference between the surface temperature and the ambient fluid temperature.

b. Temperature θ increases and heat flux from the plate decreases when θ_w is increased. In fact $\theta'(0)$ approach to the zero when θ_w is increased.

c. Irrespective of the chosen value of velocity ratio γ, an increase in the magnetic field strength leads to a thinner boundary layer and increase in the temperature and heat transfer rate from the plate.

d. Temperature and the thermal boundary layer thickness decrease with an increase in Pr. This reduction is accompanied with the larger heat transfer from the plate.

e. An augmentation in the radiation parameter Rd enhances the thermal boundary layer thickness and heat transfer from the plate with the other parameters fixed.

Table 7.1: Comparison of values of $f''(0)$ with those of Cortell [8].

γ	M	$f''(0)$	
		Cortell [8]	Present Solution
0.0	0	-0.627547	-0.627555
0.2		-0.363308	-0.363336
0.4		-0.115777	-0.115809
0.6		0.109652	0.109638
0.8		0.307378	0.307354
1.0		0.469602	0.469600
0.0	0.5		-0.929473
	1.5		-1.359455
1.0	0.5		0.835273
	1.5		1.297384

Table 7.2: Numerical values of $-\theta'(0)$ for various parametric values.

Pr	γ	M	Ec	θ_w	Rd	$-\theta'(0)$
0.72	0.6	0.5	0.2	1.5	1	0.204437
1						0.238759
3						0.399756
7	0	0.5	0.2	1.5	1	0.476978
	0.3					0.625676
	0.7					0.563905
	1					0.325771
	0.6	0	0.2	1.5	1	0.589997
		1				0.618554
		2				0.625619
		0.5	0	1.5	1	0.603442
			0.5			0.605198
			1			0.585724
			0.2	1.5	1	0.606931
				2		0.380534
				3		0.198860
				2	0	1.372612
					1	0.380534
					2	0.277017

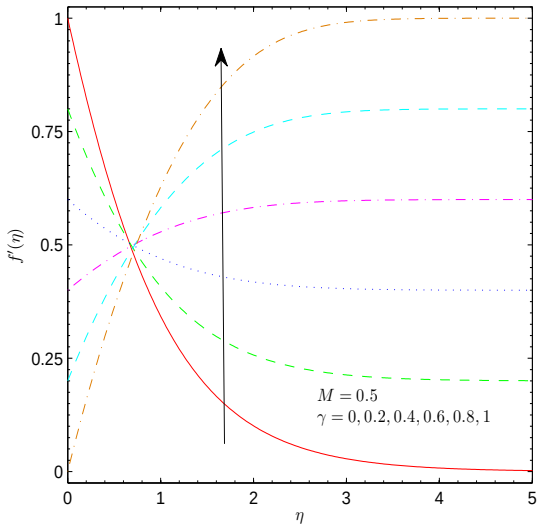

Figure 7.2: Effect of γ on f'.

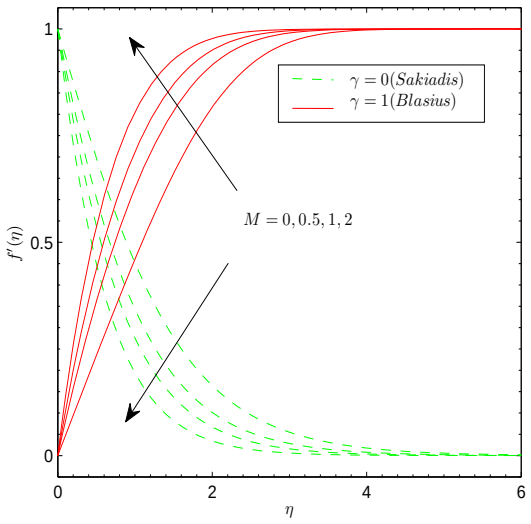

Figure 7.3: Effect of M on f'.

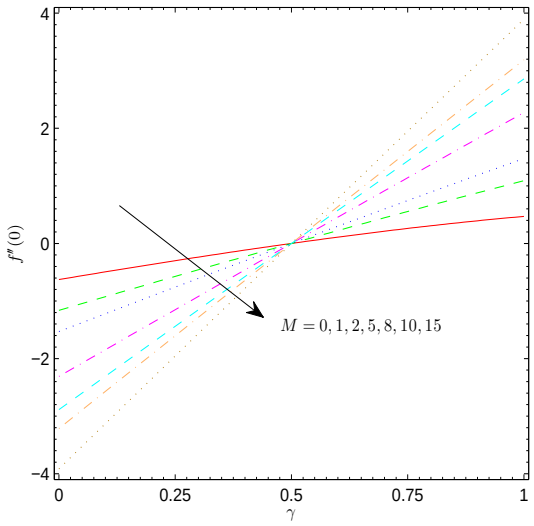

Figure 7.4: Effect of M and γ on $f''(0)$.

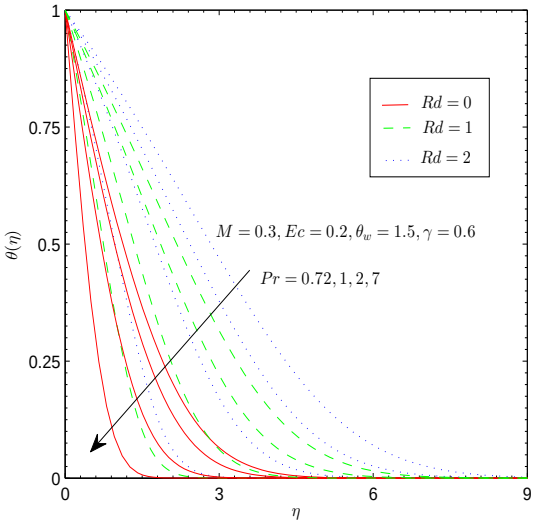

Figure 7.5: Effect of Pr and Rd on θ.

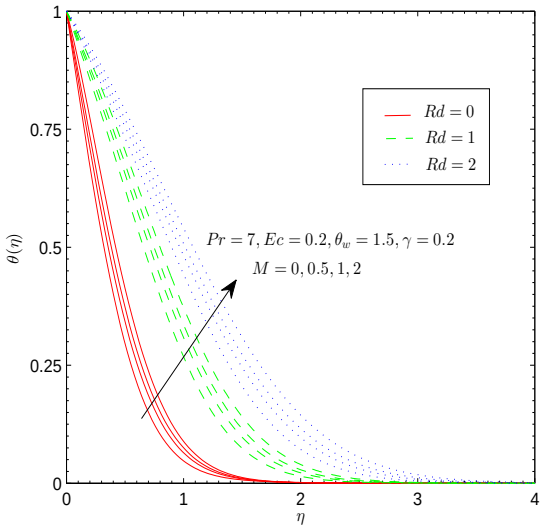

Figure 7.6: Effect of M and Rd on θ.

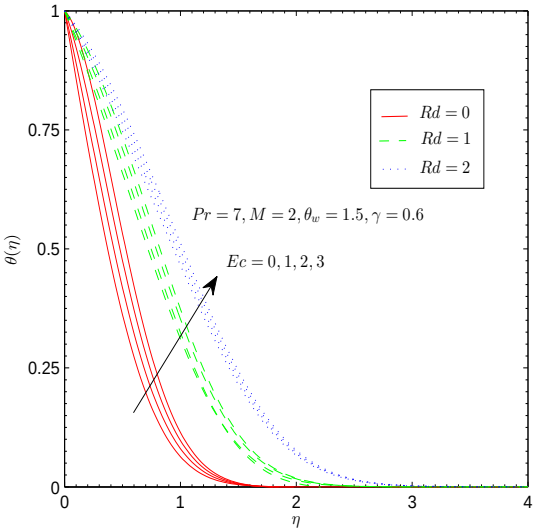

Figure 7.7: Effect of Ec and Rd on θ.

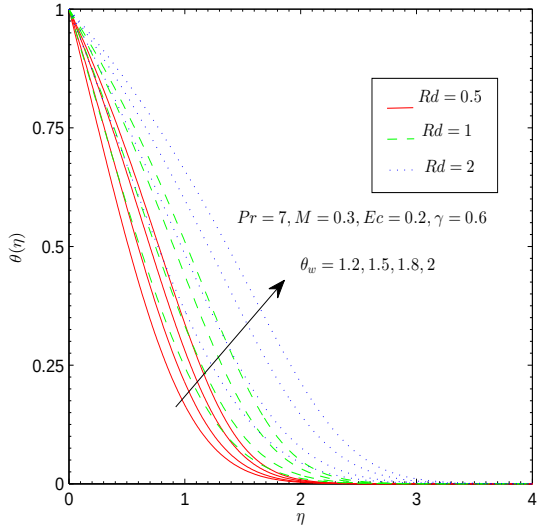

Figure 7.8: Effect of θ_w and Rd on θ.

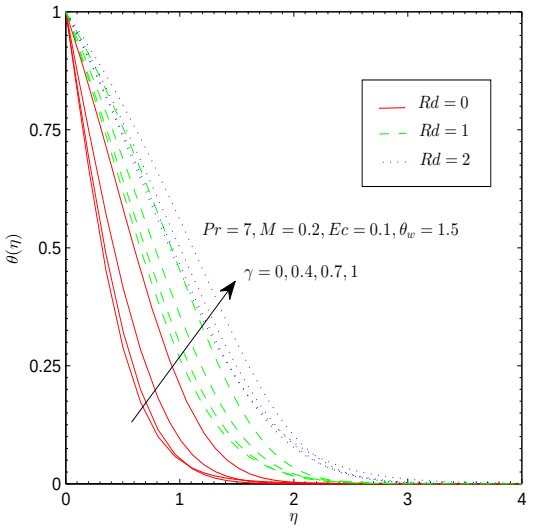

Figure 7.9: Effect of γ and Rd on θ.

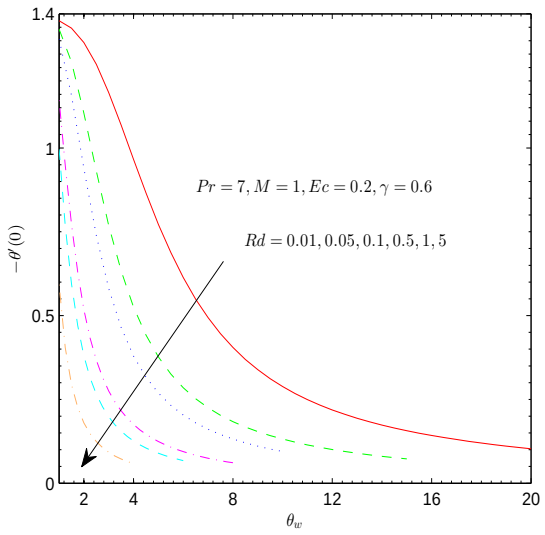

Figure 7.10: Effect of θ_w and Rd on $-\theta'(0)$.

Chapter 8

Non-linear radiation consideration in three-dimensional flow over a bi-directional stretching surface

8.1 Introduction

The steady laminar three-dimensional magnetohydrodynamic (MHD) boundary layer flow and heat transfer over a stretching sheet is investigated in this chapter. The sheet is linearly stretched in two lateral directions. Heat transfer analysis is performed by utilizing a nonlinear radiative heat flux in Rosseland approximation for thermal radiation. The developed nonlinear boundary value problems ($BVPs$) are solved numerically through fifth-order Runge-Kutta method using a shooting technique. To ascertain the accuracy of results the solutions are also computed by using built in function *bvp4c* of $MATLAB$. The behaviors of interesting parameters are carefully analyzed through graphs for velocity and temperature distributions. The dimensionless expressions of wall shear stress and heat transfer rate at the sheet are evaluated and discussed. It is seen that point of inflection of the temperature function exists for sufficiently large values of wall to ambient temperature ratio. The solutions are in excellent agreement with the previous studies in a limiting sense.

8.2 Problem Formulation

We consider the steady three-dimensional flow of an incompressible viscous fluid over a stretching sheet situated at $z = 0$. Heat transfer analysis in the presence of viscous dissipation and thermal radiation is considered. Let $U_w(x) = ax$, and $V_w(x) = by$, be the velocities of the stretching sheet in the $x-$ and $y-$ direction respectively, where a, b are positive constants. (see Fig.8.1). The uniform transverse magnetic field of strength B_0 is applied in the $z-$ direction whereas the induced magnetic field is neglected by assuming small magnetic Reynolds number.

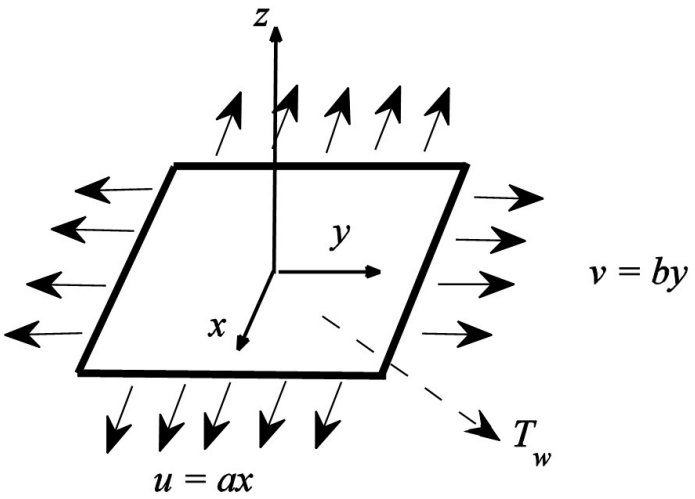

Figure 8.1: A physical sketch of the problem and coordinate system.

The boundary layer equations governing the steady three-dimensional flow are:

$$\frac{\partial u}{\partial x} + \frac{\partial v}{\partial y} + \frac{\partial w}{\partial z} = 0, \tag{8.1}$$

$$u\frac{\partial u}{\partial x} + v\frac{\partial u}{\partial y} + w\frac{\partial u}{\partial z} = \nu\frac{\partial^2 u}{\partial z^2} - \frac{\sigma B_0^2}{\rho}u, \tag{8.2}$$

$$u\frac{\partial v}{\partial x} + v\frac{\partial v}{\partial y} + w\frac{\partial v}{\partial z} = \nu\frac{\partial^2 v}{\partial z^2} - \frac{\sigma B_0^2}{\rho}v, \tag{8.3}$$

where ν is the kinematic viscosity, u, v and w are the velocity components in the $x-, y-$ and $z-$directions respectively. The boundary conditions in the present problem are:

$$\begin{aligned} &u = U_w(x) = ax,\ v = V_w(x) = by,\ w = 0, && \text{at } z = 0, \\ &u, v \to 0, && \text{as } z \to \infty. \end{aligned} \tag{8.4}$$

Invoking the following similarity transformations:

$$\eta = z\sqrt{\frac{a}{\nu}},\ u = ax\frac{df}{d\eta},\ v = ay\frac{dg}{d\eta},\ w = -\sqrt{a\nu}\,(f + g)\,. \tag{8.5}$$

Eq. (8.1) is identically satisfied and Eqs. (8.2) and (8.3) become:

$$\frac{d^3f}{d\eta^3} - \left(\frac{df}{d\eta}\right)^2 + (f+g)\frac{d^2f}{d\eta^2} - M\frac{df}{d\eta} = 0, \tag{8.6}$$

$$\frac{d^3g}{d\eta^3} - \left(\frac{dg}{d\eta}\right)^2 + (f+g)\frac{d^2g}{d\eta^2} - M\frac{dg}{d\eta} = 0, \tag{8.7}$$

with corresponding boundary conditions

$$\begin{aligned} &f(0) = 0,\ f'(0) = 1,\ g(0) = 0,\ g'(0) = c, \\ &f'(\infty) \to 0,\ g'(\infty) \to 0, \end{aligned} \tag{8.8}$$

where $c = b/a$ is velocity ratio, $M = \sigma B_0^2/\rho a$ is the Hartman number.

Physical quantities of practical interest in this study are the skin friction coefficient along $x-$ and $y-$ directions defined as under

$$\begin{aligned} C_{fx} &= \frac{\tau_{xz}}{\rho U_w^2};\ \tau_{xz} = \mu\left(\frac{\partial u}{\partial z}\right)_{z=0}, \\ C_{fy} &= \frac{\tau_{yz}}{\rho V_w^2};\ \tau_{yz} = \mu\left(\frac{\partial v}{\partial z}\right)_{z=0}, \end{aligned} \tag{8.9}$$

where $\tau's$ are the wall shear stress. Now using dimensionless quantities from Eq. (8.5) in Eq. (8.9), we get

$$\begin{aligned} &\sqrt{Re_x}C_{fx} = f''(0), \\ &c^{3/2}\sqrt{Re_y}C_{fy} = g''(0), \end{aligned} \tag{8.10}$$

where $Re_x = U_w x/\nu$ and $Re_y = V_w y/\nu$ are the local Reynolds number along $x-$ and $y-$ directions respectively.

8.3 Heat Transfer Analysis

Under usual boundary layer assumptions, the energy equation in the presence of thermal radiation and viscous dissipation effects is given by:

$$u\frac{\partial T}{\partial x} + v\frac{\partial T}{\partial y} + w\frac{\partial T}{\partial z} = \alpha\frac{\partial^2 T}{\partial z^2} - \frac{1}{\rho C_p}\left(\frac{\partial q_r}{\partial z}\right), \tag{8.11}$$

The relevant boundary conditions in this situation are:

$$T = T_w \text{ at } z = 0;\ T \to T_\infty \text{ as } z \to \infty, \tag{8.12}$$

where T is the temperature, α is the thermal diffusivity, C_p is the specific heat at constant pressure and q_r is the radiative heat flux, T_w, T_∞ are the sheet temperature and the

ambient fluid temperature respectively with $T_w > T_\infty$. Using the Rosseland approximation for thermal radiation [123] and applying to optically thick media, the radiative heat flux is simplified as:

$$q_r = -\frac{4\sigma^*}{3k^*}\frac{\partial T^4}{\partial z} = -\frac{16\sigma^*}{3k^*}T^3\frac{\partial T}{\partial z}, \tag{8.13}$$

where σ^* and k^* are the Stefan-Boltzman constant and the mean absorption coefficient respectively. Now (8.11) can be expressed as:

$$u\frac{\partial T}{\partial x} + v\frac{\partial T}{\partial y} + w\frac{\partial T}{\partial z} = \frac{\partial}{\partial z}\left[\left(\alpha + \frac{16\sigma^* T^3}{3\rho C_p k^*}\right)\frac{\partial T}{\partial z}\right]. \tag{8.14}$$

It is worth mentioning here that in the previous studies on thermal radiation T^4 in Eq. (8.13) was expanded about the ambient temperature T_∞. However in the present case this has been avoided to obtain more meaningful and practically useful results. Defining the non-dimensional temperature $\theta = (T - T_\infty)/T_w - T_\infty)$. Eq. (8.11) takes the following form

$$\frac{1}{Pr}\frac{d}{d\eta}\left[\left(1 + Rd\Big(1 + (\theta_w - 1)\theta\Big)^3\right)\frac{d\theta}{d\eta}\right] + (f + g)\frac{d\theta}{d\eta} = 0, \tag{8.15}$$

with the following boundary conditions

$$\theta(0) = 1,\ \theta(\infty) \to 0, \tag{8.16}$$

where $Pr = \nu/\alpha$ is the Prandtl number and $Rd = 16\sigma^* T_\infty^3/3kk^*$ is the radiation parameter.

The heat transfer rate at the sheet in this case can be calculated using the local Nusselt number Nu_x defined as

$$Nu_x = \frac{xq_w}{k(T_w - T_\infty)};\ q_w = -k\left(\frac{\partial T}{\partial z}\right)_{z=0} + (q_r)_{z=0}, \tag{8.17}$$

where q_w is the wall heat flux. Now using dimensionless quantities we get

$$Re_x^{-1/2}Nu_x = -\Big[1 + Rd\theta_w^3\Big]\theta'(0) = Nur, \tag{8.18}$$

where $Re_x = U_w x/\nu$ is the local Reynolds number.

8.4 Numerical Method

The dimensionless momentum equations (8.6-8.7) and the energy equation (8.15) with the relevant boundary conditions have been solved numerically by shooting method using fourth-order Runge-Kutta integration technique. Before employing the Runge-Kutta

integration scheme, first we reduce the governing differential equations into a set of first order ODEs. Let $x_1 = \eta, x_2 = f, x_3 = f', x_4 = f'', x_5 = g, x_6 = g', x_7 = g'', x_8 = \theta, x_9 = \theta'$. We obtain the following system:

$$\begin{pmatrix} x_1' \\ x_2' \\ x_3' \\ x_4' \\ x_5' \\ x_6' \\ x_7' \\ x_8' \\ x_9' \end{pmatrix} = \begin{pmatrix} 1 \\ x_3 \\ x_4 \\ Mx_3 + x_3^2 - (x_2 + x_5)x_4 \\ x_6 \\ x_7 \\ Mx_6 + x_6^2 - (x_2 + x_5)x_7 \\ x_9 \\ \frac{-Pr(x_2+x_5)x_9 - 3Rdx_9^2(\theta_w-1)\left(1+(\theta_w-1)x_8\right)^2}{1+Rd\left(1+(\theta_w-1)x_8\right)^3} \end{pmatrix}, \tag{8.19}$$

and the corresponding initial conditions are:

$$\begin{pmatrix} x_1 \\ x_2 \\ x_3 \\ x_4 \\ x_5 \\ x_6 \\ x_7 \\ x_8 \\ x_9 \end{pmatrix} = \begin{pmatrix} 0 \\ 0 \\ 1 \\ u_1 \\ 0 \\ c \\ u_2 \\ 1 \\ u_3 \end{pmatrix}. \tag{8.20}$$

The above nonlinear coupled ODEs along with initial conditions are solved using fourth-fifth order Runge-Kutta integration technique.

8.5 Numerical Results and Discussion

The influence of embedding parameters on the velocity and temperature functions is described through graphical and numerical results. Figs. 8.2 and 8.3 show the effects of magnetic field on the dimensionless $x-$ and $y-$components of velocity for different values of velocity ratio c. The generalized unidirectional stretching wall problem can be recov-

ered by choosing $c = 0$. On the other hand $c = 1$ corresponds to the axisymmetric flow due to a stretching sheet. The magnetic parameter M has a significant impact on the solutions. The presence of a magnetic field restricts the fluid motion and as a consequence the velocity decreases. With a gradual increase in M, the Lorentz force associated with the magnetic field increases and it produces more resistance to the transport phenomena. Irrespective of the value of magnetic parameter M, the velocity field f' and the boundary layer thickness are decreasing functions of velocity ratio c. Fig. 8.4 indicates that shear stress in the both $x-$ and $y-$directions increase with an increase in velocity ratio c. As a result the entrainment velocity $f(\infty) + g(\infty)$ is also an increasing function of c.

Fig. 8.5 displays the behavior of radiation parameter Rd on the temperature θ. The results are shown for different values of c. It is observed that the temperature θ decreases with an increase in c . In contrast to the linearized Rosseland approximation considered in previous studies the radiation parameter in the present study has a significant role on the thermal boundary layer as can be seen from Fig. 8.5. As expected the temperature and the thermal boundary layer thickness are increasing functions of Rd. Further the heat transfer rate at the sheet drastically decreases with an increase in Rd as the profiles become less steeper near the sheet as radiation parameter increases. The Prandtl number Pr is defined as the ratio of momentum diffusivity to the thermal diffusivity. It can be used to increase the rate of cooling in conducting flows. Temperature profiles for different values of Pr have been shown in the Fig. 8.6. Specifically, Prandtl number $Pr = 0.72, 1.0$ and 7.0 correspond to air, electrolyte solution such as salt water and water, respectively. The results are shown for $Rd = 0$ and $Rd = 1$. Fig. 8.6 indicates that temperature θ and the thermal boundary layer thickness decrease with an increase in Pr. This is due to the fact that larger Prandtl number has a relatively lower thermal diffusivity which decreases conduction and thereby increases variation in the thermal characteristics. As expected the thermal penetration is limited for the fluids with larger Prandtl number when compared with the small Prandtl number fluids. In this work the variation in the temperature θ with an increase in Pr is larger than that of previously reported works with the linearized Rosseland approximation. Figs. 8.7 and 8.8 compare the results of linear and non-linear radiation for different values of Rd when $\theta_w = 1.1$ and $\theta_w = 3$ respectively. It is seen that linear and non-linear results match each other better at $\theta_w = 1.1$ when compared with $\theta_w = 3$. The profiles show a significant deviation as the radiation parameter is gradually increased. Thus it can be concluded that linear and non-linear radiation results match up smoothly when θ_w is close to one (say $\theta_w = 1.1$) and is sufficiently small (say

$Rd < 0.5$). Fig. 8.9 plots the wall temperature gradient versus θ_w for different values of radiation parameter Rd . When $\theta_w \approx 1, \theta'(0)$ tends to a constant value for sufficiently smaller values of $Rd \approx 0.01$ which is in accordance with Cortell [113].

Table 8.1 shows the comparison of present solutions for $f''(0)$ and $g''(0)$ with those reported by Wang [5] and Liu and Andersson [9]. The present results are found in excellent agreement with those provided in [5] and [9]. We have also noticed that $|\theta'(0)|$ increases with an increase in the values of indices r and s. This observation leads to the conclusion that heat transfer rate at the sheet can be increased by increasing the variation of wall temperature along the $x-$ and $y-$directions. The numerical values of local Nusselt number $\theta'(0)$ are given for various parametric values in Table 8.2. It is noticeable that wall temperature gradient approaches the zero value as θ_w is increased indicating the existence of a point of inflection for the temperature distribution. This outcome is consistent with the findings obtained for two-dimensional flow. Irrespective of magnetic parameter M we observe a significant increase in the local Nusselt number as the thermal radiation effect intensifies. We noticed earlier in the graphical results that temperature profiles become increasingly steeper as Pr increases. As a result the Nusselt number $\theta'(0)$, being proportional to the initial slope, increases with an increase in Pr.

8.6 Concluding Remarks

MHD three-dimensional flow and heat transfer due to a bi-directional stretching sheet is investigated in presence of thermal radiation. In this work the temperature function in the radiation term of energy equation is not further expanded about the ambient temperature. This results in highly nonlinear but an interesting energy equation which is governed by an additional temperature ratio parameter θ_w. The developed differential system is solved numerically through the shooting method with fifth-order Runge-Kutta integration technique. The key points of the present work may be summarized as follows:

a. It is observed that radiation parameter has a strong effect on the thermal boundary layer for any considered value of Prandtl number. The temperature θ and the thermal boundary layer thickness increase when the thermal radiation effect strengthens.

b. The temperature and the thermal boundary layer thickness are decreasing functions of Pr. This decrease accompanies with the larger rate of heat transfer at the

bounding surface.

c. The numerical results of $|\theta'(0)|$ are compared with those of Liu and Andersson [9] in the absence of thermal radiation effects and found in an excellent agreement.

d. The current analysis for two-dimensional and axisymmetric flows can be obtained as special cases of the present study. To the best of our knowledge, this is the fundamental study of the application of nonlinear Rosseland approximation for thermal radiation in the three-dimensional boundary layer flow.

Table 8.1: Numerical values of $f''(0)$and $g''(0)$ with the previous studies for $M = 0$.

c	Present solution		Wang [5]		Liu and Andersson [9]	
	$f''(0)$	$g''(0)$	$f''(0)$	$g''(0)$	$f''(0)$	$g''(0)$
0.0	-1	0	-1	0	-1	0
0.25	-1.048811	-0.194564	-1.048813	-0.194564	-1.048813	-0.194565
0.50	-1.093095	-0.465205	-1.093097	-0.465205	-1.093096	-0.465206
0.75	-1.134486	-0.794618	-1.093097	-0.794622	-1.134486	-0.794619
1.0	-1.173721	-1.173721	-1.173720	-1.173720	-1.173721	-0.173721

Table 8.2: Heat transfer rate at the sheet$-\theta'(0)$ when $c = 0.5$.

Pr	M	θ_w	Rd	$-\theta'(0)$
7	0	-	0	2.354383
		1	1	1.593196
		2	1	0.547158
	1	-	0	2.267987
		1	1	1.507175
		2	1	0.499324
0.72	0.5	-	0	0.547237
		1	1	0.319122
		2	1	0.083342
	1.5	-	0	0.487439
		1	1	0.274844
		2	1	0.068696

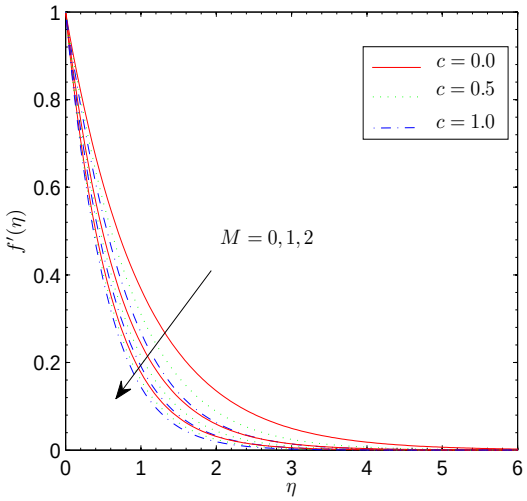

Figure 8.2: Effect of M and c on f'.

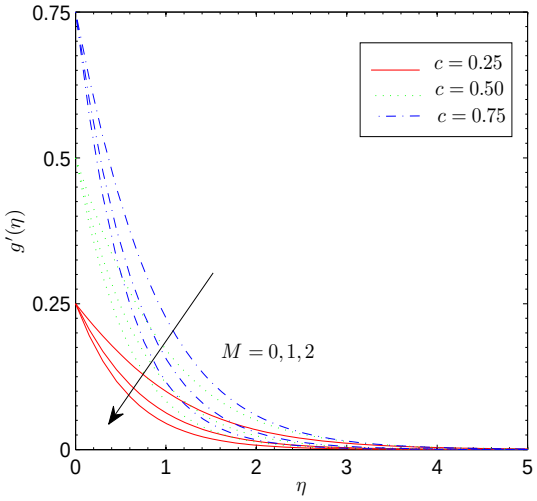

Figure 8.3: Effect of M and c on g'.

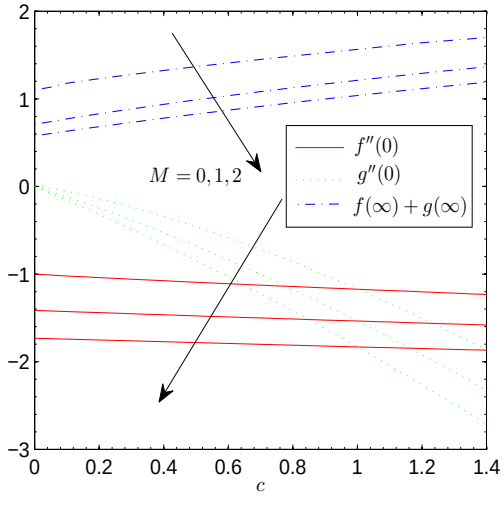

Figure 8.4: Effect of M and c on $f''(0)$ and $g''(0)$.

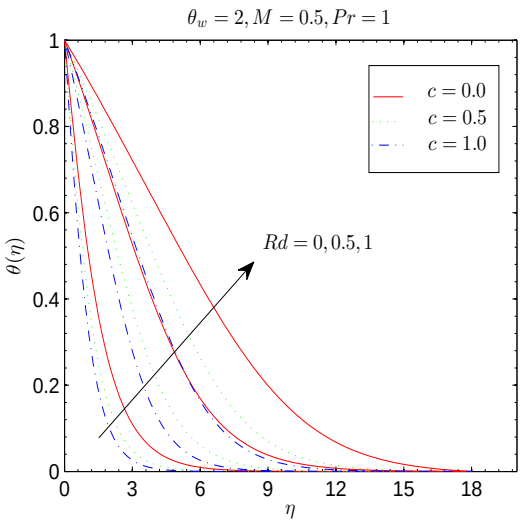

Figure 8.5: Effect of c and Rd on θ.

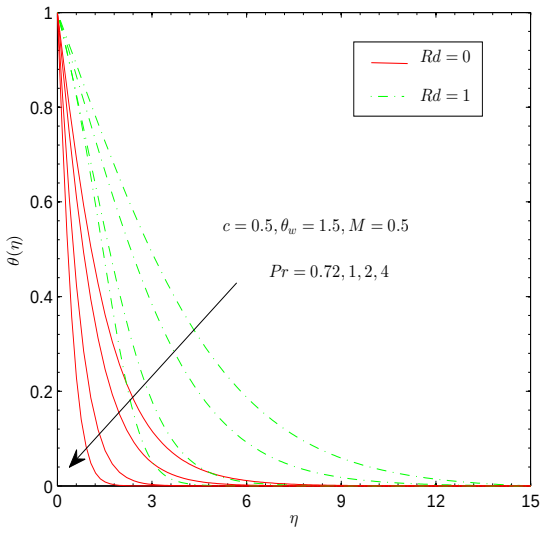

Figure 8.6: Effect of Pr and Rd on θ.

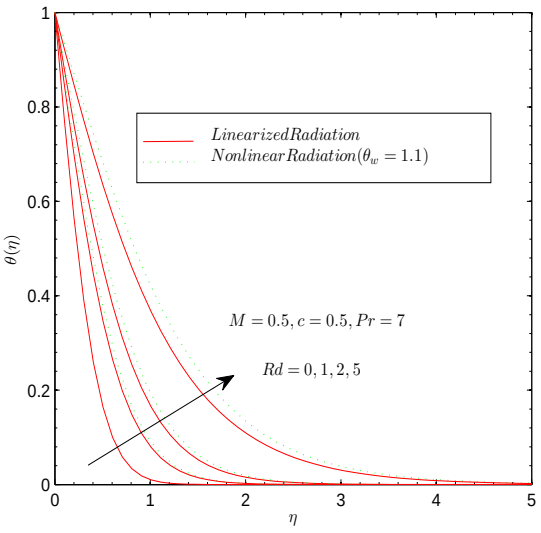

Figure 8.7: Effect Rd on θ for $\theta_w = 1.1$.

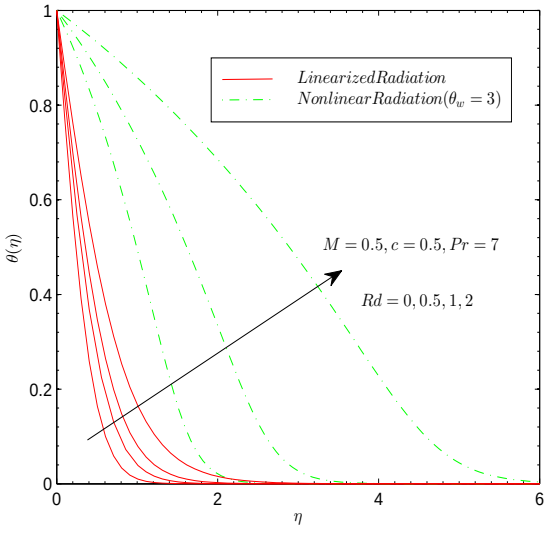

Figure 8.8: Effect Rd on θ for $\theta_w = 3$.

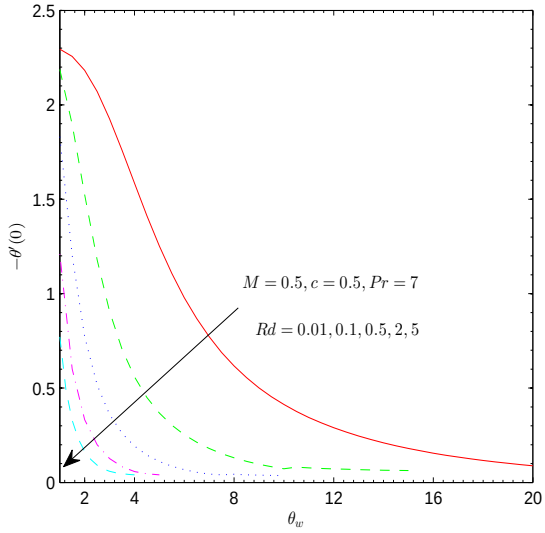

Figure 8.9: Effect of Rd and θ_w on $-\theta'(0)$.

Chapter 9

Bi-directional exponentially stretching radiative surface in a viscous fluid

9.1 Introduction

Analysis is performed to explore the characteristics of non-linear radiation heat transfer in the three-dimensional flow above an exponentially stretching sheet. The temperature is also exponentially distributed across the sheet. Local similarity solutions of the arising differential equations are computed through shooting method with fourth-fifth-order Runge-Kutta integration technique. The results corresponding to different values of temperature exponent parameter (A) reveal some interesting facts about the temperature distribution. The fluid's temperature is largely influenced with the variations in wall to ambient temperature ratio. The solutions are found in excellent agreement with the existing studies in the literature.

9.2 Problem Formulation

We consider the steady three-dimensional flow of an incompressible viscous fluid over a plane elastic sheet stretched exponentially in two lateral directions. The sheet is situated at $z = 0$. Heat transfer analysis in the presence of viscous dissipation and thermal radiation is considered. Let $U_w(x, y) = U_0 e^{(x+y/L)}$ and $V_w(x, y) = V_0 e^{(x+y/L)}$be the velocities of the stretching sheet in the $x-$ and $y-$ direction respectively, where U_o, V_0 and L are positive constants. The sheet is maintained at temperature $T_w = T_\infty + T_0 e^{A(x+y/2L)}$ and T_∞ denotes the ambient temperature (see Fig. 9.1). We have considered both positive

and negative value for temperature exponent parameter A in our analysis.

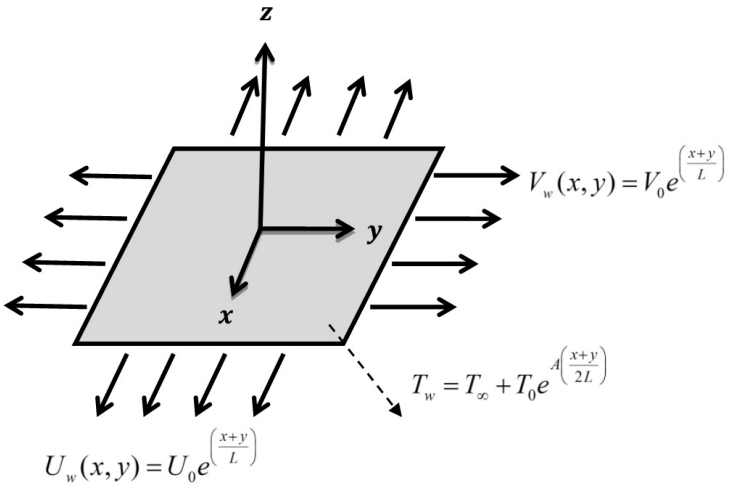

Figure 9.1: Physical configuration and coordinate system.

Under usual boundary layer assumptions, the equations governing the steady three-dimensional flow and heat transfer are:

$$\frac{\partial u}{\partial x} + \frac{\partial v}{\partial y} + \frac{\partial w}{\partial z} = 0, \tag{9.1}$$

$$u\frac{\partial u}{\partial x} + v\frac{\partial u}{\partial y} + w\frac{\partial u}{\partial z} = \nu\frac{\partial^2 u}{\partial z^2}, \tag{9.2}$$

$$u\frac{\partial v}{\partial x} + v\frac{\partial v}{\partial y} + w\frac{\partial v}{\partial z} = \nu\frac{\partial^2 v}{\partial z^2}, \tag{9.3}$$

$$u\frac{\partial T}{\partial x} + v\frac{\partial T}{\partial y} + w\frac{\partial T}{\partial z} = \alpha\frac{\partial^2 T}{\partial z^2} - \frac{1}{\rho C_p}\left(\frac{\partial q_r}{\partial z}\right), \tag{9.4}$$

The boundary conditions in the present problem are:

$$\begin{aligned} &u = U_0 e^{\frac{x+y}{L}},\ v = V_0 e^{\frac{x+y}{L}},\ w = 0,\ T = T_\infty + T_0 e^{A\left(\frac{x+y}{2L}\right)} \quad \text{at } z = 0, \\ &u, v \to 0, \qquad T \to T_\infty \qquad\qquad\qquad \text{as } z \to \infty, \end{aligned} \tag{9.5}$$

where ν is the kinematic viscosity, u, v and w are the velocity components in the $x-, y-$ and $z-$directions respectively, T is the temperature, α is the thermal diffusivity, C_p is the specific heat at constant pressure and q_r is the radiative heat flux. Using the Rosseland approximation for thermal radiation [123] and applying to optically thick media, the radiative heat flux is simplified as:

$$q_r = -\frac{4\sigma^*}{3k^*}\frac{\partial T^4}{\partial z} = -\frac{16\sigma^*}{3k^*}T^3\frac{\partial T}{\partial z}, \tag{9.6}$$

where σ^* and k^* are the Stefan-Boltzman constant and the mean absorption coefficient respectively. Now (9.4) can be expressed as:

$$u\frac{\partial T}{\partial x}+v\frac{\partial T}{\partial y}+w\frac{\partial T}{\partial z}=\frac{\partial}{\partial z}\left[\left(\alpha+\frac{16\sigma^*T^3}{3\rho C_p k^*}\right)\frac{\partial T}{\partial z}\right]. \tag{9.7}$$

It is worth mentioning here that in the previous studies on thermal radiation T^4 in Eq. (9.6) was expanded about the ambient temperature T_∞. However in the present case this has been avoided to obtain more meaningful and practically useful results. Invoking the following similarity transformations:

$$\begin{aligned}&\eta=e^{\frac{x+y}{2L}}\sqrt{\frac{U_0}{2\nu L}}z,\ u=U_0e^{\frac{x+y}{L}}\frac{df}{d\eta},\ v=U_0e^{\frac{x+y}{L}}\frac{dg}{d\eta},\\&w=-e^{\frac{x+y}{2L}}\sqrt{\frac{\nu U_0}{2L}}\left(f+g+\eta\frac{df}{d\eta}+\eta\frac{dg}{d\eta}\right),\ \theta=\frac{T-T_\infty}{T_w-T_\infty}.\end{aligned} \tag{9.8}$$

Eq. (9.1) is identically satisfied and Eqs. (9.2-9.3) and (9.7) become:

$$\frac{d^3f}{d\eta^3}-2\left(\frac{df}{d\eta}+\frac{dg}{d\eta}\right)\frac{df}{d\eta}+(f+g)\frac{d^2f}{d\eta^2}=0, \tag{9.9}$$

$$\frac{d^3g}{d\eta^3}-2\left(\frac{df}{d\eta}+\frac{dg}{d\eta}\right)\frac{dg}{d\eta}+(f+g)\frac{d^2g}{d\eta^2}=0, \tag{9.10}$$

$$\frac{1}{Pr}\frac{d}{d\eta}\left[\left(1+Rd\Big(1+(\theta_w-1)\theta\Big)^3\right)\frac{d\theta}{d\eta}\right]+(f+g)\frac{d\theta}{d\eta}-A\theta\left(\frac{df}{d\eta}+\frac{dg}{d\eta}\right)=0, \tag{9.11}$$

with the corresponding boundary conditions

$$\begin{aligned}&f(0)=0,\ f'(0)=1,\ g(0)=0,\ g'(0)=\lambda,\ \theta(0)=1,\\&f'(\infty)\to 0,\ g'(\infty)\to 0,\ \theta(\infty)\to 0,\end{aligned} \tag{9.12}$$

where $\lambda=V_0/U_0$ is velocity ratio, $Pr=\nu/\alpha$ is the Prandtl number and $Rd=16\sigma^*T_\infty^3/3kk^*$ is the radiation parameter.

Physical quantities of practical interest in this study are the skin friction coefficient along $x-$ and $y-$ directions respectively and the local heat transfer rate at the sheet in this case can be calculated using the local Nusselt number Nu_x defined as under

$$\begin{aligned}&C_{fx}=\frac{\tau_{xz}}{\rho U_0^2/2};\ \tau_{xz}=\mu\left(\frac{\partial u}{\partial z}\right)_{z=0},\\&C_{fy}=\frac{\tau_{yz}}{\rho U_0^2/2};\ \tau_{yz}=\mu\left(\frac{\partial v}{\partial z}\right)_{z=0},\\&Nu_x=\frac{xq_w}{k(T_w-T_\infty)};\ q_w=-k\left(\frac{\partial T}{\partial z}\right)_{z=0}+(q_r)_{z=0},\end{aligned} \tag{9.13}$$

where $\tau's$ are the wall shear stress and q_w is the wall heat flux. Now using dimensionless quantities from Eq. (9.8) in Eq. (9.13), we get

$$\begin{aligned} e^{-3\left(\frac{x+y}{2L}\right)}\sqrt{\frac{Re}{2}}C_{fx} &= -f''(0), \\ e^{-3\left(\frac{x+y}{2L}\right)}\sqrt{\frac{Re}{2}}C_{fy} &= -g''(0), \\ e^{-\left(\frac{x+y}{2L}\right)}\frac{L}{x}\sqrt{\frac{2}{Re}}Nu_x &= -\left[1+Rd\theta_w^3\right]\theta'(0) = Nur, \end{aligned} \tag{9.14}$$

where $Re = U_0 L/\nu$ is the Reynolds number. Using Eq. (9.8), the vertical component of velocity at far field boundary can be expressed as

$$w(x,y,\infty) = -e^{\frac{x+y}{2L}}\frac{\nu}{L}\sqrt{\frac{Re}{2}}\left[f(\infty)+g(\infty)\right]. \tag{9.15}$$

9.3 Numerical Method

The dimensionless momentum equations (9.9), (9.10) and the energy equation (9.11) subject to the boundary conditions (9.12) have been solved numerically by shooting method with fourth-fifth-order Runge-Kutta integration technique. Before employing the Runge-Kutta integration scheme, first we reduce the governing differential equations into a set of first order ODEs. Let $x_1 = \eta, x_2 = f, x_3 = f', x_4 = f'', x_5 = g, x_6 = g', x_7 = g'', x_8 = \theta, x_9 = \theta'$. We obtain the following system:

$$\begin{pmatrix} x_1' \\ x_2' \\ x_3' \\ x_4' \\ x_5' \\ x_6' \\ x_7' \\ x_8' \\ x_9' \end{pmatrix} = \begin{pmatrix} 1 \\ x_3 \\ x_4 \\ 2(x_3+x_6)x_3 - (x_2+x_5)x_4 \\ x_6 \\ x_7 \\ 2(x_3+x_6)x_6 - (x_2+x_5)x_7 \\ x_9 \\ \frac{-Pr((x_2+x_5)x_9 - A(x_3+x_6)x_8) - 3Rdx_9^2(\theta_w-1)\left(1+(\theta_w-1)x_8\right)^2}{1+Rd\left(1+(\theta_w-1)x_8\right)^3} \end{pmatrix}, \tag{9.16}$$

and the corresponding initial conditions are:

$$\begin{pmatrix} x_1 \\ x_2 \\ x_3 \\ x_4 \\ x_5 \\ x_6 \\ x_7 \\ x_8 \\ x_9 \end{pmatrix} = \begin{pmatrix} 0 \\ 0 \\ 1 \\ u_1 \\ 0 \\ \lambda \\ u_2 \\ 1 \\ u_3 \end{pmatrix}. \tag{9.17}$$

The above nonlinear coupled ODEs along with initial conditions are solved using fourth-fifth order Runge-Kutta integration technique.

9.4 Numerical Results and Discussion

In this section, the physical interpretation to the behaviors of embedded parameters is given through graphs for velocity and temperature distributions. In order to validate the solutions, we compare our results with those obtained by Magyari and Keller [6] and Liu et al. [10] in the absence of thermal radiation. A very good agreement is found as can be seen in Tables 9.1 and 9.2. Fig. 9.2 shows the profiles of velocity components for different values of velocity ratio parameter λ. Larger values of λ indicates larger velocity of the stretching sheet along the y-direction compared to $x-$direction. Due to this reason the $y-$component of velocity increases and while the $x-$component of velocity simultaneously decreases when λ is increased. It is also important to note that $\lambda = 0$ corresponds to two-dimensional flow case and $\lambda = 1$ indicates the axisymmetric flow. Fig. 9.3 plots the skin friction coefficients and entrainment velocity against the velocity ratio parameter λ. Here the results of wall shear stress are complimenting the results shown in Fig. 9.2. Entrainment velocity is negative showing the downward flow in vertical direction which is the consequence of bi-directional stretching sheet.

Fig. 9.4 captures the influence of Prandtl number Pr and radiation parameter Rd on dimensionless temperature function. The Prandtl number Pr, being the ratio of momentum diffusivity to thermal diffusivity, controls the relative thickness of the momentum and

thermal boundary layers. Larger Prandtl number decreases thermal diffusion and hence offers less penetration depth for thermal boundary layer. As a consequence temperature θ decreases and thermal boundary layer thins with an augmentation in Pr. The decrease in temperature function with an increase in Pr becomes significant when radiation parameter changes from $Rd = 0$ to $Rd = 1$. The temperature profiles become increasingly steeper with an increase in Pr indicating larger heat transfer rate from the sheet. On the other hand, the influence of radiation parameter on temperature profiles is qualitatively opposite, that is, as Rd increase, the temperature profiles become broader and change from normal shape to S-shaped thicker profiles. Fig. 9.5 perceives the impact of temperature exponent parameter A on the local fluid's temperature with the variations in velocity ratio λ. An increase in λ enhances the entrainment intensity of cold fluid (from the ambient) towards the hot fluid near the sheet. As a result temperature θ decreases with an increment in λ. This outcome is consistent with the findings reported by Liu et al. [10]. It can be seen that when $A \geq 0$, the temperature profiles monotonically decay from unity to zero with increasing dimensionless distance. Interestingly, for range of values of $A < 0$, temperature θ first increases and then asymptotically reaches the zero value as η is increased showing the existence of "Sparrow-Gregg Hills (SGH)". Physically for sufficiently smaller values of A, the sheet's temperature becomes less than the fluid's temperature near the vicinity of the sheet which leads to the reverse heat flow close to the sheet. In this situation the reduced Nusselt number $-\theta'(0)$ is expected to be negative which will be demonstrated later.

Fig. 9.6 shows that increasing values of θ_w correspond to an increase in wall temperature (T_w) which eventually rises the fluid's temperature. In accordance with Pantokratoras and Fang [110] the profiles become S-shaped when θ_w is gradually increased indicating the existence of point of inflection (i.e. $-\theta'(0) = 0$). It is worth pointing here that when $\theta_w \approx 1$, the corresponding profiles represent the case of linearized radiative heat flux, a fact that is evident from Eq. (9.11). The influence of radiation parameter Rd on the temperature θ for both linear and non-linear radiative heat flux cases can be analyzed from Fig. 9.7. It is found that rise in temperature function with the variation in Rd is quite significant in non-linear radiative heat flux case when compared with the case of linear thermal radiation. We notice that thermal boundary layer thins and profiles change to S-shape when Rd tends to zero value (a phenomenon also depicted by Pantokratoras and Fang [110]). Fig. 9.8 plots the dimensionless heat flux versus θ_w for different values of Prandtl number Pr and radiation parameter Rd. We observe that in case of linearized

radiative heat flux ($\theta_w \approx 1$), the wall heat flux approaches to a constant finite value as Rd tends to zero. Notably, this outcome is not true in case of non-linear radiative heat flux. Fig. 9.9 shows the variation of wall temperature gradient versus Pr with the variations in λ and A. The wall temperature gradient approaches zero for vanishing Prandtl number $Pr \to 0$. Further $\theta'(0)$ is positive for $A < 0$ and negative for $A \geq 0$, which is consistent with the results given in Fig. 9.5 and Table 8.2.

9.5 Concluding Remarks

Numerical study on non-linear radiative heat transfer problem for three-dimensional flow of viscous fluid past an exponentially stretching sheet is presented here. The temperature is exponentially varied along the sheet. A local similarity solution is achieved by means of shooting method with Runge-Kutta integration technique. The important points of this study are as under:

a. The energy equation is governed by an additional temperature ratio parameter θ_w which is an indicator of wall to ambient temperature difference.

b. The temperature θ increases with an increase in θ_w. Further, the wall temperature gradient smoothly descends to zero with an augmentation in θ_w.

c. Temperature decreases and thermal boundary layer thins when Pr is increased. Moreover, significant variations in temperature profiles are accounted when thermal radiation effect is stronger.

d. The Nusselt number $(-\theta'(0))$ is negative when $A < 0$ indicating the reverse heat flow close to the wall regions.

e. The results are found in excellent agreement with Magyari and Keller [6] and Liu et al. [10].

Table 9.1: Comparison of results of skin friction coefficients with Liu et al. [10] for different values of λ when $Rd = 0$.

λ	$-f''(0)$	$-g''(0)$	$-[f(\infty) + g(\infty)]$
0.0	1.28180919	0	0.90564398
	(1.28180856)	0	(0.90564383)
0.5	1.56989016	0.784945082	1.10918343
	(1.56988846)	(0.78494423)	(1.10918263)
1.0	1.81275445	1.81275445	1.28077511
	(1.81275105)	(1.81275105)	(1.28077378)

Table 9.2: Comparison of results of wall temperature gradient with Magyari and Keller [6] and Liu et al. [10] when $\lambda = Rd = 0$.

Pr	A	$-\theta'(0)$		
		Magyari & Keller [6]	Liu et al. [10]	Present
1	-1.5	-0.377413	-0.37741256	-0.37740378
	0	0.549643	0.54964375	0.54964817
	1	0.954782	0.95478270	0.95478658
	3	1.560294	1.56029540	1.56031491
5	-1.5	-1.353240	-1.35324050	-1.3532587
	0	1.521243	1.52123900	1.52124805
	1	2.500135	2.50013157	2.50010963
	3	3.886555	3.88655510	3.88655864
10	-1.5	-2.200000	-2.20002816	-2.20003325
	0	2.257429	2.25742372	2.25743435
	1	3.660379	3.66037218	3.66023389
	3	5.635369	5.62819631	5.62812884

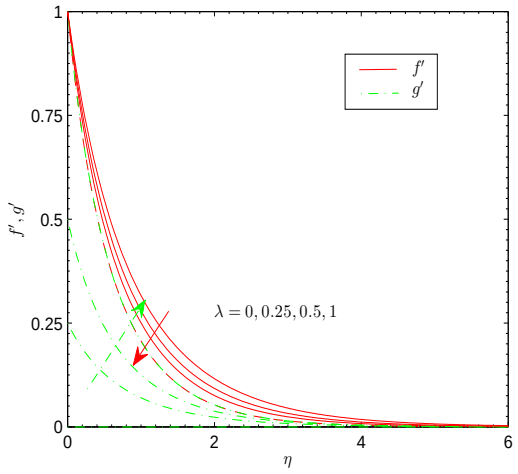

Figure 9.2: Effect of λ on $f'(\eta)$ and $g'(\eta)$.

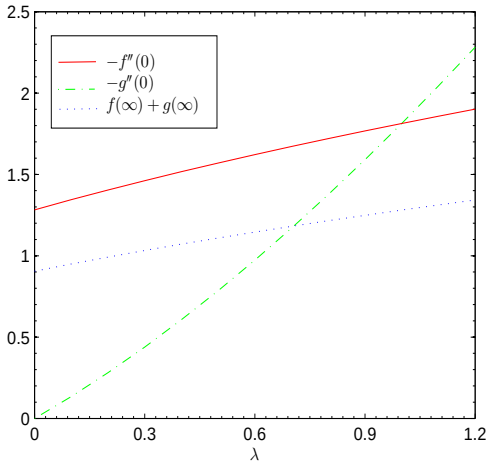

Figure 9.3: Effect of λ on $-f''(0), -g''(0)$.

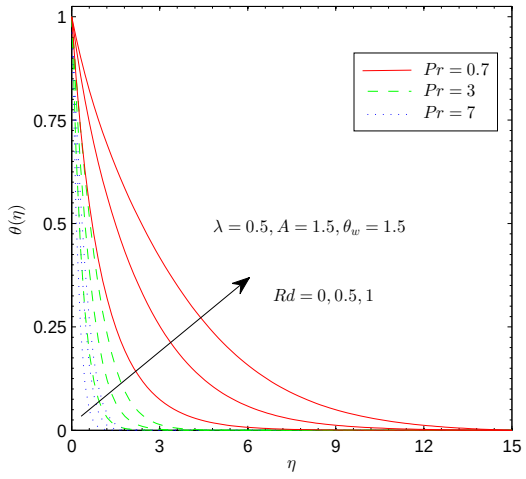

Figure 9.4: Effect of Rd and Pr on θ.

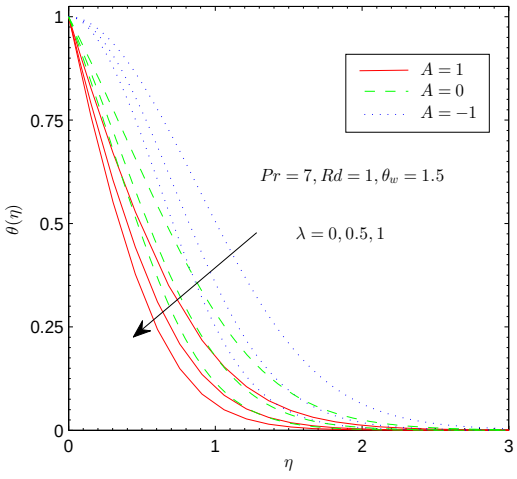

Figure 9.5: Effect of λ and A on θ.

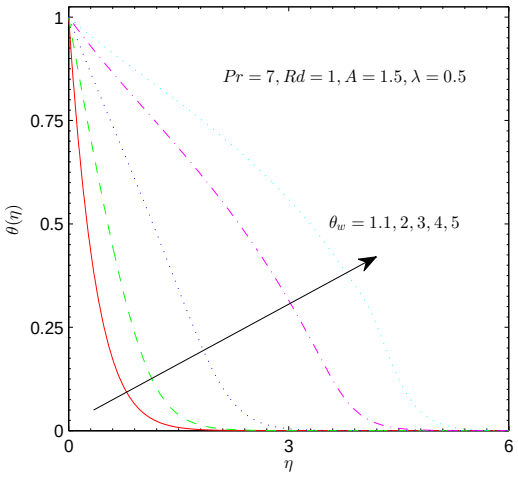

Figure 9.6: Effect of θ_w on θ.

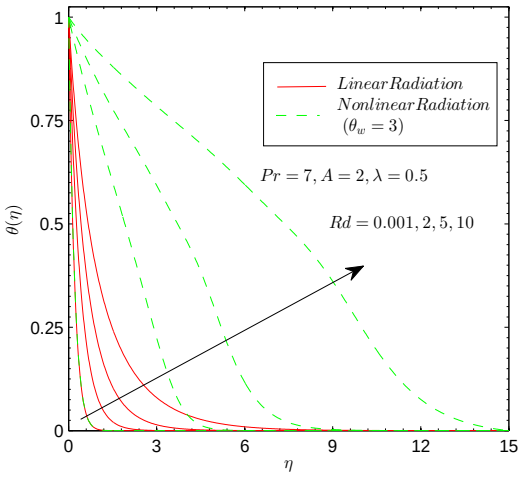

Figure 9.7: Effect of Rd on θ.

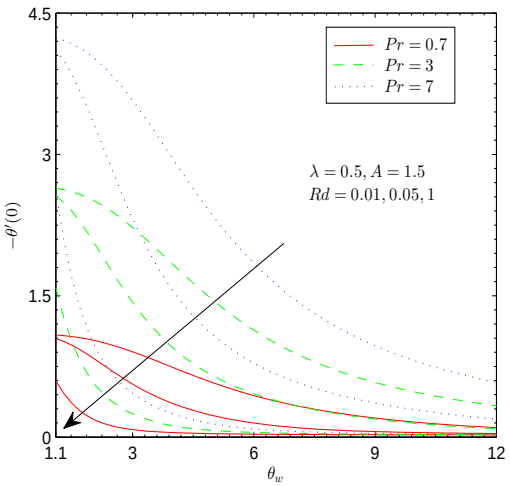

Figure 9.8: Effect of Rd, θ_w and Pr on $-\theta'(0)$.

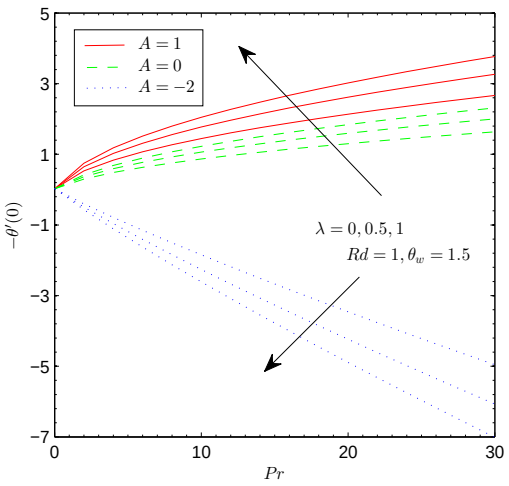

Figure 9.9: Effect of A, Pr and λ on $-\theta'(0)$.

Bibliography

[1]. H. Blasius, Grenzschichten in FlussigkeitenmitKleinerReibung, Z. Angew. Math. Phys. 56 (1908) 1-37.

[2]. B. C. Sakiadis, Boundary-layer behavior on continuous solid surfaces. I. Boundary-layer equations for two-dimensional and axisymmetric flow, AIChE J 7 (1961) 26-28.

[3]. L. J. Crane, Flow past a stretching plate, Zeitschrift für angewandte Mathematik und Physik ZAMP 21 (1970) 645-647.

[4]. K. R. Rajagopal, A note on unsteady unidirectional flows of a non-Newtonian fluid, Int. J. Non-Linear Mech. 17 (1982) 369-373.

[5]. C. Y. Wang, The three-dimensional flow due to a stretching flat surface, Phys. Fluids 27 (1984) 1915–1917.

[6]. E. Magyari and B. Keller, Heat and mass transfer in the boundary layers on an exponentially stretching continuous surface, J Phys D: Appl Phys 32 (1999) 577-585.

[7]. T. R. Mahapatra and A.S. Gupta, Heat transfer in stagnation-point flow towards a stretching sheet, Int. J. Heat Mass Transf. 38 (2002) 517-521.

[8]. R. Cortell, Flow and heat transfer in a moving fluid over a moving flat surface, Theor. Comput. Fluid Dyn. 21 (2007) 435–446.

[9]. I. Liu and H. I. Andersson, Heat transfer over a bidirectional stretching sheet with variable thermal conditions, Int. J. Heat Mass Transf. 51(2008) 4018–4024.

[10]. I. C. Liu, H. H. Wang and Y. F. Peng, Flow and heat transfer for three-dimensional flow over an exponentially stretching surface, Chem. Eng. Commun. 200(2013) 253–268.

[11]. W. Ostwald, Ueber die rechnerische Darstellung des Strukturgebietes der Viskosität, Kolloid Zeitschrift 47 (1929) 176-187.

[12]. W. R. Schowalter, The application of boundary layer theory to power-law pseudo-plastic fluids: Similar solutions, AIChE J. 6 (1960) 24-28.

[13]. H. I. Andersson, K. H. Bech and B. S. Dandapat. Magnetohydrodynamic flow of a power-law fluid over a stretching sheet," Int. J. Non-Linear Mech. 27 (1992) 929-936.

[14]. K. V. Prasad, D. Pal, and P. S. Datti, MHD power-law fluid flow and heat transfer over a non-isothermal stretching sheet, Comm. Nonlinear Sci. and Num. Sim. 14 (2009) 2178-2189.

[15]. T. R. Mahapatra, S. K. Nandy and A.S. Gupta, Magnetohydrodynamic stagnation-point flow of a power-law fluid towards a stretching surface, Int. J. Non-linear Mech. 44 (2009) 124-129.

[16]. M. Z. Salleh, R. Nazar and I. Pop, Boundary layer flow and heat transfer over a stretching sheet with Newtonian heating, J. Taiwan Inst. Chem. Eng. 41 (2010) 651-655.

[17]. M. Kumari, I. Pop and G. Nath, Transient MHD stagnation flow of a non-Newtonian fluid due to impulsive motion from rest, Int. J. Non-Linear Mech. 45 (2010) 463-473.

[18]. P. M. Patil, S. Roy and A. J. Chamkha, Mixed convection flow over a vertical power-law stretching sheet, Int. J. Num. Meth. Heat & Fluid Flow 20 (2010) 445-458.

[19]. A. Postelnicu and I. Pop, Falkner–Skan boundary layer flow of a power-law fluid past a stretching wedge, App. Maths. Comp. 217 (2011) 4359-4368.

[20]. P. T. Griffiths, S. O. Stephen, A. P. Bassom and S. J. Garrett, Stability of the boundary layer on a rotating disk for power-law fluids, J. Non-Newtonian Fluid Mech. 207 (2014) 1-6.

[21]. K. Sadeghy, A. H. Najafi and M. Saffaripour, Sakiadis flow of an upper-convected Maxwell fluid, Int. J. Nonlinear Mech. 40 (2005) 1220-1228.

[22]. K. Sadeghy, H. Hajibeygi, S.M. Taghavi, Stagnation point flow of upper-convected Maxwell fluids, Int. J. Non-Linear Mech.41 (2006) 1242–1247.

[23]. T. Hayat, Z. Abbas and M. Sajid, Series solution for the upper-convected Maxwell fluid over a porous stretching plate, Phys. Lett. A 358 (2006) 396-403.

[24]. T. Hayat and M. Sajid, Homotopy analysis of MHD boundary layer flow of an upper-convected Maxwell fluid, Int. J. Eng. Sci. 45 (2007) 393-401.

[25]. M. Kumari and G. Nath, Steady mixed convection stagnation-point flow of upper convected Maxwell fluids with magnetic field, Int. J. Nonlinear Mech. 44 (2009) 1048-1055.

[26]. A. Alizadeh-Pahlavan, V. Aliakbar, F. Vakili-Farahania and K. Sadeghy, MHD flows of UCM fluids above porous stretching sheets using two-auxiliary-parameter homotopy analysis method, Comm. Nonlinear Sci. Num. Simul. 14 (2009) 473-488.

[27]. T. Hayat, Z. Abbas and M. Sajid, MHD stagnation-point flow of an upper-convected Maxwell fluid over a stretching surface, Chaos, Solitons and Fractals 39 (2009) 840-848.

[28]. B. Raftari and A. Yildirim, The application of homotopy perturbation method for MHD flows of UCM fluids above porous stretching sheets, Comp. Math. Appl. 59 (2010) 3328-3337.

[29]. S. Mukhopadhyay, Heat transfer analysis of the unsteady flow of a Maxwell fluid over a stretching surface in the presence of a heat source/sink, Chin. Phys. Let. 29 (2011) DOI: 10.1088/0256-307X/29/5/054703.

[30]. T. Hayat, Z. Iqbal, M. Mustafa and A. Alsaedi, Momentum and heat transfer of an upper-convected Maxwell fluid over a moving surface with convective boundary conditions, Nucl. Eng. Des. 252 (2012) 242-247.

[31]. M. S. Abel, J. V. Tawade and M. M. Nandeppanavar, MHD flow and heat transfer for the upper-convected Maxwell fluid over a stretching sheet, Meccanica 47(2012) 385-393.

[32]. T. Hayat, M. Mustafa, S. A. Shehzad and S. Obaidat, Melting heat transfer in the stagnation-point flow of an upper-convected Maxwell (UCM) fluid past a stretching sheet, Int. J. Numer. Meth. Fluids 68 (2012) 233-243.

[33]. S. Shateyi, A new numerical approach to MHD flow of a Maxwell fluid past a vertical stretching sheet in the presence of thermophoresis and chemical reaction, Bound. Val. Prob. 196 (2013) DOI:10.1186/1687-2770-2013-196.

[34]. S. Nadeem. R. Ul Haq and Z. H. Khan, Numerical study of MHD boundary layer flow of a Maxwell fluid past a stretching sheet in the presence of nanoparticles, J. Taiwan Inst. Chem. Eng. 45 (2014) 121-126.

[35]. M. Mustafa, J. A. Khan, T. Hayat, and A. Alsaedi, Simulations for Maxwell fluid flow past a convectively heated exponentially stretching sheet with nanoparticles, AIP Advances 5 (2015) 037133.

[36]. M. Mustafa, J. A. Khan, T. Hayat, and A. Alsaedi, Sakiadis flow of Maxwell fluid considering magnetic field and convective boundary conditions, AIP Advances 5 (2015) 027106.

[37]. M. Jalil, S. Asghar and S. M. Imran, Self similar solutions for the flow and heat transfer of Powell-Eyring fluid over a moving surface in a parallel free stream, Int. J. Heat Mass Transf. 65 (2013)73-79.

[38]. A. Mushtaq, M. Mustafa, T. Hayat, M. Rahi and A. Alsaedi, Exponentially stretching sheet in a Powell–Eyring fluid: Numerical and series solutions, Z. Naturforsch. 68a (2013) 791-798.

[39]. T. Javed, N. Ali, Z. Abbas and M. Sajid, Flow of an Erying-Powell non-Newtonian fluid over a stretching sheet, Chem. Engg. Commun. 200 (2013) 327-336.

[40]. A. V. Roşca and I. Pop, Flow and heat transfer of Powell–Eyring fluid over a shrinking surface in a parallel free stream, Int. J. Heat Mass Transf. 71 (2014) 321-327.

[41]. M. Poonia and R. Bhargava, Finite element study of Eyring–Powell fluid flow with convective boundary conditions, J. Thermophys. Heat Transf. 28 (2014) 499-506.

[42]. T. Hayat, S. Asad, M. Mustafa and A. Alsaedi, Radiation effects on the flow of Powell-Eyring fluid past an unsteady inclined stretching sheet with non-uniform heat source/sink, PloS ONE 9 (2014) doi:10.1371/journal.pone.0103214.

[43]. S. Panigrahi, M. Reza and A. K. Mishra, MHD effect of mixed convection boundary-layer flow of Powell-Eyring fluid past nonlinear stretching surface, Appl. Math. Mech. (2014) doi: 10.1007/s10483-014-1888-6.

[44]. A. J. Hunt, Small particle heat exchangers, J Renew Sustain Energy (1978) Lawrence Berkeley Lab Report NumberLBL-7841.

[45]. G. K. Batchelor, Brownian diffusion of particles with hydrodynamic interaction, J. Fluid Mech. 74 (1976) 1-29.

[46]. K. L. Walker, G. M. Homsy and F. T. Geyling, Thermophoretic deposition of small particles in laminar tube flow, J. Coll. Interf. Sci. 69 (1979) 138-147.

[47]. S. T. Pratsinis and K. S. Kim, Particle coagulation, diffusion and thermophoresis in laminar tube flows, J. Aeros. Sci. 20 (1989) 101-111.

[48]. F. Trieb and J. Nitsch, Recommendations for the market introduction of solar thermal power stations, Renew. Ener. 14 (1998) 17-22.

[49]. P. F. Lin and J. Z. Lin, Prediction of nanoparticle transport and deposition in bends. Appl. Math. Mech. Engl. Ed. 30 (2009) 957-968.

[50]. J. Z. Lin, P. F. Lin and J. H. Chen, Research on the transport and deposition of nanoparticles in a rotating curved pipe, Phys. Fluids 21(2009) 122001.

[51]. T. P. Otanicar and J. S. Golden, Comparative environmental and economic analysis of conventional and nanofluid solar hot water technologies, Environmental science & technology 43 (2009) 6082-6087.

[52]. H. Tyagi, P. Phelan and R. Prasher (2009) Predicted efficiency of a low-temperature nanofluid-based direct absorption solar collector, J. Solar Ener. Eng. 131 (2009) 041004.

[53]. K. V. Wong and O. D. Leon, Applications of Nanofluids: Current and Future, Advan. Mech. Engg. (2010) Article ID 519659.

[54]. O. Mahian, A. Kianifar, S. A. Kalogirou, I. Pop and S. Wongwises, A review of the applications of nanofluids in solar energy, Int. J. Heat Mass Transf. 57 (2013) 582-594.

[55]. H. Masuda, A. Ebata, K. Teramae and N. Hishinuma, Alteration of thermal conductivity and viscosity of liquid by dispersing ultra-fine particles (dispersion of c-Al2O3, SiO2 and TiO2 ultra-fine particles), NetsuBussei (in Japanese) 4 (1993) 227–233.

[56]. S. U. S. Choi, Enhancing thermal conductivity of fluids with nanoparticle, in: D.A. Siginer, H.P. Wang (eds.), Developments and Applications of Non-Newtonian Flows, ASME FED, 231 (1995) 99-105.

[57]. S. U. S. Choi and J. A. Eastman, Enhancing thermal conductivity of fluids with nanoparticles. in: The Proceedings of the 1995 ASME International Mechanical Engineering Congress and Exposition, San Francisco, USA, ASME, FED 231/MD 66 (1995) 99–105.

[58]. J. Buongiorno, Convective transport in nanofluids, ASME J. Heat Transf. 128 (2006) 240–250.

[59]. J. Buongiorno and L. W. Hu, Nanofluid heat transfer enhancement for nuclear reactor application. Proceedings of the ASME 2009 2nd Micro/Nanoscale Heat & Mass Transfer International Conference, DOI: 10.1115/MNHMT2009-18062.

[60]. G. Huminic and A. Huminic, Application of nanofluids in heat exchangers: A review, Renew. Sust. Ener. Reviews 16 (2012) 5625-5638.

[61]. D. A. Nield and A. V. Kuznetsov, The Cheng–Minkowycz problem for natural convective boundary-layer flow in a porous medium saturated by a nanofluid, Int. J. Heat Mass Transf. 52 (2009) 5792-5795.

[62]. A. V. Kuznetsov and D. A. Nield, Natural convective boundary-layer flow of a nanofluid past a vertical plate, Int. J. Therm. Sci. 49 (2010) 243-247.

[63]. W. A. Khan and I. Pop, Boundary-layer flow of a nanofluid past a stretching sheet, Int. J. Heat Mass Transf. 53 (2010) 2477-2483.

[64]. O. D. Makinde and A. Aziz, Boundary layer flow of a nanofluid past a stretching sheet with a convective boundary condition, Int. J. Therm. Sci. 50 (2011) 1326-1332.

[65]. M. Mustafa, T. Hayat, I. Pop, S. Asghar and S. Obadiat, Stagnation-point flow of a nanofluid towards a stretching sheet, Int. J. Heat Mass Transf. 54 (2011) 5588-5594.

[66]. S. Ahmad, A. M. Rohni and I. Pop, Blasius and Sakiadis problems in nanofluids, Acta Mechan. 218 (2011) 195-204.

[67]. A. Rasekh, D. D. Ganji and S. Tavakoli, Numerical solutions for a nanofluid past over a stretching circular cylinder with non-uniform heat source, Front Heat Mass Transf. (2012) http://dx.doi.org/10.5098/hmt.v3.4.3003.

[68]. H. R. Ashorynejad, M. Sheikholeslami, I. Pop and D. D. Ganji, Nanofluid flow and heat transfer due to a stretching cylinder in the presence of magnetic field, Heat Mass Transf. 49 (2013) 427–436.

[69]. W. Ibrahim, B. Shankar and M. M. Nandeppanavar, MHD stagnation-point flow and heat transfer due to nanofluid towards a stretching sheet, Int. J. Heat Mass Transf. 56 (2013) 1-9.

[70]. M. Sheikholeslami, M. Hatami and D. D. Ganji, Analytical investigation of MHD nanofluid flow in a semi-porous channel, Powder Tech. 246 (2013) 327-336.

[71]. M. V. Karwe and Y. Jaluria, Fluid flow and mixed convection transport from a moving plate in rolling and extrusion processes, ASME J. Heat Transf. 110 (1988) 655–661.

[72]. C. H. Chen, Mixed convection cooling of a heated continuously stretching surface. Heat Mass Transf. 36 (2000) 79–86.

[73]. F. P. Incropera, Fundamentals of heat and mass transfer. John Wiley & Sons (2011).

[74]. A. Aziz, W. A. Khan, Natural convective boundary layer flow of a nanofluid past a convectively heated vertical plate, Int. J. Therm. Sci. 52 (2012) 83-90.

[75]. M. J. Uddin, W. A. Khan and A. I. Ismail, MHD free convective boundary layer flow of a nanofluid past a flat vertical plate with Newtonian heating boundary condition, PLoS One 7 (2012) doi:10.1371/journal.pone.0049499.

[76]. A. V. Kuznetsov and D. A. Nield, The Cheng–Minkowycz problem for natural convective boundary layer flow in a porous medium saturated by a nanofluid: A revised model, Int. J. Heat Mass Transf. 65 (2013) 682-685.

[77]. O. D. Makinde, W. A. Khan and Z. H. Khan, Buoyancy effects on MHD stagnation point flow and heat transfer of a nanofluid past a convectively heated stretching/shrinking sheet, Int. J. Heat Mass Transf. 62 (2013) 526-533.

[78]. M. Mustafa, S. Hina, T. Hayat and B. Ahmad, Influence of induced magnetic field on the peristaltic flow of nanofluid, Meccan. 49 (2014) 521-534.

[79]. N. A. Yacob, A. Ishak, I. Pop and K. Vajravelu, Boundary layer flow past a stretching/shrinking surface beneath an external uniform shear flow with a convective surface boundary condition in a nanofluid, Nanoscale Res. Letts. 6 (2011) doi:10.1186/1556-276X-6-314.

[80]. M. A. A. Hamad and M. Ferdows, Similarity solution of boundary layer stagnation-point flow towards a heated porous stretching sheet saturated with a nanofluid with heat absorption/generation and suction/blowing: A Lie group analysis, Comm. Nonlinear Sci. Num. Simul. 17 (2012) 132-140.

[81]. M. Turkyilmazoglu, Exact analytical solutions for heat and mass transfer of MHD slip flow in nanofluids, Chemical Engineering Science 84(2012)182–187.

[82]. W. A. Khan and I. Pop, Boundary layer flow past a stretching surface in a porous medium saturated by a nanofluid: Brinkman-Forchheimer model, Plos One 7(2012) doi:10.1371/journal.pone.0047031.

[83]. M. Mustafa, Junaid A. Khan, T. Hayat, and A. Alsaedi, Boundary Layer Flow of Nanofluid Over a Nonlinearly Stretching Sheet With Convective Boundary Condition, IEEE T. NANOTECHNOL. 14 (2015) 159.

[84]. J. A. Khan, M. Mustafa, T. Hayat, M. Sheikholeslami, and A. Alsaedi, Three-dimensional flow of nanofluid induced by an exponentially stretching sheet: an application to solar energy, PloS one 10 (2015) e0116603.

[85]. J. A. Khan, M. Mustafa, T. Hayat, and A. Alsaedi, Three-dimensional flow of nanofluid over a non-linearly stretching sheet: An application to solar energy, Inter. J. Heat Mass Transf. 86 (2015) 158-164.

[86]. A. Rapits and C. Perdikis, Viscoelastic flow by the presence of radiation, ZAMP 78 (1998) 277–279.

[87]. M. A. Seddeek, Effects of radiation and variable viscosity on MHD free convection flow past a semi infinite flat plate with an aligned magnetic field in the case of unsteady flow, Int. J. Heat Mass Transf. 45 (2002) 931-935.

[88]. A. Raptis, C. Perdikis and H. S. Takhar, Effect of thermal radiation on MHD flow, Appl. Math. Comput. 153 (2004) 645-649.

[89]. R. C. Bataller, Radiation effects in the Blasius flow, Appl. Math. andComput. 198 (2008) 333-338.

[90]. A. Ishaq, Mixed convection boundary layer flow over a horizontal plate with thermal radiation, Heat Mass Transf. 46 (2009) 147-151.

[91]. K. Bhattacharyya, Effects of radiation and heat source/sink on unsteady MHD boundary layer flow and heat transfer over a shrinking sheet with suction/injection, Front. Chem. Sci. Eng. 5 (2011) 376-384.

[92]. R. Cortell, A numerical tackling on Sakiadis flow with thermal radiation, Chin. Phys. Lett. 25 (2008) 1340-1342.

[93]. T. Hayat, M. Mustafa and M. Sajid, Influence of thermal radiation on Blasius flow of a second grade fluid, Z. Naturforsch. 64a (2009) 827-833.

[94]. B. J. Gireesha, A. J. Chamkha, S. Manjunatha, and C. S. Bagewadi, Mixed convective flow of a dusty fluid over a vertical stretching sheet with non-uniform heat source/sink and radiation, International Journal of Numerical Methods for Heat & Fluid Flow, 23 (2013) 598-612.

[95]. T. Hayat, Z. Iqbal, M. Mustafa and A. Alsaedi, Stagnation-point flow of Jeffrey fluid with melting heat transfer and Soret and Dufour effects, Inter. J. Numer. Methods Heat Fluid Flow 24 (2014) 402-418.

[96]. T. Hayat, S. Asad, M. Mustafa and A. Alsaedi, Radiation effects on the flow of Powell-Eyring fluid past an unsteady inclined stretching sheet with non-uniform heat source/sink, PLoS ONE 9 (2014), doi: 10.1371/journal.pone.0103214.

[97]. T. R. Mahapatra, S. Mondal and D. Pal, Heat Transfer due to Magnetohydrodynamic Stagnation-Point Flow of a Power-Law Fluid towards a Stretching Surface in the Presence of Thermal Radiation and Suction/Injection, Thermodynamics. 2012 (2012) Article ID 465864 http://dx.doi.org/10.5402/2012/465864.

[98]. M. S. Khan, I. Karim, L. E. Ali and I. Islam, Unsteady MHD free convection boundary-layer flow of a nanofluid along a stretching sheet with thermal radiation and viscous dissipation effects, Int. Nano Lett. 24 (2012) (1-9).

[99]. T. G. Motsumi and O. D. Makinde, Effects of thermal radiation and viscous dissipation on boundary layer flow of nanofluids over a permeable moving flat plate, Phys. Scr. 86 (2012) 045003 (doi:10.1088/0031-8949/86/04/045003).

[100]. F. M. Hady, F. S. Ibrahim, S. M. A. Gaied and M. R. Eid, Radiation effect on viscous flow of a nanofluid and heat transfer over a nonlinearly stretching sheet, Nanosca. Res. Lett. 7(2012) doi: 10.1186/1556-276X-7-229.

[101]. N. A. A. Mat, N. M. Arifin, R. Nazar and F. Ismail, Radiation effect on Marangoni convection boundary layer flow of a nanofluid, Mathem. Sci. 6 (2012) doi: 10.1186/2251-7456-6-21.

[102]. R. B. Mohamad, R. Kandasamy and I. Muhamin, Enhance of heat transfer on unsteady Hiemenz flow of nanofluid over a porous wedge with heat source/sink due to solar energy radiation with variable stream condition, Heat Mass Transf. 49 (2013) 1261-1269.

[103]. R. Kandasamy, I. Muhamin and R. Mohamad, Thermophoresis and Brownian motion effects on MHD boundary-layer flow of a nanofluid in the presence of thermal stratification due to solar radiation, Int. J. Mech. Sci. 70 (2013) 146-154.

[104]. M. S. Shadloo, A. Kimiaeifar and D. Bagheri, Series solution for heat transfer of continuous stretching sheet immersed in a micropolar fluid in the existence of radiation, Int. J. Num. Meth. Heat & Fluid Flow 23 (2013) 289-304.

[105]. M. Ferdows, M. S. Khan and O. A. Beg, Numerical study of transient magnetohydrodynamic radiative free convection nanofluid flow from a stretching permeable surface, Proc IMechE Part E J Process Mechanical Engg. 0 (2013) 1–16.

[106]. M. S. Khan, M. M. Alam and M. Ferdows, Effects of magnetic field on radiative flow of a nanofluid past a stretching sheet, Procedia Engg. 56 (2013) 316-22.

[107]. M. S. Khan, I. Karim, M. S. Islam and M. Wahiduzzaman, MHD boundary layer radiative, heat generating and chemical reacting flow past a wedge moving in a nanofluid, Nano Convergence 2014 (2014) http://dx.doi.org/10.1186/s40580-014-0020-8.

[108]. E. Magyari and A. Pantokratoras, Note on the effect of thermal radiation in the linearized Rosseland approximation on the heat transfer characteristics of various

boundary layer flows, Int. Commun. Heat Mass Transf. 38 (2011) 554-556.

[109]. M. M. Rahman and I. A. Eltayeb, Radiative heat transfer in a hydromagnetic nanofluid past a non-linear stretching surface with convective boundary condition, Meccan. 48 (2013) 601-615.

[110]. A. Pantokratoras and T. Fang, Sakiadis flow with nonlinear Rosseland thermal radiation, Physic. Scrip. 87 (2013) 015703(5 pages).

[111]. A. Pantokratoras and T. Fang, Blasius flow with non-linear Rosseland thermal radiation, Meccan. 49 (2014) 1539-1545.

[112]. A. Mushtaq, M. Mustafa, T. Hayat and A. Alsaedi, Effect of thermal radiation on the stagnation-point flow of upper-convected Maxwell (UCM) fluid over a stretching sheet, J. Aerosp. Engg. 27 (2014). doi: 10.1061/(ASCE)AS.1943-5525.0000361.

[113]. R. Cortell, Fluid flow and radiative nonlinear heat transfer over a stretching sheet, J. King Saud University-Science 26 (2014) 161-167. doi.org/10.1016/j jksus.2013.08.004.

[114]. A. Mushtaq, M. Mustafa, T. Hayat and A. Alsaedi, Nonlinear radiative heat transfer in the flow of nanofluid due to solar energy: A numerical study, J. Taiwan Inst. Chem. Eng. 45 (2014) 1176-1183.

[115]. M. Mustafa, A. Mushtaq, T. Hayat and B. Ahmad, Nonlinear radiation heat transfer effects in the natural convective boundary layer flow of nanofluid past a vertical plate: a numerical study, PLoS ONE 9 (2014) doi: 10.1371/journal.pone.0103946.

[116]. R. Cortell, MHD (magneto-hydrodynamic) flow and radiative nonlinear heat transfer of a viscoelastic fluid over a stretching sheet with heat generation/absorption, Energy 74 (2014) 896-905.

[117]. A. Mushtaq, M. Mustafa, T. Hayat and A. Alsaedi, On the numerical solution of the nonlinear radiation heat transfer problem in a three-dimensional flow, Z. Naturforsch. 69a (2014) 705-713.

[118]. A. Pantokratoras, Natural convection along a vertical isothermal plate with linear and non-linear Rosseland thermal radiation, Int. J. Therm. Sci. 84 (2014) 151-157.

[119]. M. Mustafa, A. Mushtaq, T. Hayat and A. Alsaedi, Radiation effects in three-dimensional flow over a bi-directional exponentially stretching sheet, J. Taiwan Inst. Chem. Eng. 47 (2015) 403-409.

[120]. M. Mustafa, A. Mushtaq, T. Hayat and A. Alsaedi, Model to Study the Nonlinear Radiation Heat Transfer in the Stagnation-Point Flow of Power-Law Fluid Int. J. Num. Meth. Heat and Fluid Flow 25 (2015) In press.

[121]. R. B. Bird, W.E. Stewart and E.N. Lightfoot, Transport Phenomena, Wiley, New York (1960).

[122]. H. Schlichting, K. Gersten and K. Gersten, Boundary-layer theory, Springer Science & Business Media (2000).

[123]. S. Rosseland, Astrophysik and atom-theorestischegrundlagen, Springer Berlin (1931).